A comparative first-principles magnetic ground states study in pristine and reduced $LaMnO_{3-x}$ $(0.0 \leq x \leq 0.04)$: Role of magnetic quasi-particles

P. Srikanth Patnaik[1], Tilak Das[1]*, Sergio Tosoni[2] and G. P. Das[3]

[1]Department of Physics, Indian Institute of Technology Kharagpur, Kharagpur - 721302, India

[2]Dipartimento di Scienza dei Materiali, Università di Milano-Bicocca, via Cozzi 55, 20125 Milano, Italy

[3]Research Institute for Sustainable Energy, TCG Centres for Research and Education in Science and Technology, Sector V, Salt Lake, Kolkata 700091, India

Abstract

The earth abundant oxides with fidelity to form quasi-particles are yet to be explored for energy storage applications in batteries, supercapacitors and *spintronics*. The present theoretical study has provided a systematic description of Mn(3*d*)-O(2*p*) electronic-correlation in two bulk oxides of La-manganites, $LaMnO_3$(LMO) with orthorhombic (o-) and rhombohedral (r-) bulk crystal symmetry. Thus, an investigation is done herein through the determination of accurate on-site Hubbard *U* from first-principles density functional perturbation theory (*i.e.*, self-consistent Hubbard *U*, say U_{self}) in both of these pristine LMOs and applied on partially reduced manganites model, $LaMnO_{3-x}(0.0 \leq x \leq 0.04)$. The correlation treatments within the density functional theory with on-site Hubbard *U* (DFT+*U*) not only on metal sites but also on the non-metals, are found to be quite crucial while searching for correct magnetic ground states and metal-insulator transitions pertaining to the reductions of Mn^{3+} ions and intrinsic Jahn-Teller (JT) distortions in LMOs. Thus, point-defects induced transport and magnetic symmetry breaking helps to unravel the mesmerizing magnetic ground states of LMOs as debated in the last several decades. The U_{self} is also applied for determining the geometries, structural descriptors, magnetic ground states, magnetic-exchange (ME) interactions and electronics structures of LMOs in close comparison to other known on-site U_{eff} calculations. The present U_{self} helps to better visualize the strong-correlation and non-local itinerant character of Mn(3*d*) occupancies in LMOs. Our study provides that a weaker and positive sign of ME interactions ($J_{\perp}$, $J_{\parallel}$) from the native $Mn^{3+}(3d^4)$—O—$Mn^{3+}(3d^4)$ skeleton of the o-LMO with JT-distortions is viable, while these are an order larger and also positive in other non-JT case r-LMO. However, in the reduced format, we predict more negative out-of-plane ME interactions ($J_{\perp}$) in o-LMO_{3-x} made out of the $Mn^{2+}(3d^5)$—• —$Mn^{2+}(3d^5)$ skeletons (• = Oxygen vacancy) immersed inside $Mn^{3+}(3d^4)$—O—$Mn^{3+}(3d^4)$ chains. We discussed the formation of A-type anti-ferromagnetic (AFM) polarons and ferromagnetic (FM) doublons type magnetic quasi-particles in these manganites in variation of JT-distortions. This has essentially shed light on the decade old enigma of the AFM ground state search in o-LMO and opens future scope of studies in FM insulating r-LMO – a milestone that reshuffles the scope of the first-principles calculations with DFT+*U*. With enhance O-vacancy concentrations, the o-LMO_{3-x} results charge-transfer insulating type due to AFM mono-polarons formations. But, Nagaoka-type FM polarons (doublons) in r-LMO_{3-x} shows orbital selective Mott-insulating nature in contrast to the FM ordered metallic types in the pristine. These observations are also consistent with recent model studies from Samajdar and Bhatt, 2024 and would enlighten further scope of applications of JT-type perovskites in catalysis to spintronics and towards the orbitronics, guided by magnetic quasi-particles.

Keywords: La-Manganites; Density functional theory; Self-consistent Hubbard *U*; Jahn-Teller distortions; Magnetic quasi-particles; Magnetic-exchange; Oxygen vacancy;

*Corresponding Author's E-mail: tilak.das@phy.iitkgp.ac.in

1. Introduction

Magnetic ground states, electronic structures and associated physical properties of oxides pertaining to the point-defects, line-defects and/or planar-defects are mesmerizing phenomena in condensed matter physics –

defects induced magnetism [1,2]. Out of different oxides, perovskite type 3*d*-metal oxides are explored through optoelectronic device applications due to its very promising low energy consumptions and Earth abundance [3,4,5]. These physical properties are guided by the physics of the intrinsic metal-insulator transitions, defect-centres guided transport and magnetic properties [6,7]. It is more interesting while such physical properties are present in the same stoichiometric phases along with the same chemical compositions but different symmetry groups (crystals types) – either studies from experimental measurements or corroborated with first-principles calculations. For example, transition metal (TM) oxides with orthorhombic or rhombohedral symmetry in Lanthanum manganites ($LaMnO_3$, hereafter LMOs) are few such oxide compounds with possible loss-free spintronics applications, which is explored even very recently [8,9,10,11,12]. Upon doping (holes or electrons), quite puzzling and novel charge- and spin-transport properties may arise. Taking into account the complex orbital-, charge-, and spin-ordering under competitive JT (Jahn-Teller) distortions and hence, the better understanding of magnetic ground states of LMOs is still fertile topic of research in condensed matter physics. This can not only open up possibilities for new technological device applications beyond spintronics but also explored for larger colossal magnetoresistance (CMR) [13,14,15,16], orbitronics (orbital angular moments or say, orbital selective non-local electronic correlation) related devices in the *point-defects induced* ferromagnetic or anti-ferromagnetic ground state of oxides [17,18].

First-principles calculation within the standard DFT (density functional theory) level [19,20] is known to be workhorse in understanding such physical and physio-chemical properties of ABO_3 oxides and their A-site or B-site mixed alloys for at least last several decades and even today [21,22]. However, some obvious drawbacks prevail when one takes into account the relative stabilization of the actual magnetic ground state of the oxide composed of strongly correlated *d*- and or *f*-metal ions. Here, overall thermochemical stabilities, electronic structures, and band gap predictions become more challenging at the same footing to the known experimental (exp.) data [23,24,25]. Not only with the 3*d*-metal based binary or ternary oxides, it is even true in some non-oxides with half-filled or partially filled *d*-orbital's electronic-correlation treatments [26,27,28,29]. In particular, a strongly-correlated electronic correlations impacts, and self-interactions along with the JT-deformation issues are mediated in one of such 3*d*-metal oxides – the present La-manganite $LaMnO_3$. The structural descriptions and physical properties within the standard DFT are thus, severely unfitted in the standard electronic structure theory calculations [30,31,32], and opens the paradox in ground state determinations of LMOs from fully first-principles theory (see next).

More specifically, this scenario is even more complex in the case of the half-filled or nearly half-filled 3*d*-metal oxides *i.e.*, LMOs which seems to be an exceptional critical case to measure the sign and quantification of the $Mn^{3+}(3d^4)$—$Mn^{3+}(3d^4)$ magnetic-exchange (ME) interactions as discussed by seminal papers from Zener, 1951-1960 [70], meanwhile by J. Kanamori, 1959 [33], and even a quarter century before by Park, 1996 [34] and Pickett & Singh, 1996 [13]. It is very recently also, undertaken by Stepanov & Biermann, 2024 [17]. Thus, though in the last 6-7 decades researchers have measured or hypotheses the major ME terms in different perovskites including the present La-manganite, but yet the actual sign of the $Mn^{3+}(3d^4)$—$Mn^{3+}(3d^4)$ chains in

the variation of the electrons (or holes) doping, is still under debate and need more clarifications, at least theoretically [35,36,37].

On the other hand, on-site effective Hubbard correlation-correction with DFT (*i.e.*, DFT+U_{eff}) has become a widely used tool in the first-principles approaches for describing properties of metal oxides' electronic and magnetic structures quite accurately [38,39,40,41,42,43,44,45]. Very often, preference of U_{eff} comes from the ad-hoc choices referring to the treatment of known experimental (exp.) geometries or from the thermochemical properties referential. However, these are criticized and limited to some extents and nonetheless, weaken the predictive powers of fully first-principles calculations of lattice positions and volumes [46]. For example, in case of the current orthorhombic LMO (o-LMO), the earlier theoretical studies have yielded very curious and contradictory results, for example, the ground state stabilization energy estimation from first-principles levels. A better understanding of the Mott-Hubbard vs. the charge-transfer insulator type in the anti-ferromagnetic (AFM) ground state of the o-LMO, pertaining to the class of solid solutions of $La_{1-x}A_xMnO_3$ manganites (A= Ca, Ba, Sr *etc*.) has begun already 2-3 decades before [47,48].

Besides, the pristine rhombohedral LMO phase (r-LMO) is known to be a ferromagnetic (FM) and half-metallic character at room temperature, and it lacks JT-distortions [12]. *True* & *Conventional* half-metallic vs. the *Transport* half-metallic phases for example, in the family of $La_{1-x}A_xMnO_3$ manganites (A = Ca, Ba, Sr) have been earlier discussed by Nadgorny *et al.*, 2001 [49]; and separately by Dowben & Skomski, 2004 [50]. This possibly has become matter of concern that how at the elevated temperature, and associated defects, inhomogeneity, interfaces in the manganites destroy the spin-polarization for half-metals even at the zero temperature [51]. The description is less complicated in the pristine rhombohedral manganite r-LMO with ideal crystal structures (no defects) using the first-principles calculations. Due to lack of the accurate treatment of self-interactions and correlation effects in the ground state DFT theory, authors also undertook better computational set-up to handle these localized vs. itinerant Mn-3*d* electrons [12].

The difficulty of correct magnetic ordering and electronic structural descriptions to unfold origin of the CMR in o-LMO has recently been discussed by the Jang *et al.*, 2018 [52]. The authors compared data from the spin-density functional (SDFT) vs. the spin-unpolarized charge-density (CDFT) functional theory with Hubbard U and Hund's exchange J through DFT+U_{eff} calculations. Authors highlighted the need for self-consistent approach for better first-principles predictions of Mn-3*d* electronic correlations to get consistent structure and properties due to strong couplings of spin-charge-orbital and lattice in particular for the o-LMO.

Thus, in the present article we have proposed determination of the spin-polarized spin-density functional based first-principles self-consistent Hubbard on-site U terms, U_{self} (hereafter, PBE+U_{self}). The U_{self} is determined either on Mn(3*d*) solely or combined on both Mn(3*d*) & O(2*p*) orbitals in these two LMOs for the very first time, and the necessity for the Hubbard on-site term on the O(2*p*) is thus, pointed out – a quantification of the Mn(3*d*)-O(2*p*) hybridization and O-2*p* correlation corrections. The nature of the electronic band structure is revisited in the given range of the effective U terms from literatures (see later), and then the fundamental electronic band edges compositions, band gap values, and orbital overlaps are estimated in these LMOs, while

the transport character (insulator vs. half-metallic) in the bulk is correlated with presence and absence of intrinsic JT-distortions.

A soft-reduction of LMOs into a set of partially reduced compounds with compositions $LaMnO_{3-x}$; $0 \leq x \leq 0.20$ had also been earlier discussed by Hansteen *et al.*, 2004 [165]. This was also later reported by Cortés-Gil *et al*., 2006 [53] on the stabilization of A-type AFM spin ordering in the reduced $LaMnO_{3-d}$; $0 \leq d \leq 0.03$. It was indeed, highlighted even earlier about the unavailability of the pristine stoichiometric LMOs by Jonker, 1956 [54]. The presence of the Mn^{3+}/Mn^{2+} sub-lattices at the ambient exp. conditions of synthesizing the o-$LaMnO_{3-x}$ (o-LMO_{3-x}) is viable on stabilizing its AFM magnetic ground states by introducing the negative ME interactions. This was later supported by overlapped orbital symmetry rules by Kanamori, 1959 [33]. At room temperature stable structure with oxygen deficiency o-LMO_{3-x} is thus possible, while it maintains the basal-plane lattice parameters in quite excellent agreement to the pristine one by less than $\pm 1.2\%$, in presence of Oxygen vacancy (O_v) concentration $x \leq 0.20$ [165]. In the meantime, a partial expansion of the out-of-plane lattice by $3.0 - 4.0\%$ was noticed, although. Thus, a systematic first-principles calculations dealing with the pristine and reduced LMOs are quite demanding whether electron doping would have actually any role to stabilize the magnetic ground states of these LMOs and less understood till date in best of our knowledge. This indeed would reshape existing understanding of the available ground state determination using the DFT+*U* methods in a JT-distorted oxides at affordable computational loads and modest accuracies; and unravel the limitations of DFT+*U* correlation treatments vs. JT-distorted structural models of other *A*MnO_3 perovskites. Hence, the standard DFT plus on-site Hubbard *U* term (DFT+*U*) is known to be very robust for the defect formation energies, magnetic ground states search or even ion intercalation energies calculations [55]. Earlier discussions also include one of our observations on 3*d*- and 4*d*-layered oxides that how a better electronic correlations treatment in the DFT+U_{self} approaches allowed to get better electronic structure, and magnetic ground state description [56,57,58].

How the transport and magnetic properties of bulk LMOs in presence of electron doping *i.e.*, in case of native point-defects via oxygen vacancies? Especially, in the bulk o-LMO the AFM spin-ordering among the Mn sub-lattices is found to be more dominant while compared to the known existence of the oxygen vacancies [59,60]. However, this is less known for the r-LMO. An estimation of the relative ground state energies of these LMOs from first-principles calculations with on-site Hubbard U_{eff} corrections is a way to improve the predictive powers of the first-principles calculations both quantitatively and qualitatively, systematically. Hence, with the possible scope of using the current LMOs for the low energy consumption optoelectronics, spintronics and indeed, for clean energy applications, the proposed theoretical tool must be optimized and transferable for the broader communities in physics, chemistry and materials sciences. This has been undertaken herein with possible implications of the current theoretical propositions. More specifically, a relative understanding of these two competitive o-LMO and r-LMO phases from the electronic and magnetic properties modelling are still missing to the best of our knowledge – *a comparative theoretical study in the pristine and reduced LMOs is thus quested*. So, results of the electronic and magnetic properties are also compared with the data from our proposition by

using PBE+U_{self} and compared to the existing standard ad-hoc PBE+U_{eff} methods. Then, the role of the spin-orbit coupling (SOC) is further explored and taken into account for the search of pristine magnetic ground states anisotropy of these LMOs. The impact of spin-orbital ordering and hence, the addition of the SOC is visualized at the correct on-site correlations in LMOs on the electronic structures, estimation of relative stabilities and orbital ordering.

Thus, we shed light on the magnetic quasi-particles formation and their characters out of the two types of O-vacancies, O_v (say, type V_{O1} and V_{O2}, see later) from the present theoretical study. The spin-, charge- and orbital-selective ordering of these correlated electrons along with geometry of the JT-tilted MnO_6–MnO_6 octahedrons in the pristine LMOs versus the MnO_6 – MnO_5 deformations is explored via reduced LMO_{3-x} models. We, thus also have shed light on the electron- and spin-localizations via AFM electron polarons and Nagaoka-type FM polarons (doublons) quasi-particles quantification in the strong-correlations regime to the itinerant characters of the Mn-3*d* electrons in the mixed ionic states of $Mn^{3+}(3d^4)$ and $Mn^{2+}(3d^5)$ in LMOs.

The current manuscript is organized in the following few sections and sub-sections, where in the next **Section 2**, we have provided the background and known physical properties and electronic structure calculations on the LMOs. In the **Section 3**, we describe the computational and methodological details with the brief theoretical formulation of calculating the possible first two magnetic-exchange (ME) terms in these LMOs. In the final **Section 4**, results are discussed following the impact of the self-consistent Hubbard U_{self} term and spin-orbital coupling effect (so called SOC). More specifically, in the first part of the results **Section 4**, a sub-section on the geometry, magnetic-ground states and electronic properties are discussed at the different PBE+U_{eff} methods (ad-hoc Hubbard *U*) and validates our calculation strategies (**Sections 4.1-4.3**); and a next sub-section provides the detail of the structure and properties from self-consistent Hubbard U_{self} based calculations from PBE+U_{self} computed volume, in closer resemblance with the known experimental predictions. Role of SOC in both phase of LMOs is also discussed either on the PBE+U_{eff} or PBE+U_{self} ground states, respectively. The novelty is also supported with the results from the choice of PBE+U_{self} which is applied for both on the Mn(3*d*) & O(2*p*) sub-lattices as the pristine LMOs are unlike natural earth abundant compared to the partial reduced phase LMO_{3-x} ($0.01 < x < 0.04$) (**Sections 4.4-4.5**). In the last sub-section of the **Section 4.6**, the details analysis of the projected DOS, electron polaronic and doublons quasi-particle physics are discussed on the relative stabilities of ground states. Finally, a possible conclusions and future perspective from the current research are given in **Section 5** and **Section 6**, respectively.

2. Electronic structure and properties of LMOs: Theory and experiments

The pristine orthorhombic o-LMO phase is assigned with the space group *Pbnm* (no. 62, point group D_{2h}^{16}) and a formula unit (f.u.) = 4 [61,62]; while the rhombohedral r-LMO phase belongs to the space group *R-3c* (no. 167, point group D_{3d}^{6}) with f.u. = 2 [63]. The bulk o-LMO phase shows JT-distortion of the Mn-O-Mn skeletons, where the basal-plane Mn^{3+}—$O2^{2-}$—Mn^{3+} motifs are separated by ~3.990Å and show ferro-magnetic type (FM) ME interactions. On the other side, the out-of-plane chains of the Mn^{3+}—$O1^{2-}$—Mn^{3+} is partially contracted

(separated by ~3.846Å); and *ideally* these would be anti-FM type (say, AFM) ME interactions. In r-LMO, a uniform FM-type ME interactions are viable in all crystallographic directions, with more regular square-cages of the Mn^{3+}—O^{2-}—Mn^{3+} motifs and more regular Mn-Mn distances are noted (~3.965Å in both planes). It also lacks JT-distortions within these Mn^{3+}—O^{2-}—Mn^{3+} skeletons. An accurate reproduction of the JT-distortions from first-principles calculations is challenging [35,64], while the nature and absolute value of the electronic band gap made out of the correct valence and conduction bands compositions in LMOs are also demanding. Meanwhile, it is also expected to maintain the right magnetic ground states and transport properties at the same theoretical level [65,66].

Earlier much interest was on the hole doped o-LMO in the scarcity of the pristine r-LMO bulk phase with the stoichiometric ferromagnetic $La_{1-x}A_xMnO_3$ manganites (*A* = Ca, Ba, Sr *etc*.) [67,68] and the references therein. Authors have argued on the anomalous Mn-O ordering at the lower temperature (much below to the Curie temperature, T_C) for a class of manganites (with FM ground state). The correlation with the stronger spin-phonon coupling as a result of the anomalous spin dynamical behaviour in such pseudo LMOs was proposed. In the meanwhile, the work from Qian *et al.*, 2002 also tried to unfold the temperature dependent net spin-moment measurements at the Mn-sites of $La_{1-x}A_xMnO_3$ manganites by using the novel spin-polarized *x*-ray absorption spectroscopy (XAS) – a recipe to distinguish the FM vs. AFM magnetic sites [69]. In the regime of the CMR with half-metallic nature, it was discussed from theoretical calculations [13] by considering the quantification of the Mn(3*d*)-O(2*p*) electronic-correlations in the two end members of manganites *i.e.*, $LaMnO_3$ and $CaMnO_3$. Authors had enlightened the necessity of the broken cubic symmetry of perovskites to validate the AFM ground states in manganites; and the limitation from the Zener's "double-exchange" picture at some extend for these FM half-metallic manganites for CMR [70]. The extended scenario of electron (or hole) doping concentrations in many ABO_3 type oxides was discussed in manganites by de Gennes, 1960 [71]. However, not much was highlighted on these two pristine phases of current LMOs with two crystal symmetries at the variations of JT-distortions.

Superior performance of the hybrid exchange-correlation functionals from range-separated version in the post-DFT approaches, *i.e.*, GW or hybrid functional calculations by eliminating the conventional self-interactions issues – were applied for binary oxides, quasi-2D semiconductors, and also for halide perovskites [72,73,74,75,76,77,78,79,80] or even for the current o-LMO [81,82]. Though the higher rung of exchange-correlation predicts the AFM insulating type for o-LMO but in exp. structures [83,84,85] and also, the r-LMO was not undertaken at same footing of calculations [86,87,88]. Primarily, these intrinsic properties, *i.e.*, AFM stabilization in the pristine o-LMO with JT-distortions is supposed to be inaccessible in any electronic structure theory based on the first-principles. Secondly, by using the higher-rung exchange-correlation functional in simultaneously predicting the correlated electronic structures of these two competitive bulk phases (one an insulator and another metal) simultaneously, is absolutely overlooked and not productive due to computationally expensive nature of tasks.

A broad range of Hubbard's on-site *U* terms (U_{eff}) is available in the literature to study properties of pristine or A-site doped bulk o-LMO. The U_{eff} is either determined from ad-hoc choice or from the (semi-)empirical bonded

non-bonded inter-atomic interaction choice. For example, Satpathy *et al.*, 1996 [89], had proposed a constrained LDA based determination of the U_{eff} term for hole doped La-manganites, with U = 10.1 eV on Mn(3*d*) and the exchange J value is approximately 0.90 eV. This is also according to other observations closer in agreement to the other prototype binary Mn-oxide MnO (on-site U_{Mn} = 6.9 eV); however, the known photoemission measured value U_{Mn} = 7.5 eV on Mn(3*d*) in o-LMO [90]. A critical transition from the A-type AFM to the long-range E-type AFM magnetic ordering is discussed by I. Solovyev, 2009 [91] who took into account the JT-distortions and out-of-plane ME interactions with a proposed Hubbard on-site U for Mn(3*d*) = 2.15 eV; and an exchange term J = 0.85 eV along with the non-sphericity B = 0.09 eV in case of the o-LMO.

Finally, another (semi-)empirical U_{eff} term arises from the competitive behaviour of the Mott-Hubbard vs. charge-transfer type insulating nature of the o-LMO by imposing also the Hubbard U term on the O(2*p*) orbitals along with Mn(3*d*) [92]. Hence, this type different choice is proposed herein by Gavin and Watson, 2017 [92]. Because of the existing exp. observations of the O(2*p*) orbitals closer to the Fermi level in polycrystalline o-LMO phase, and authors suggested an effective U terms, U_{eff} = 4.5 eV, and U_{eff} = 5.5 eV, respectively on Mn(3*d*) and O(2*p*) orbitals. This not only resulted a better exp. geometries and band gaps, also the charge-transfer nature of the o-LMO is produced simultaneously. Nonetheless, such an intermediate U_{eff} value was procured for the Mn(3*d*) = 4.5 eV on the exp. geometry of o-LMO and also accepted by Trimarchi & Binggeli, 2005 to better understand the pressure induced elastic properties change of o-LMO [56]. However, these studies overlooked about the correct ME terms in these LMOs. Thus, it requires a careful revisit of these issues on the understanding of complex electron-correlations in these LMOs structures with/out JT-distortions. Since, natural or synthetic single-crystalline LMOs are unlike and the role of electron doping on the magnetic ground states may assist to scrutinize the failure or/and success of the applied first-principles electronic structure calculations and its efficacy in the current manganites.

Despite the nature of the calculated electronic fundamental band gaps, E_g (Mott-Hubbard or charge-transfer insulator?) in o-LMO that was estimated from the DFT and post-DFT tools – a broad range of E_g values are available from the exp. literature. For example, to estimate the optical band gap on polycrystalline samples by the Jung *et al.*, 1997 [93] from the optical reflectivity data between 100 meV to several 10s of eV optical excitations, through Kramers-Kronig transformation. A separation of the top of valence to the bottom of conduction band was estimated from other exp. data by using the XPS (X-ray photoelectron spectroscopy) and XAS (X-ray absorption spectra) of the Mn(3*d*)-O(2*p*) orbitals ordering led to E_g = 1.1 to 1.9 eV [34,94]. In fact, authors from Park *et al.*, 1996 [34] have predicted and showed evidence of the stronger small polarons at the Fermi level on the *charge* fluctuations and resulting a metal-insulator gap transition of ~1.5 eV in class of $La_{1-x}A_xMnO_3$ manganites (A = Ca, Pb). While the valence band XPS data combined with Ultra-violet photo-electron spectra (UPS), Saitoh *et al.*, 1996 provides a value 1.7-1.9 eV [95]; and it shows reasonable agreement with the ellipsometry measurements of the dielectric function and related minimum optical band gap transition of 1.9 eV by Kovaleva *et al.*, 2004 [96]. More latest results from the Magneto-optical Kerr spectroscopy measurements on the poly-crystalline samples of $La_{1-x}Sr_xMnO_3$, provide a minimum band gap E_g ~1.5 eV for x = 0.00 [97]. So, in this context we propose to use the latest experimental data on the crystalline samples, which resulted E_g

~1.5-1.7 eV band gap in o-LMO from the known exp. measurements, while the r-LMO is a metallic (*i.e*., half-metallic) compound [12,98].

3. Theory and computational details

All first-principles density functional theory (DFT) based spin-polarized calculations are performed using plane-waves and ultrasoft pseudopotentials (USPP) for these composing elements La, Mn and O from the SSSP pseudopotential data base and implementation within the DFT package QUANTUM ESPRESSO version 6.8 (QE6.8) [99,100,101]. In these USPP valence configurations for La atom, we took 11 valence electrons [Xe]$5s^2 5p^6 5d^1 6s^2 4f^0$, 15 valence electrons for Mn atom [Ar]$3s^2 3p^6 3d^5 4s^2$, and 6 valence electrons for O atom [He]$2s^2 2p^4$. Total energy convergence 0.136×10^{-10} eV for ionic relaxations and a single-point self-consistency cycle (scf) energy convergence were ensured with a kinetic energy cut-off 120 Ry and cut-off for charge-density 700 Ry. For the structural relaxation, force convergence up to 0.257×10^{-3} eV/Å was ensured for the given conversed Monkhorst-Pack (MP) type [102] *k*-mesh $15 \times 15 \times 9$ and $11 \times 11 \times 11$, in the 1st Brillouin-zone integrations, respectively for the orthorhombic and rhombohedral unit-cells. It is worth to mention here that to design exp. known magnetic ground state AFM and FM type initial spin on the Mn sub-lattices, we took 20 (f.u. = 4) and 10 (f.u. = 2) atoms, respectively for the o-LMO and r-LMO bulk phases.

The FM order is defined as the parallel spins of all Mn(3*d*) spin-moments with a square cage-type Mn-O-Mn skeleton (see later **Fig. 1**), while the AFM of A-type is made out of the anti-parallel spins along the out-of-plane of the two FM-type Mn-O-Mn sub-lattices from in-plane layers, and finally the G-type AFM is made out of the in-plane AFM type Mn-O-Mn sub-lattices spins interact also anti-parallelly along with the 1st nearest neighbour of out-of-plane Mn-O-Mn sub-lattices of LMOs. The choice of the PBE-GGA exchange-correlation, along with effective Hubbard $U_{\text{eff}} = (U - J)$ terms on ground state search in LMOs is found to be suitable either on the pristine or strained o-LMO [42,43,103], despite its limited and clean applicability known in the present pristine and reduced LMOs.

Spin-polarized ground state density was obtained from in-built generalized gradient approximation (GGA), as formulated by Perdew-Bruke-Ernzerhof (PBE) [104] along with additional on-site Hubbard *U* and or Hubbard *U* with Hund's exchange term *J*. In some specific cases, different types on-site correction via PBE+*U* [105] with Hund's exchange *J*, and rotationally invariant approach PBE+U_{eff}+*B* [106,107] was used for ground state calculations and predicted magnetic properties, where *B* is a non-sphericity term. In all cases as available in the USPP implementations, the choice of the Hubbard projector is chosen to be Orthogonalized Atomic Orbitals (OAO) to ensure the reasonable application of the Hubbard on-site +*U* potentials on the Hubbard manifolds only once on the overlap reasons, and also found to be an important feature for the treatment such Mn-O bond strengths in such correlated oxides [58,108,112].

In the context of proposing an effective on-site Hubbard *U* from self-consistent Hubbard parameter (U_{self}) is determined in the linear response scheme [109] within density functional perturbation theory (DFPT) formalism

in the QE6.8 for the Mn(3*d*) and or O(2*p*) orbitals in bulk LMOs [110,111,112]. BFGS algorithm [113] was used for the structural relaxations (either for lattice positions or both positions and cell volume relaxations) along with theses above mentioned exchange-correlation using the Marzari-Vanderbilt (m-v) smearing technique and a broadening parameter 0.01-0.001 Ry [114]. Thus, with the virtue of the DFPT technique based self-consistent Hubbard on-site U_{eff} for Mn(3*d*) or Mn(3*d*) & O(2*p*) for LMOs are determined by using the QE6.8 Code. We have used a minimum size supercell *i.e.*, a unit-cell for the o-LMO and r-LMO structure, respectively for DFPT runs using the AFM and FM magnetic ground state with the *q*-point grid of 3×3×3 for both LMOs. This was found to be sufficient vs. $2 \times 2 \times 2$ and $4 \times 4 \times 4$ to reach convergence on the determination of the U_{self} values. The ground state density was used for DFPT runs with Gamma centred *k*-mesh with a grid size $6 \times 6 \times 3$ ($6 \times 6 \times 6$) for o-LMO (r-LMO) with m-v smearing and broadening 0.001 Ry. The effective *U*-terms which were determined from self-consistent Hubbard on-site U_{self} for the LMO phases, are shown in the **Table S1** in Supporting Information (SI). More technical details about the implementation and use can be found from Refs. [115,116,117].

For the postprocessing of the total and atom/orbital decomposed density of states (*i.e.*, DOS and pDOS), we have used tetrahedron method with energy resolution 0.01 eV and gaussian type broadening 0.01 Ry. These conditions were also preserved along with Gaussian-like broadening for the electronic bands structure calculations (bands dispersion) at the different level of the PBE+*U* exchange-correlation functionals with or without spin-orbit coupling (SOC).

In the PBE+U_{self} set-ups, the calculated ME interactions in these two periodic crystal systems o-LMO and r-LMO with 4 f.u. in super-cell was used, in either case. We have used these following equations (**Eq. 1-2**) to decouple its in-plane and out-of-plane magnetic-exchange (ME) values, $J_{\parallel}$ and $J_{\perp}$ respectively. These two unknown parameters $J_{\perp}$ and $J_{||}$ are calculated from the three known values in these crystal systems, which are the relative energies differences in A-type AFM (AFM) and G-type AFM (GFM) in their symmetry broken symmetry model vs. the total energy from the FM spin-ordering on the Mn-sites [81,118]. However, values of the nearest neighbour (NN) atoms in out-of-plane or in-the-plane direction of the origin Mn-atom are different, say *n* and *m* respectively. For example, in the o-LMO system with Mn-O-Mn square-cage model (see later **Fig. 1**), we have these following two equations from the mapping of 1st NN Mn-atoms in such periodic Mn-sub-lattices under the given space group symmetry [119,120,121],

$$\frac{1}{4}(E_{AFM} - E_{FM}) = 8 \times n \times J_{\perp} \quad \ldots\ldots\ldots \text{(Eq.1)},$$

$$\frac{1}{4}(E_{GFM} - E_{FM}) = (8 \times n \times J_{\perp} + 8 \times m \times J_{||}) \ldots\ldots\ldots\ldots\ldots\ldots \text{(Eq.2)}.$$

Here, $n = 1$, and $m = 2$, are independent sub-lattice types for out-of-plane and in-plane, respectively of the bulk LMOs host with 8*n* or 8*m* inequivalent such positions. In the left-hand side of these equations, the number 4 is the f.u. in the given supercells of LMOs. Here, *J* are expressed in meV per Mn-ions of LMOs.

All spin-polarized calculations in the present set of single/double oxygen vacancy formation energy studies, are done by using plane-wave DFT code VASP5.4.4 [122]. The core-valence treatment was done by using PAW pseudopotentials [123] for the composing elements La, Mn and O in the similar valence electrons configurations that was used in the present QE6.8 DFT code and USPP based calculations. A kinetic-energy cut-off 600 eV was sufficient for final conversed results in the VASP5.4.4 code. The full optimized (atoms and cell parameters) bulk unit-cell of the o-LMO (see main text **Table 3**) are used to create 16 (or 32) f.u., supercell of o-LMO (total 80 or 160 atoms, respectively) for the defect calculations with one/two O1 or O2 vacancies were created in the host LMOs (vacancy concentration: 1/16 = 6.25% or 1/32 = 3.12% per f.u., *i.e.*, $0.02 \leq x \leq 0.04$). The same for the r-LMO was however, 24 f.u. (total 120 atoms supercell, defect concentration: 1/24 = 4.26% per f.u. *i.e.*, $0.00 \leq x \leq 0.02$). In the formation energies estimation, spin-polarised atomic positions relaxed calculations were done within A-AFM (or FM) spin-ordered ground states for o-LMO_{3-x} (or r-LMO_{3-x}) supercell models, and a single-point FM (or AFM) ground state scf-runs was done on the last optimized structures in the actual stable ground state (see more details in the **Section S1**). Thus, in the formation energy stability checks, we preserved the same cell volume for different magnetic ordered state calculations with/out O_v vacancy models.

4. Results and Discussions

4.1 Role of ad-hoc PBE+U methods on experimental bulk phases

To initiate our discussions based on the calculated and analysed data from the currently proposed PBE+U_{self}, we review, revisit and correlate existing findings from previous ad-hoc PBE+U_{eff} calculations. As mentioned before, here choices have been proposed majorly from 3 different propositions, for example 1) the constrained LDA calculations [89] on the orthorhombic phase upon *A*-cation doping, while the other two [91,92] comes from the 2) exp. observation either as a Mott-Hubbard type [17] or 3) Charge-transfer type insulator [95] character of the bulk o-LMO. No clean proposition on the application of the on-site Hubbard *U* term for the Mn(3*d*) sites in r-LMO phase is available. Thus, results are rationalized with the known exp. data of the hole doped o-LMO compounds, concerning to the FM spin-ordering and metallic only, irrespective to the scenario of JT-distortions in LMOs [124,142]. Thus, three categories of the on-site U_{eff} parameters are viable and applied for the same o-LMO. These are now onwards called as the smaller, larger and medium on-site U_{eff} values in the current research on LMOs, respectively. The primary one from the proposition by I. Solovyev, 2009 is provided with U_{eff} = 1.3 eV on Mn(3*d*) along with Hund's exchange *J* value, and a non-sphericity *B* term (smaller) [91]. The larger *U* value comes from the Satpathy *et al.*, 1996 with U_{eff} = 9.22 eV for Mn(3*d*) electrons and also a partially different Hund's *J* exchange terms [89]. Finally, a medium U_{eff} value is proposed by Gavin & Watson, 2017 with on-site U_{eff} for both Mn(3*d*) = 4.5 eV and O(2*p*) = 5.5 eV [92]. Thus, the failure of the first-principles tools with ad-hoc *U* correction is profound with no clear proposition for the same 3*d*-electronic correlations treatment in current LMOs even with same Mn^{3+} ionic states. In the given set-ups of PBE+U_{eff}, we have

systematically applied these three U_{eff} choices on the experimental (exp.) structures of LMOs as a primary goals to benchmark our current calculations.

In **Table 1**, we have tabulated important geometries related parameters and physical properties of the exp. bulk LMOs, including the relative stabilization energies, spin-magnetic moments in the Mn and O ions. The electronic fundamental band gaps (E_g) of o-LMO as obtained from the present analysis of PBE+U_{eff} calculations, are also tabulated. The relative stability is the primary step to get into the essential magnetic ground state searching of these LMOs. Note that in the **Table 1** and later analysis, the ΔE_{FM} is defined vs. the AFM spin-magnetic ordering stability of these LMOs (say, ΔE_{FM} vs. ΔE_{AFM} = 0.0 eV per f.u.). While the positive sign of ΔE_{FM} presents the AFM type spin-ordering, the negative sign of it assigns for the FM spin-ordering preference in the current theoretical analysis.

It is quite obvious that the relative stability, ΔE_{FM} in meV per f.u. of r-LMO phase is very much robust in stabilizing the FM ground state in all applied PBE+U_{eff} choices (three), as expected for metallic character oxides with stronger FM type ME. Increasing the U_{eff} on Mn(3*d*), these ΔE_{FM} values are -349.0 meV per f.u. at U_{eff} = 1.3 eV; -616.0 meV per f.u. at U_{eff} = 4.5 eV; and -713.0 meV per f.u. at U_{eff} = 9.22 eV. Thus, the FM stability is profound with enhanced *U* correlation corrections for the current r-LMO. An enhanced FM type ME among these itinerant character Mn-3*d* electrons is thus, further enhanced with increasing U_{eff} values. In all U_{eff} set-ups, a clean half-metallic nature is also reproduced in these current calculations from the electronic bands dispersion plots which are shown in **the Figure S1-S4** of the Supporting Information (SI).

However, the situation has become more complex if we look into the o-LMO phase, where one can see that the relative stabilization energies, ΔE_{FM} are very different either in sign or in absolute value as a function of *U* corrections. More specifically, only at U_{eff} = 1.3 eV, it retains as the AFM (A-type) ground state (ΔE_{FM} = +4.0 meV/f.u.). However, a FM spin-ordering is dominating with other two choices of U_{eff} = 4.5 eV and 9.22 eV on Mn(3*d*) *i.e.*, a reverse result of magnetic ground state for o-LMO. Thus, it raises a concern of using the higher on-site *U* values on Mn-site in such JT-distorted oxides. A prime failure of the ad-hoc on-site *U* corrections in the first-principles electronic structure theory is clear now. Although, we saw an insulating nature of o-LMO in all three set-ups of U_{eff}, while it is metallic for r-LMO which also lacks JT-distortions – as a primary difference in geometrical descriptors. These phenomena in some abrupt ways are in accordance to the known exp. evidences, and discussed in earlier **Section 2**, this further demands microscopic justifications.

In fact, this smaller effective U_{eff} value (about one order less) with, U_{eff} = 1.30 eV on Mn(3*d*) was used later through the standard DFT+*U* method by Hashimoto *et al.*, 2010 [65,55] and estimated values of the out-of-plane magnetic-exchange (ME) terms of the Mn^{3+}—$O1^{2-}$—Mn^{3+}, say $J_{\perp}$ and in-plane ME, say $J_{||}$ from the Mn^{3+}—$O2^{2-}$—Mn^{3+} motifs [125,126]. Authors obtained a ratio that differed from the known experimental ratio of $J_{\perp}/J_{||}$ = -0.699 vs. -0.833 in calculations in o-LMO [96]. Indeed, this is also restricted with their choice of the exp. geometry of o-LMO, and limits predictive power of the first-principles theory. Also, in the earlier reports from the Evarestov *et al.*, 2005 [127], authors showed a wide range of these ME values in o-LMO bulk phase as a function of the different LCAO basis-sets and hybrid functionals. Here, predictions are done on the exp.

structure and none of the non-local exchange-correlations turn out to be accurate enough to reach the exp. ME values *i.e.*, $J_{\parallel}$ = +0.83 meV and $J_{\perp}$ = -0.58 meV per Mn-ions of o-LMO. To the best of our knowledge, we do not find any exp. data on such magnetic-coupling ME terms, that is measured for the pristine r-LMO phase. Except the fact that some of the proto-type FM metallic compounds with the doped o-LMO with cations Ca or Pb *etc*. which resulted a FM metallic phase. Therefore, exp. measurements provide uniform ME terms in the range, $J_{\perp} \sim J_{\parallel} \sim$ +2.198 to +2.375 meV per Mn-ion [128,129]. A positive sign indicates it as the FM type ME interaction in all directions of the pseudo r-LMO crystal. Thus, compared to the weaker FM type ordered $J_{\parallel}$ values in o-LMO (+0.83 meV per Mn-ion), the same in the pseudo r-LMO has about 2-3-fold stronger ME term in- or out-of-plane directions from these exp. observations. More details are discussed based on our calculations in the later **Section 4.5**.

Hence, the magnetic-exchange strengths along the in-plane and out-of-plane are crucial for current LMOs to predict the FM or AFM magnetic ground states – that indirectly defines the strengths of the Mn-O bonds through pure or mixed co-valency. A failure of these predictions in first-principles calculations were thus, questioned at the given PBE+U_{eff} set-ups due to inconsistent anticipation of ΔE_{FM} at the first-principles levels (see **Table 1**). Not only that, we also have noticed that the trend in the electronic band gaps E_{g} is also quite nonlinear with the increase of the U_{eff} values on Mn(3*d*), yielding E_g = 0.51 eV, 1.08 eV and 0.78 eV, respectively from smaller to larger U_{eff} choice (see also **Figure S1-S4**). It is unlike to happen for other higher-rung exchange-correlation functionals which usually show in oxides and non-oxides a linear trend [78]. Moreover, in the o-LMO an indirect E_{g} is present between the top of valence band at $U - \text{Z}$ *k*-path and the conduction band bottom at the Γ-point of the 1st Brillouin-zone (IBZ) as like other theoretical studies [130,131,132].

Table 1: Calculated stabilization energies ΔE_{FM} vs. AFM ground state as the reference set to ΔE_{AFM} = 0.0 eV per f.u.; per site spin-magnetic moments of Mn-site ($|M_{\text{Mn}}|$), O-site ($|M_{\text{O}}|$) and total spin-moment, $|M_{\text{tot}}|$ at the stable magnetic ground states and the band gap of bulk LMOs from different PBE+U_{eff} method on the exp. geometry *i.e.*, PBE+U_{eff} from I. Solovyev, 2009 [91], Gavin & Watson, 2017 [92] and Satpathy *et al.*, 1996 [89], respectively.

Parameters	**Orthorhombic LMO (o-LMO)**			**Rhombohedral LMO (r-LMO)**		
	PBE+U_{eff} (I. Solovyev. 2009)	**PBE+U_{eff} (Gavin & Watson, 2017)**	**PBE+U_{eff} (Satpathy, 1996)**	**PBE+U_{eff} (I. Solovyev. 2009)**	**PBE+U_{eff} (Gavin & Watson, 2017)**	**PBE+U_{eff} (Satpathy , 1996)**
ΔE_{AFM} in meV/f.u.	0.00	0.00	0.00	0.00	0.00	0.00
ΔE_{FM} in meV/f.u.	+4.0	-16.0	-61.0	-349.0	-616.0	-713.0

$\|M_{tot}\|$ per cell in μ_B	15.86	17.13	18.51	8.33	8.96	9.93
$\|M_{Mn}\|$ per Mn^{3+}site ($3d^4$) in μ_B	Mn = 3.16	Mn = 3.39	Mn = 3.61	Mn = 3.40	Mn = 3.64	Mn = 3.85
$\|M_O\|$ per site in μ_B	O2= 0.055	O2 = 0.010	O2= 0.092	O = 0.027	O = 0.061	O = 0.153
Band gap, E_g in eV	0.51 Indirect	1.08 Indirect	0.78 Indirect	Half-Metallic	Half-Metallic	Half-Metallic

To better explain these predictions of E_g, we have also plotted the total and atom projected electronic density of states (DOS) from the current three types of the PBE+U_{eff} methods, with smaller (I. Solovyev, 2009), medium (Gavin & Watson, 2017) and larger (Satpathy *et al.*, 1996) U_{eff} values on the Mn(3*d*) orbitals, and shown in the **Figure S5** (o-LMO) and **Figure S6** (r-LMO). Nevertheless, in both LMOs, the range of the valence band width (VBW) is also expanded linearly with increase of the U_{eff} values, which results VBW = 0.0-6.0 eV with smaller U_{eff}, shown in panel **Figure S5.a)** and gradually, it increases to 0.0-7.0 eV to 0.0-9.0 eV, respectively with the medium and larger U_{eff} values (other two DOS panels **in Figure S5.b-c**). With the applied larger U_{eff} value, the Mn(3*d*) orbitals are pushed to the bottom of the valence band (VB) – a much profound charge-transfer like nature is thus, visible due to O(2*p*)-Mn(3*d*) transitions. Since, the O(2*p*) orbitals are dominating on the top of the VB *i.e.*, closer to the Fermi level, E_F = 0.0 eV and empty Mn(3*d*) orbitals are at the bottom edge of the conduction band (CB), in particular at the larger U_{eff} set-up.

From **Figure S5**, one can also see that it is consistent with the earlier theoretical data [81]. The band gap opening at smaller and medium U_{eff} values is in between the occupied $3d$:t_{2g}^3-e_g^1 majority and empty $3d$:t_{2g}^0-e_g^0 minority orbitals, while role of the O(2*p*) states is marginal vicinity to the Fermi level, E_F = 0.0 eV (More details are discussed later in **Section 4.3-4.4**). Thus, it predicts the possible Mott-Hubbard insulating nature for the o-LMO at the lower and medium U_{eff} values in contrast to the exp. transport data [91,95]. While, in the larger U_{eff} value it turns out to be charge-transfer type, but in all these cases the underestimation of the E_g value is about 50-70% vs. exp. values 1.5-1.7 eV, along with stronger FM stability. We noted that partial improvement of E_g at the intermediate U_{eff} values, along with the on-site U term is also essential for the O(2*p*) orbitals in o-LMO.

Thus, though the medium U_{eff} corrections shows better electronic band gap, E_g estimation to 1.08 eV vs. 0.78 eV or 0.51 eV in bulk o-LMO, it is still not acceptable at this stage due to failure to show an actual AFM magnetic ground state stability and Mott-type insulator. So, the nature of the VB and CB compositions for the *Mott-Hubbard vs. charge-transfer* insulator type is very weakly interpreted. The weaker anticipation of AFM ordering in the medium U_{eff}, it is likely to showing a charge-transfer type bands structure in o-LMO which become more profound with further enlarged U_{eff} = 9.2 eV *i.e.*, a linear trend, see also **Figure S5.c**.

However, this larger U_{eff} at higher computational cost, also costs about a 50% reduction of the band gap, E_g on the exp. geometry of the o-LMO than the known exp. values and this is even worse than the medium U_{eff} set-up. In addition, an enhanced octahedral crystal-field splitting is observed with higher U values due to modifications of Mn(3*d*) and O(2*p*) orbital hybridizations. This makes the Mn(3*d*) pDOS significantly modified at the VB top edge than the lower or medium U_{eff} values (see **Figure S5**) – a major drawback of the applied DFT+*U* set-up with larger U_{eff} values, in spite of the better charge-transfer band gap type was resulted for o-LMO. However, the CB width was weakly described vs. known exp. data which is expected to be localized around the +7.0 eV energy range above the E_F = 0.0 eV level, but unable to show (**Figure S5.c**). [95].

Though, the empty Mn(3*d*):t_{2g} orbitals in o-LMO is pushed upward quite strongly even beyond the La(4*f*) orbitals at the given larger U_{eff} value, it still retains the *p-d* transition, at the cost of the weaker (semi-)covalent character of the Mn-O bonds as proposed from seminal works from Goodenough, 1951 [134]. Besides, the non-degeneracy of the O2-2*p* pDOS is also lifted with enlarged U_{eff} on the Mn(3*d*), which also results in the deposition of an extra magnetic moments on O2-sites in o-LMO (brown dashed lines in DOS plots) as shown in the **Table 1** with $|M_O|$ spin-moments. In fact, with the applied *U* on O-2*p*, it gives profound covalent character in o-LMO phase which prevails with a quenched magnetic moment on the O2-sites $|M_O| = 0.01\mu_B$ vs. 0.06-0.09 μ_B without U_{eff}, on O-2*p* orbitals. Also, while in the o-LMO phase with/out additional Hubbard *U* potential on O-2*p* mainly has affected the in-plane O-atoms (O2-site) with visible O-site dependent non-degenerate O-2*p* orbitals between the up- and down-spins (see also **Figure S5**), but it lacks in the r-LMO phase. The absence of the possible JT distortions of the host r-LMO lattice leads to lack of such O-site dependent non-degeneracy O-2*p* orbitals, which is connecting the MnO_6 octahedrons either in-plane or out-of-plane directions. Moreover, these O-sites in r-LMO, we have identical non-degeneracy in the up- and down-spin channels and restricted by the rhombohedral crystal-field symmetry and uniform orbital ordering (see also **Figure S6**).

Earlier theoretical studies in o-LMO bulk phase by Hashimoto *et al.*, 2010 provided relative stability energies at the given PBE+*U* method with U_{eff} = 14.0 eV also, on the La(4*f*) orbitals using PAW and QMAS code [65]. In their observation, this larger U_{eff} on La(4*f*) orbitals provides right AFM magnetic stability of o-LMO, but neither we known how it will affect the relative stability of r-LMO nor the origin of band gap E_g opening and band compositions were disclosed.

Similarly, looking at **Figure S6** (see also bands dispersion in **Figure S4**), one can clearly note that the half-metallic nature of the bulk r-LMO phase is preserved. This also has analogous *p-d* orbital hybridization on the occupied up-spin (majority) channel than o-LMO, but the pseudo band gap is opened only in between the down-spin (minority) channels. This half-metallic pseudo band gap from down-spins (minority channels) is increased with the applied effective U_{eff} values on the Mn(3*d*), and this is consistent also with the enhanced FM relative stabilization energies discussed just before (see also **Table 1**). The trend can be explained from Zener's double-exchange (DE) mechanisms [70].

Thus, the available ME interactions become more profound and uniform FM-type in all directions in r-LMO from DE mechanism with atom-like O-2*p* ground state situation but, absent in the o-LMO. The linear dependence of O-2*p* spin-moments, $|M_O|$ in the r-LMO does not hold tightly whether additional *U* is applied on

the O(2*p*) orbitals or not. The estimated values are in the range 0.03-0.15 μ_B per O-site, a linear dependency is noted with applied on-site *U*. In r-LMO phase, the minority pseudo band gap E_g in the down-spin channel is no longer due to Mn(3*d*) and O(2*p*) transitions, but from O-2*p* to empty La-4*f* orbitals.

It is worth to mentioning hereafter that the nature of the $Mn^{3+}(3d^4)$ spin-moments ($|M_{Mn}|$) with four unpaired electrons in Mn-3*d*:t_{2g}^3-e_g^1 occupancies in LMOs, are also showing linear dependence with the applied on-site Hubbard *U* on Mn(3*d*). In spite of the choice of additional presence of the on-site U_{eff} term on O(2*p*), it retains same either in o-LMO and r-LMO (see also **Table 1**). Here, the calculated total magnetic moment per Mn^{3+} sites is $|M_{Mn}|$ = 3.16, 3.39 and 3.61μ_B in o-LMO (or 3.40, 3.64, 3.85μ_B for r-LMO), respectively, at the given smaller, medium and larger U_{eff} values. This is an exact increase of about 10-15% on Mn(3*d*) spin-moments and reasonable compared to the known exp. values in the bulk o-LMO, exp. $|M_{Mn}|$ = 3.87μ_B on the polycrystalline samples [34] or 2.9μ_B in another Ba-doped o-LMO polycrystalline samples within the FM ground state – a pseudo r-LMO model [133].

No exp. data of the measured $|M_{Mn}|$ is thus, clearly known for pristine r-LMO phase, and our predictions from first-principles cannot be directly compared. We expected that in an ideal valence band $Mn^{3+}(3d^4)$ occupancies in r-LMO phase with 4 unpaired electrons, it would be assigned by maximum spin-moments per Mn-site, $|M_{Mn}|$ = 4.0μ_B. We stress that based on the earlier predictions by Goodenough, 1951 [134], due to flatter <Mn-O-Mn angles (in-the-plane and out-of-plane) in r-LMO phase than the o-LMO, it plays an important role in stabilizing the FM ground state with half-metallic nature – a competition of covalent and/or semi-covalent like Mn-O bonds with competitive super-exchange (SE) and DE type interactions. Thus, we would discuss in the next impacts of the cell volume and atomic positions relaxations on geometries and these physical properties of LMOs.

4.2 Role of ad-hoc PBE+U on full-optimized LMO structures

In order to better understand such reverse scenario *i.e.*, a weaker AFM magnetic ground state stability (ΔE_{FM} = +4.0 meV per f.u.) and insulating type o-LMO determined by only at lower U_{eff} value, we undertook few checks. On the other hand, a FM ground state ordering (ΔE_{FM} = -349 meV per f.u.) with a half-metallic nature is very robust in r-LMO, and the trend is irrespective to all U_{eff} values. So, we further explore the effect of *J* and *B* terms to decouple the choice of PBE+U_{eff} set-up (lower U_{eff} value model) as proposed by I. Solovyev, 2009 [91] formalism using the higher and medium U_{eff} set-up of PBE+*U* calculations. Thus, it is crucial now to know the nature of the electronic band's hybridization and widths in the pseudo ground states with FM and AFM ordering in o-LMO and r-LMO phase, respectively. The associated pDOS are shown in **Figure S7** and **Figure S8**. It is very much remarkable from these DOS figures that the o-LMO within FM ordering shows a half-metallic nature while, the r-LMO in AFM ordering is likely to be an insulator with clean VB splitting between O(2*p*)-Mn(3*d*) orbitals. Results are summarized in the **Table S2**, in similar analogy to the main text **Table 1**. The AFM ground state of the r-LMO 3*d*-metal oxide without JT-distortion is unphysical due to an artefact from pDOS peak at the Fermi level, E_F = 0 eV, and not solvable in first-principles electronic structure theory. A detail of *U* and *J*

dependence of the relative stabilities and magnetic phase diagram of o-LMO can be found in Ref. [52], which highlights the role of CDFT+*U* vs. SDFT+*U* set-up on the difference of magnetic ground states and *U* correlation on Mn-sites. This clearly indicated the proposed U set-up in I. Solovyev, 2009 is definitely low and not recommended in the first-principles predictions of structure-properties in LMOs.

As similar to **Table 1**, ΔE_{AFM} = 0.0 eV is taken as the reference for relative ground state stability. More specifically, the estimated ΔE_{FM} per f.u. of LMOs, now systematically sheds light on choice free technical aspects in these current DFT+*U* calculations, and best elucidated in the current study [135]. As mentioned before, the current lower U_{eff} method (I. Solovyev, 2009) is based on the rotationally invariant approach, so called PBE+U_{eff} +*B* [106,107] with *U* = 2.15 eV, Hund's exchange term *J* = 0.85 eV and non-sphericity term *B* = 0.09 eV [91]. We have also, not seen any such major changes in the trend of the stabilization energies of these bulk LMOs either from the PBE+U_{eff} or PBEsol+U_{eff} approaches [136,137]. Thus, in the PBE+*U* set-up, we decided to plug-in additional features of the exchange *J* and non-sphericity term B along with the on-site effective Hubbard *U* terms. Next, we approach with PBE+U_{eff}+B with two sets of calculations. Let's say that in one case, U_1(Mn) = 4.5 eV and in other one U_2(Mn) = 9.22 eV are plugged in the similar footing with U_{eff} values from Gavin & Watson, 2017 and Satpathy *et al.*, 1996.

We noticed that such a choice in the lower bound of U_{eff} from I. Solovyev, 2009 set-up and integrating into the PBE+U_1 or PBE+U_2 methods, for example, Hund's *J* and *B* term on the atomic position relaxations of LMOs, makes the electronic structures predictions worse. First, we noticed that the change in relative stability from calculated ΔE_{FM} are not remarkably different in either choice of U_1 and U_2. The estimated ΔE_{FM} = -17.0 meV and -61.0 meV per f.u., respectively at U_1 and U_2 set-ups, in o-LMO exp. structures, thus FM stability is still profound. Thus, these makes the o-LMO phase energetically more disfavoured as an AFM insulator, as we previously noticed without the Hund's exchange *J* and non-sphericity *B* term [138]. Though the trend of the band-edge compositions from these pDOS plots differed by minor for the medium U_1 = 4.5 eV, but it appears that there is an enhance *p-d* hybridization (more covalence). This is accompanied by the quenched $|M_O|$ moments and a partially reduced E_g for o-LMO compared to the lower U_{eff} = 2.15 eV (**Figure S9.a**).

Similarly, in the other r-LMO case within the higher on-site correlations U_1 and U_2 set-ups led to the more likely a *p-d* transitions around Fermi level but still maintain the half-metallic nature (see **Figure S10**). Thus, the lack of the JT-distortions would be one of the viable geometry aspects that causes the r-LMO likely to be insulator nature in the AFM spin ordering, while the same actually makes it fit to be a half-metallic in FM spin ordering. This possibly is guided by the Zener's double-exchange (DE) due to non-local itinerant Mn(3*d*) electrons across the FM vs. AFM spin-ordering [70]. A competition of SE and DE is now becoming a guiding factor of the transport character of these LMOs. Though the opening of E_g out of the electronic transitions at IBZ (1st Irreducible Brillouin zone) high-symmetry *k*-points remain similar from bands dispersion analysis, and this is insensitive to larger U_2 vs. the partially smaller U_1 with the same set-up of *J* and *B* terms **(**see **Figure S11**). In fact, once this additional Hund's *J* and *B* terms were introduced in the PBE+U_{eff} +*B* set-ups, it also contributes to the reduction of the E_g of o-LMO phase from 1.08 eV to 0.81 eV (*i.e.*, worsening of the situation) by approximately 25% reduction, see also **Table S2**.

Finally, positions optimization of all lattices within PBE+U_1 set-up does change the electronic structures marginally, but not the magnetic ground state stability trend. However, it enhances the absolute ΔE_{FM} values by about 4-8 (1-2) times in case of o-LMO (r-LMO), and shown in the parentheses of the first two columns of **Table S2**. Indeed, due to the lattice positions relaxation a reverse ground state stability is resulted (*i.e.*, ΔE_{FM} = +4.0 meV in exp. structure vs. -33.0 meV in relax structure per f.u.) within the current test using PBE+U_1 as compared to the PBE+U_{eff} set-up from I. Solovyev, 2009. More specifically, the FM ground state turns out to be the most stable even in the o-LMO phase vs. AFM spin-ordering, while the r-LMO remains intact to the FM ground state without much change of the absolute value before or after the atomic positions relaxed calculations in PBE+U_1 set-up. The relaxation caused also stronger reduction of E_g ~0.51 eV from exp. structure vs. 0.40 eV while relaxed the bulk structure from PBE+U_{eff} set-up of I. Solovyev, 2009 in o-LMO. Finally, from the unfavoured impacts of PBE+U_{eff}, we observed less important changes on bands dispersion plot of o-LMO vs. only atomic positions relaxed geometry (see **Figure S12**). In fact, this reduction of the E_g became more prominent while atoms were allowed to relax vs. the exp. structure if one uses the PBE+U_1 set-up in o-LMO (*i.e.*, two-fold increase of U_{eff}). We saw E_g is reduced from 0.81 eV to 0.56 eV (31.0% reduction) in the same o-LMO from PBE+U_1 set-up and also true for PBE+U_{eff} proposition of I. Solovyev, 2009 (see **Figure S13**).

In the same set-ups of PBE+$U_{1,2}$ the half-metallic nature of the r-LMO remains same even after atomic positions relaxation, with an expansion of the minority spin-channels pseudo gap, which is enlarged from 3.2 to 4.8 eV (see **Figure S14**). Finally, we also noticed enhanced $|M_O|$ spin-moments in the r-LMO phase with the plug-in of the J and B terms in the PBE+U_1 set-up, resulting more O(2p) density on the top of the valence band (see also **Table S2**). Similar analysis with PBE+U_2, seems to provide same conclusions, and thus less important herein due to such unfavourable and unimportant impacts in these LMOs and not reported herein.

Thus, JT-distortions in LMOs is unlike to be the prime source of modulating the insulating (or the transport) character but crucial to assigning of magnetic ground states *i.e.*, FM or AFM ordered exchange types. This eventually explains the need for proper electronic-correlations treatment in current La-manganites, in particular for the electronic structure descriptions. So, the correct estimation of the non-local or dynamical electronic correlations in these LMO is extremely vital. Though these PBE+$U_{1,2}$ methods were not fruitful at all, we found this is an important task to revisit the role of Hund's J and non-sphericity B terms. Thus, the geometry changes due to full relaxation of the host LMOs including volume changes, the Mn-O bond lengths and Mn-O-Mn angles, while systematic impacts on the properties and relative energetics are also noted. This will allow us to decouple the local and non-local strong correlations and/or itinerant character of Mn(3d) electrons which will be discussed in the later sub-sections. The comparisons are done with the proposition of PBE+U_{eff} from Gavin & Watson, 2017 with applied U_{eff} values Mn(3d) = 4.5 eV and O(2p) = 5.5 eV which is better and reasonable than the PBE+U_1 set-up [92].

Geometry of oxide crystals are described in principle, from the lattice vectors and local metal and non-metal polyhedral distortions with the virtue of the electronic correlation effects as the nature's glue. Thus, important changes around the MnO_6 octahedrons in the LMOs crystals are observed after the full relaxed (Full-Optm.) calculations. Here, the lattice parameters are expanded by less than 1.0% for the o-LMO, while unit-cell

parameters remain unchanged in r-LMO upon Full-Optm. lattice relaxations. The in-plane $(Mn\text{-}Mn)_{\perp}$ and out-of-plane $(Mn\text{-}Mn)_{\parallel}$ distances vs. the *c*-axis of the unit-cell are also noted, and the associate effects on the Mn-O-Mn angles in the analogous planes of the MnO_6-octahedrons of LMOs are tabulated in the **Table 2**. The calculated in-plane $(Mn\text{-}Mn)_{\parallel}$ distance after Full-Optm., is changed by less than 0.1 Å (+2.0%) in the o-LMO, and unaffected for the r-LMO. However, other out-of-plane $(Mn\text{-}Mn)_{\perp}$ distance shows no visible changes in all case. This indeed affects the Mn-O-Mn angles mostly in the o-LMO phase, but absent in r-LMO phase.

A schematic view of the square-cage like Mn-O-Mn sub-lattices are shown in the **Fig. 1** for o-LMO in panel **a)** and r-LMO in panel **c)**, where La-sublattices are hidden for simplicity in these top panels. We can clearly see that there is a distinct rotation of the MnO_6 octahedral axis vs. *c*-axis by 90° in the basal plane of o-LMO without any gliding angles in the adjacent MnO_6-layers belong to the top and bottom sides of the 1st NN layers, and shown in panels **b-d)**. However, in the r-LMO phase, it shows a marginal gliding angles at alternate basal-plane MnO_6-layers. Thus, a clean presence of the JT-distortions is visible for o-LMO but not in r-LMO due to simultaneous clockwise and anti-clockwise rotations of the MnO_6 motifs in the former case. The La-sites are also displaced in the adjacent top-bottom basal layers in o-LMO due to JT-distortions, while these are in a uniform overlapped along a line in the r-LMO.

Now, looking more carefully to the relative stabilization energies, in the **Table2** for o-LMO phase (ΔE_{FM} ~20-40 meV per f.u.), which is twice of an order in magnitude less as compared to the r-LMO (ΔE_{FM} ~629 meV per f.u.) and also its origin yet to explore. In o-LMO atomic positions relaxation caused the ΔE_{FM} to expand double with -Ve sign (*i.e.*, towards the FM ground state), while the full relaxation let it back to the opposite ground state stabilization energies *i.e.*, AFM ordered (but still FM type). This could be due to the competitive changes in both, Mn-O bond-lengths and <Mn-O-Mn angles, mediated via JT-distortion phenomena in o-LMO. More specifically, the <Mn-O-Mn angle is reduced about 3.0° (more buckled) while optimized with atomic positions only, and reduced further additionally by 2.0° while fully relaxed *i.e.*, total of ~5-6° reduction and maintained by the JT-distortions strictly. Such angles changes are almost invisible and/or absent in case of the r-LMO, which thus holds a same relative stabilities and half-metallic character before and after the full relaxations (Full-Optm.). The 1st step angle changes in o-LMO might have influenced the ΔE_{FM} values that can be due the deviation from GK-rules for 180° angles as compared to the ideal super-exchange mechanism in a cubic ABO_3 perovskites.

Table 2: Calculated geometry, stabilization energies ΔE_{FM} vs. AFM ground state, per site spin-magnetic moments Mn^{3+} site ($|M_{Mn}|$), oxygen-site ($|M_O|$) and total spin-moment, $|M_{tot}|$ and band gap, E_g in the AFM and FM ground states of the respective o-LMO and r-LMO phases on exp. geometry or atomic positions relaxed (atom relaxed) or full-relaxed structure (Full-Optm.) using PBE+U_{eff} exchange-correlation functional in DFT. Applied U_{eff} values for Mn(3*d*) = 4.5 eV and O(2*p*) = 5.5 eV [92].

Parameters	**o-LMO**	**r-LMO**

	PBE+U_{eff} (exp.)	**PBE+U_{eff} (Position-Optm.)**	**PBE+U_{eff} (Full-Optm.)**	**PBE+U_{eff} (exp.)**	**PBE+U_{eff} (Position-Optm.)**	**PBE+U_{eff} (Full-Optm.)**
Lattice Parameters	*a* = 5.537Å; *b* = 5.747Å; *c* = 7.693Å; α=β=γ= 90°	*a* = 5.537Å; *b* = 5.747Å; *c* = 7.693Å; α=β=γ= 90°	*a* = 5.584Å; *b* = 5.958Å; *c* =7.703Å; α=β=γ= 90°	*a* = 5.564Å; *b* = 5.564Å; *c* = 5.564Å; α=β=γ= 61.04°	*a* = 5.564Å; *b* = 5.564Å; c = 5.564Å; α=β=γ= 61.04°	*a* = 5.564Å; *b* = 5.564Å; *c* = 5.564Å; α=β=γ= 60.98°
Mn-O bond-lengths (Å)	Mn-O1: 2×1.968; Mn-O2 = 2×1.906; 2×2.180;	Mn-O1: 2×1.980; Mn-O2 = 2×1.933; 2×2.167;	Mn-O1: 2×1.991; Mn-O2 = 2×1.943; 2×2.272;	Mn-O = 6×2.026;	Mn-O = 6×2.025;	Mn-O = 6×2.024;
Mn-Mn distance (Å)	$(Mn\text{-}Mn)_{\perp}$ = 3.846 Å $(Mn\text{-}Mn)_{\parallel}$ = 3.990 Å	$(Mn\text{-}Mn)_{\perp}$ = 3.846 Å $(Mn\text{-}Mn)_{\parallel}$ = 3.990 Å	$(Mn\text{-}Mn)_{\perp}$ = 3.851 Å $(Mn\text{-}Mn)_{\parallel}$ = 4.083 Å	$(Mn\text{-}Mn)_{\perp}$= $(Mn\text{-}Mn)_{\parallel}$ = 3.965 Å	$(Mn\text{-}Mn)_{\perp}$= $(Mn\text{-}Mn)_{\parallel}$ = 3.965 Å	$(Mn\text{-}Mn)_{\perp}$= $(Mn\text{-}Mn)_{\parallel}$ = 3.964 Å
<Mn-O1-Mn / <Mn-O2-Mn (°)	155.4°/155.1°	152.5°/153.4°	150.6°/151.1°	156.3°/156.3°	156.4°/156.4°	156.5°/156.5°
ΔE_{AFM} in meV/f.u.	0.00	0.00	0.00	0.00	0.00	0.00
ΔE_{FM} in meV/f.u.	-20.0	-42.0	-20.0	-629.0	-628.0	-629.0
$\lvert M_{tot}\rvert$ per cell in μ_B	16.95	17.10	17.30	8.99	8.99	8.99
$\lvert M_{Mn}\rvert$ per Mn^{3+} site ($3d^4$) in μ_B	Mn = 3.41	Mn = 3.46	Mn = 3.48	Mn = 3.65	Mn = 3.65	Mn = 3.65
$\lvert M_O\rvert$ per O-site in μ_B	O2 = 0.016	O2 = 0.024	O2 = 0.029	O = 0.064	O = 0.064	O = 0.064
Band gap, E_g in eV	1.06 Indirect	0.90 Indirect	1.21 Indirect	Half-metallic	Half-metallic	Half-metallic

Since, we know that the sub-lattice of Mn^{3+}—O^{2-}—Mn^{3+} forms a square-cage like arrangement through the O^{2-}-ions with angles <Mn-O-Mn ~150°, the super-exchange mechanism is unavoidable. This eventually show FM type magnetic exchange due to the less than half-filled Mn-3*d* orbitals of the $Mn^{3+}(3d^4)$ ions in the Mn^{3+}—O^{2-}—Mn^{3+} chains. In o-LMO, in-plane and out-of-plane angles <Mn-O-Mn are buckled by ∼5°-6° as result of such MnO_6 octahedral deformation from Full-Optm., which remains off in the r-LMO with an absolute value about <Mn-O-Mn = 156.0°. Thus, though the buckling of angle <Mn-O-Mn has a larger deviation (∼30°-35°) from the ideal angle <Mn-O-Mn = 180° in an ideal cubic perovskites, a less than half-filled Mn^{3+} ions in these Mn^{3+}—O^{2-}—Mn^{3+} motifs would favour the FM type SE interactions as proposed also earlier by the Goodenough-Kanamori (GK) rules [134]. This tells a weak but still positive sign Mn^{3+}—O^{2-}—Mn^{3+} interactions and thus, prevails FM insulating ordering in La-manganites o-LMO, irrespective to the quality or quantity of the exchange-correlation in the first-principles calculations or electronic structure theory, in principle.

Thus, the actual sign of the ME in the Mn-O-Mn chain must be weaker/stronger +Ve (FM-type) depending on the spin aligning direction lines out-of-plane/in-plane, respectively of the super-exchange mechanism in the given $3d^4$-$3d^4$ occupancies with or without JT-effects in LMOs [33]. However, this FM ordered ME energies (or in terms of relative energy) is about an order of magnitude larger in the r-LMO phase than the o-LMO due to stiffer Mn-O-Mn angles. Thus, the origin of one order higher relative stability might be explained from the basal-plane angles change of <Mn-O2-Mn by ∼5°-6° (*i.e.*, 150° vs. 156°) in the final full-optimized structures of o-LMO. More alternately impacts from the buckled Mn-O-Mn skeletons in the o-LMO vs. the flatter and uniform in r-LMO is now visible. In the **Fig. 2.a-f)**, we have shown the respective electronic atom/orbital projected DOS of these two phases to better understand the geometry induced electronic structure and associated relative stabilities. Due to the lattice position relaxations, we had 18.0% reduction of the band gap, E_g in o-LMO, but it increases approximately by 14.0% while doing Full-Optm. cell volume in comparisons to the exp. bulk lattice, see **Fig. 2.a**). However, no visible changes in the half-metallic character of the r-LMO is found, see **Fig. 2.d-f**). In the pDOS, the trends of valence bands composition in the r-LMO remains unchanged regardless to the different type of relaxations starting from exp. bulk structure and a clean 3*d*-orbitals are dominating around the Fermi-level, and yielding a half-occupied spin-channels, across the E_F = 0.0 eV in r-LMO. Despite the accuracy of the absolute E_g in o-LMO or half-metallicity of r-LMO as estimated from the present PBE+U_{eff} set-up (Gavin & Watson, 2017 [92]), the nature of valence bands composition around the Fermi level is profound across these LMOs made with Mn-3*d* orbitals. A competition of the DE and SE mechanisms is yet unclear from this analysis.

At the room temperature even 10.0-15.0% JT-distortion pointing along the longer-shorter bonds of Mn^{3+}—$O2^{2-}$—Mn^{3+} sub-lattices, makes the Mn-3*d* orbital-ordering (OO) more complicated. Hence the degeneracy of the Mn(3*d*) manifolds shows anomalous OO in the t_{2g} and e_g orbitals occupancies and transition temperatures, T_{KK} = 550 K vs. T_{JT} = 1150 K across the orthorhombic to tetragonal modulated via JT-distortions, in particular for o-LMO [139,140].

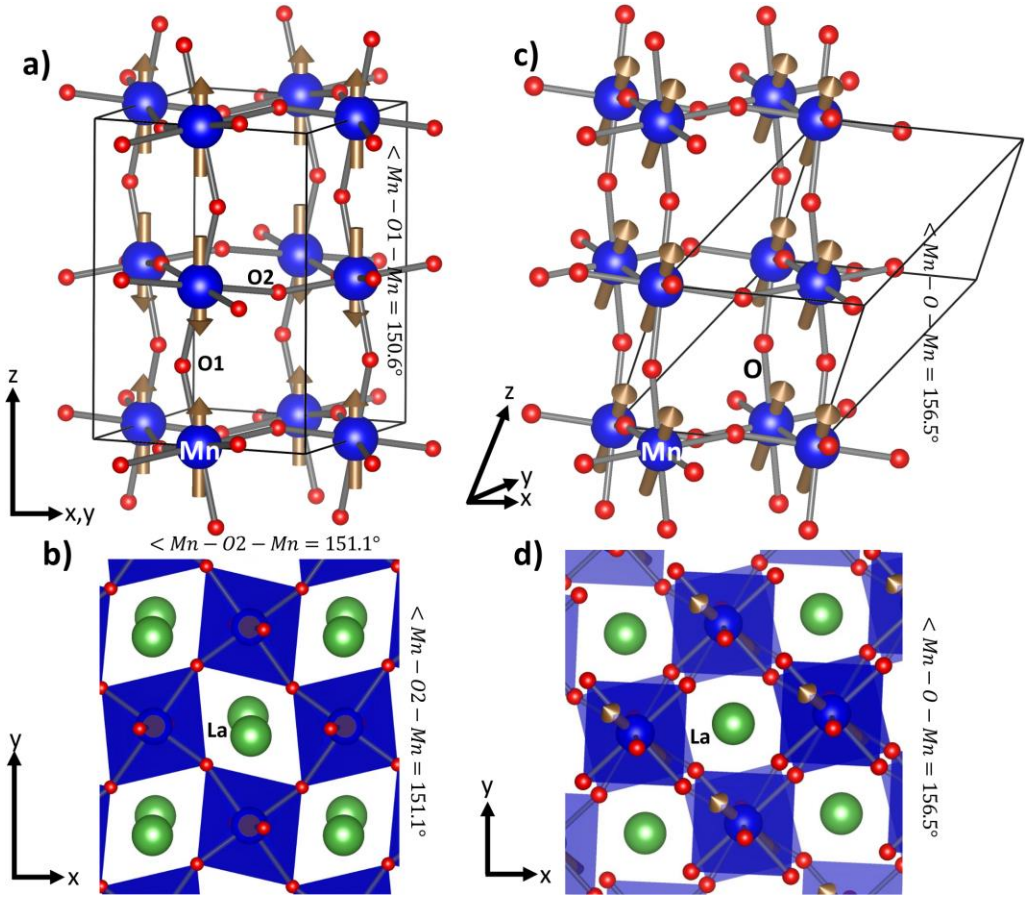

Fig. 1: A schematic view of the square Mn-O-Mn sub-lattices connected through O^{2-} anions (truncated after 3-layers of Mn-Mn plane, while La atoms are hidden) with A-AFM type magnetic ordering (fat arrows) for o-LMO **a-b)**, and FM type for r-LMO crystals **c-d)** in side/top views at upper/lower panels, respectively. The Mn-atoms (Mn) are marked with larger blue solid balls and O-atoms (O1/O2 or O) in smaller red solid balls. In both cases, ideal orthorhombic or rhombohedral unit-cell is marked with solid black line box, containing 4 formula-units (f.u.). Mn-O-Mn angles are also labelled in the Full-Optm. unit-cell in both cases in-plane and out-of-plane, see also **Table 2**.

It was earlier predicted that the presence of such cooperative JT-distortions along with simultaneously change of the basal-plane and out-of-plane MnO_6-octahedral distortion parameters Q_2 and Q_3, respectively resulted more complicated two types of OO induced E_g opening in o-LMO phase in the given AFM magnetic ground states [141,142,143]. This is one of the guiding factors to E_g opening and support the Mott-insulator like nature of the o-LMO, see **Fig. 2.b-c)** which must disobey the FM ordering from the first-principles calculations (see **Table 2**). Indeed, this is also in contrast to the exp. spectroscopic measurement reporting charge-transfer type insulating character of the same o-LMO phase [142,144]. Thus, the predictive power of the current first-principles calculation with the Gavin & Watson, 2017 proposition is deteriorated, as soon as we perform the Full-Optm. the bulk crystal of LMOs.

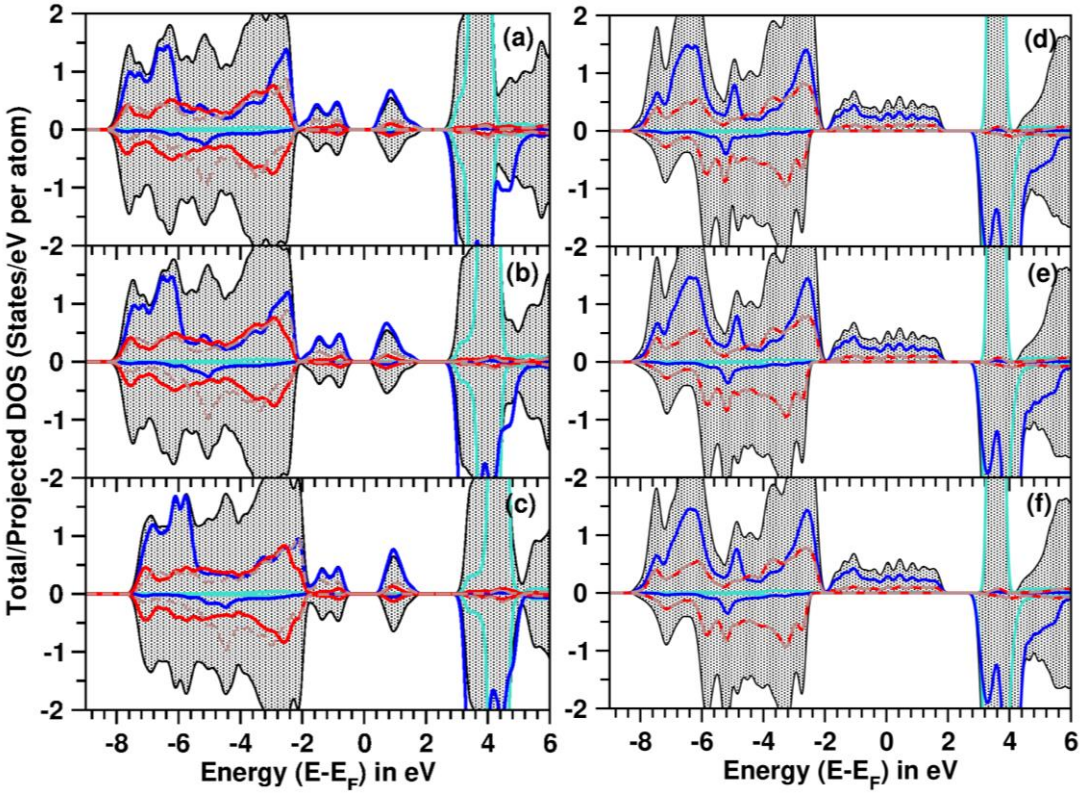

Fig. 2: Calculated atom/orbital projected electronic density of states (pDOS) per eV per atom of o-LMO phase in the AFM ground state using exp. structure panel **a)**, on the atomic position relaxed structure **b)**, and on the Full-Optm. (atomic positions and volume relaxed) structure **c)**. Similarly, pDOS for the r-LMO phase in the FM ground state are shown in panels **d-f**), respectively. Total DOS and pDOS are presented with black shaded area, total La(4*f*) are presented with cyan thick lines, total Mn(3*d*) are shown with blue thick lines, while O(2*p*) orbitals of O1 (out-of-plane) and O2 (in-plane) are marked with red and dashed brown lines, respectively in all plots. In all cases Fermi level, E_F is set to zero energy scale.

Thus, the exp. known dynamical (non-local) itinerant character of these Mn(3*d*) electrons in the r-LMO is a viable observation, irrespective to the PBE+U_{eff} calculations on exp. cell or position relaxed or even in full-relaxed unit-cells. This eventually tells that the choice of the Gavin & Watson, 2017 is an abruptly a reasonable choice for r-LMO, hence, we quested about the transferability of the current PBE+U_{eff} set-up for the class of 3*d*-metal oxides. This is also in a way, *anti-correlated* to the observed relative stabilization energies as well. Statistically an enhanced (deterioration) ΔE_{FM} value makes the o-LMO phase more likely metallic (reduced band gap) type, *i.e.*, *anti-correlation*, and the unchanged order of the ΔE_{FM} in the r-LMO phase does not leave the half-metallic type, say the *correlation* trend. These tasks will be undertaken in the next sub-sections of results and discussions **Sections 4.5-4.6**, at the limit of the various Mn-3*d* occupancies models of $3d^5$-$3d^5$, $3d^5$-$3d^4$ and $3d^4$-$3d^4$ and hypotheses of orbital overlapping symmetries [33]. Now, the OO at the given set-up of PBE+U_{eff}, in particular effects from two different types of electronic correlations (dynamical or non-dynamical) in the Mn^{3+}($3d^4$) ions in two LMOs are explored, next.

4.3 Mn(3d) electron-correlations: Role of ad-hoc PBE+U_{eff} method

Simultaneous change of the basal-plane <Mn-O2-Mn angles vs. *c*-axis affected the JT-distortions in o-LMO which results reversal of sign and absolute values of the relative stability by manipulating the SE and DE terms. However, in r-LMO phase no such change is observed followed by a constant $|M_O|$ magnetic moments per oxygen sub-lattices, thus more uniform itinerant Mn-3*d* electronic correlation. Here, JT-distortions induces a monotonous change on the OO in Mn-3*d* orbitals and its hybridization with O2-2*p* (a non-degenerate type), which can be seen in the orbital projected DOS plots in the **Fig. 3**. Here, we show the 3*d*-orbital decomposed DOS of these Mn-sites of o-LMO in **Fig.3.a)** and for r-LMO in **Fig.3.b)**.

From our present calculations, major occupied Mn($3d^4$) orbitals in the VB is extended up to 0.0-7.8 eV energy range below the Fermi level, $E_F = 0$ eV. One majority Mn(3*d*):e_g state at the top of VB at 0.0 to -1.0 eV, is just below the E_F, followed by three Mn(3*d*):t_{2g} occupied orbitals at -1.0 eV to -1.5 eV range, similar to the earlier study [144]. In the higher energies CB, couple of empty majority orbitals are located at +1.0 eV to +2.0 eV from Mn(3*d*):e_g and Mn(3*d*):t_{2g} orbitals; and finally three empty minority levels are at +5.0 eV, +6.5 eV and +7.0 eV, respectively from Mn(3*d*):e_g, Mn(3*d*):t_{2g} and Mn(3*d*):e_g orbitals. In the r-LMO case, we found similar e_g-character dominates the top of VB with a tail extended across the Fermi-level, $E_F = 0.0$ eV from the other t_{2g}-characters of Mn(3*d*), see **Fig. 3.b)**. The pDOS are more degenerate in r-LMO than the o-LMO. Thus, the OO in Mn(3*d*) is much irregular and different than the known exp. measured trends, in particular for the o-LMO [141,142]. This is also corroborated with the underestimation of the E_g (1.2 eV calculated vs. 1.5-1.7 eV in exp. data) in the o-LMO phase, due to uncertainty of OO in Mn(3*d*)-O(2*p*) hybridizations and overlapping [94,95]. Unfortunately, no such comparative exp. photoemission or absorption spectra analysis of the occupied and unoccupied bands of the pristine r-LMO is known.

A systematic connection is found also with the JT-distortion via <Mn-O2-Mn angles, which is expanded marginally to 156° in r-LMO vs. 151° in o-LMO (see also **Fig. 1**), comparing with the relative Mn(3*d*) orbital-ordering and positions. In spite of the similar order of the buckling angle <Mn-O2-Mn change by 30-35° from the ideal cubic lattice, the trend of the Mn-3*d* band gap opening is markedly different in these two LMOs. Overall impacts from the crystal-field splitting of the Mn(3*d*) orbitals is found to the OO at the -2.0 eV energy range from the E_F level. This also results an energy level locations Mn(3*d*):t_{2g} < Mn(3*d*):e_g in the r-LMO, because of the more stiffer and regular MnO_6 octahedrons (see also **Fig. 3.b**). Hence, a mixture of the multiple linearly dispersed majority bands from Mn(3*d*):(t_{2g}+ e_g) electrons around the Fermi level, $E_F = 0.0$ eV could be source to the half-metallic nature of r-LMO, with peculiar spin- and orbital-ordering. Indeed, we noticed that multiple Dirac-cones like features in majority spin-channel are present with a splitting about few tens of meV between the valence band (highest occupied) and conduction band (lowest unoccupied) edges in this r-LMO phase (see **Figure S14-S15**).

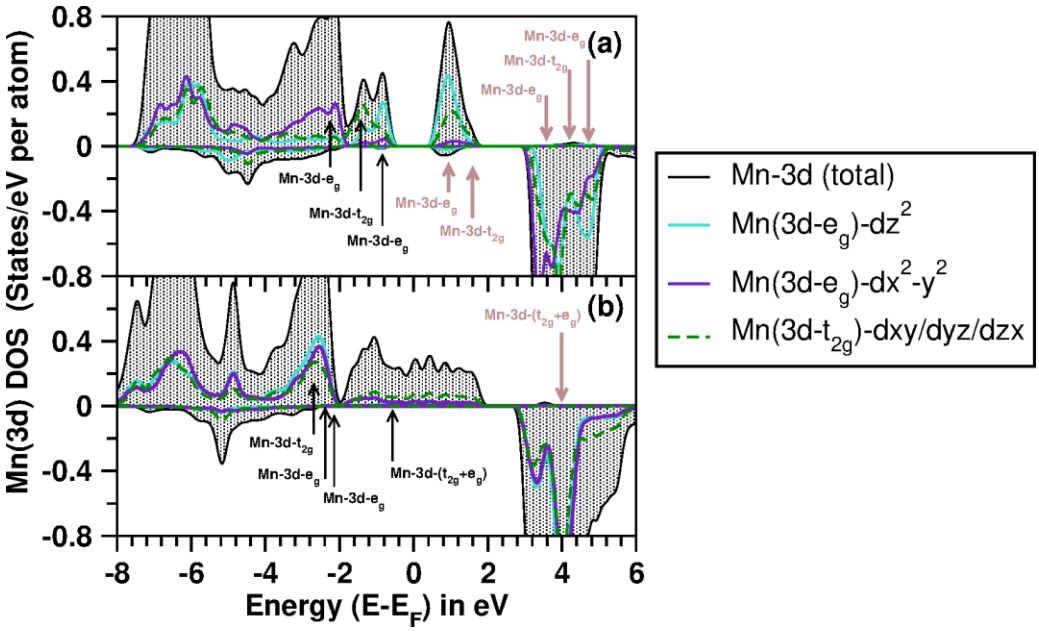

Fig. 3: Calculated Mn(3*d*) orbitals projected density of states per eV per atom of o-LMO bulk crystal in panel **a)**, and for r-LMO in panel **b)**, on the full-optimized (atomic positions and volume relaxed) structures using PBE+U_{eff} exchange-correlation. Applied U_{eff} values for Mn(3*d*) = 4.5 eV and O(2*p*) = 5.5 eV [92]. Different 3*d*-manifolds are labelled (marked with arrows) with colour solid or dashed lines, while the total Mn(3*d*) is shown with the black shaded area in each plot. In both panels Fermi level, E_F = 0.0 eV is set.

Finally, we see overall trend of the OO in Mn(3*d*) is less reasonable in the current PBE+U_{eff} set-up upon the full optimized LMOs bulk crystals. In addition, empty minority levels are actually accumulated around the 4.0-5.0 eV above Fermi level (E_F) for either LMOs, which is unlike in an exp. spectroscopic data (see next sections). Indeed, this is underestimated in energy scale as compared to the known exp. range 5.0-7.5 eV above the E_F = 0 eV level [95].

The net spin-magnetic moments on the Mn(3*d*) orbitals are also correlated with the calculated 3*d*-orbiral's eigen-values *i.e.*, 3*d*-orbital occupancies from current PBE+U_{eff} calculations and these are summarized in the **Table S3**. Here, the calculated spin-magnetic moments ($|M_{Mn}|$) are 3.5μ_B and 3.7μ_B in the respective o-LMO and r-LMO phase are due to identical Mn(3d^4) occupancies. This $|M_{Mn}|$ is integrated over the atomic sphere radii of these Mn^{3+} ions in these LMOs. From this table, relatively more localized electrons in one of the Mn(3dz^2):e_g orbital (up/down occupancies = 0.840/0.086 in r-LMO vs. 0.640/0.083 in o-LMO), results an enhanced absolute spin-moments $|M_{Mn}|$ in the r-LMO phase vs. o-LMO. Above all, partial occupancies in either phase of LMOs with minority DOS of Mn-3*d*:t_{2g} shows a partially delocalized feature due to unbalanced occupancies from current ad-hoc PBE+U_{eff} method [92]. Hence, the requirement of the more suitable on-site correlation in LMO is quested for correct orbital occupancies and OO, which would be discussed in the next sub-sections. Now, we initiate the role of spin-orbit coupling (SOC) effects on the stability energies and overall spin-orbital ordering

trends using different spin-orbital quantum number (m_j) projected DOS of the composing elements, La, Mn and O within the PBE+U_{eff} +SOC set-up (see **Section 4.4**).

4.4 Role of spin-orbit coupling: Mn(3d) Occupancies

The interplay of the spin degrees-of-freedom along with atomic structures and orbital motion of electrons are crucial for technologies in high-performance computing and memory devices [145]. Beyond weaker spin-orbit (SOC) based Si-technologies, the recent generation ABO_3 solid-state materials with appreciated electronic bands structure and its composition are very crucial to controlling the orbitronics, spintronics, and optoelectronics properties [146,147,148]. The current LMOs are one of the such important examples in the magnetic semiconductor family [149,150]. The SOC is thus, quite crucial factor for tuning the spin-orbital ordering, hence the band gap opening along with the magnetic ground state stabilization in LMOs [26]. In spite of the similar ionic states of the $Mn^{3+}(3d^4)$ in both LMOs, the role of the correct spin-orbital ordering is now vital for better understanding of the out-of-plane ME interactions.

Thus, the impact of SOC on the 3*d*-orbital occupancies of Mn atoms and its role on ground state stability of LMOs, we have done a set of calculations on the Full-Optm. crystal structure using the PBE+U_{eff} and added SOC as the single-point calculations. In the noncollinear full-relativistic picture, the SOC inclusion is available in the pseudopotential implementations in the current QE6.8 code (see method **Section 3**). Then, the electronic bands dispersions and pDOS plots are also done within PBE+U_{eff} +SOC set-up. The total and pDOS of the different major orbital-quantum (l) numbers and corresponding m_j values for the La(4*f*): $l = 3$, $m_j = \frac{5}{2}$ and $\frac{7}{2}$; for Mn(3*d*): $l = 2$, $m_j = \frac{3}{2}$ and $\frac{5}{2}$; and for O(2*p*): $l = 1$, $m_j = \frac{1}{2}$ and $\frac{3}{2}$ are plotted and labelled with colour solid or dashed lines, while the total DOS of the bulk unit-cell of LMOs are shown with black shaded area, see also **Figure S16**. In o-LMO, the OO of Mn(3*d*) orbitals is resulted more likely a Mott-Hubbard insulator, in contrast to the earlier exp. evidences of charge-transfer type insulator from spectroscopic measurements [95].

About the total energy calculations with SOC, we have noted from the **Table S4** that the relative stabilization energies, ΔE_{FM} is reduced by about 50.0% (-20.0 meV vs. -9.25 meV per f.u.) in the bulk o-LMO phase. So, the FM stability for the o-LMO has now become more weaker once the SOC is introduced even with unfitted PBE+U_{eff} set-up calculated spin-polarized charge-density (as discussed in the previous sections). Besides, the FM stability retains the same in r-LMO *i.e.*, ΔE_{FM} = -629.0 vs. -629.1 meV per f.u. – a prototype LMO without JT-distortions with more relatively non-local Mn(3*d*) electronic correlations than o-LMO. In fact, the choice of the spin-axis along in-plane (or basal-plane) was found energetically stabler vs. other possible spin-canting along face- or body-diagonals of the bulk o-LMO phases, and consistent with the known earlier exp. data [26]. From the band dispersion plots in figure **Fig. 4.a-b)**, we can clearly see the VB and CB edge shifts (red dashed line plots) in the 1st Brillouin zone around the Femi level, E_F = 0.0 eV. There is a substantial improvement of the E_g in the bulk o-LMO and which is just 5-15% smaller than the exp. value (calculated E_g ~1.46 eV vs. exp. 1.50-1.70 eV; see also **Fig. 4.a**). Thus, an excellent improvement of the calculated E_g of the o-LMO magnetic

semiconductor is observed at the given PBE+U_{eff}+SOC level; and consistent with earlier works in 3*d*-4*d*-metal oxides [80,151]. Meanwhile, the r-LMO is still maintaining the half-metallic nature except a few tens of meV change in the Dirac cone gaps around the Fermi energy, E_F = 0.0 eV as shown in the **Fig. 4.b)**.

The calculated absolute spin-magnetic moment is 3.48μ_B (or 3.65μ_B) on the Mn(3*d*) site with SOC is noted, which indicates a high-spin state of these Mn^{3+} ions in o-LMO (or r-LMO) host. Net absolute spin-moment of the bulk o-LMO unit-cell is 17.45 μ_B due to four Mn^{3+} ions in o-LMO and 8.99 μ_B (2 Mn^{3+} ions) in r-LMO. Due to AFM spin-alignment of these Mn(3*d*) sites, we had net spin-moments along three crystallographic directions are M_x=M_y=M_z = 0.00μ_B in o-LMO, while for r-LMO phase we got M_x=M_y=0.00 and M_z = 8.00μ_B in the FM spin ordering of two Mn^{3+} ions vs. spin-axis <100> or <001>, respectively in these two LMOs. The spin-moments are aligned along the most favourable spin-axis *i.e.*, basal-plane in o-LMO (or non-basal-plane in r-LMO). Thus, SOC does not show any important anisotropic spin-quantization referential axes in the r-LMO, and hence, no visible splitting of band-edges around the E_F = 0.0 eV. This could be claimed from lattice symmetry constrains (*i.e.*, centre of inversion) with at least 3 times more centre-of-inversions than the o-LMO phase.

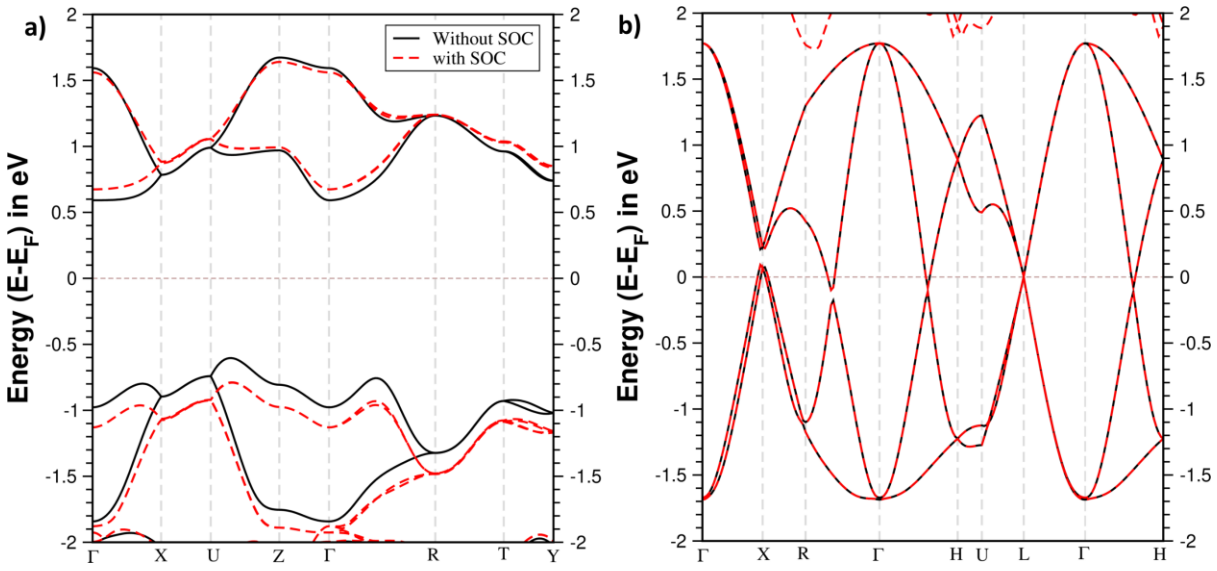

Fig. 4: Calculated electronic band structures dispersion (majority spins) of bulk crystals of o-LMO panel **a)**, and r-LMO in panel **b)** on the full-optimized structure by using PBE+U_{eff} without SOC (black solid line plots) and with SOC (red dashed line plots) exchange-correlation set-ups. Applied U_{eff} values are Mn(3*d*) = 4.5 eV and O(2*p*) = 5.5 eV. Fermi level is marked with thin brown dashed line set on the *y*-axis at zero of the energy scale with E_F = 0.0 eV.

To summarize up to now, at least, one issue is related to the improve relative stability is due to the choice of medium U_{eff} value in the current PBE+U_{eff} methods from the Gavin & Watson, 2017 exchange-correlation set-up [92] vs. the lower U_{eff} from I. Solovyev, 2009 in the first-principles predictions (see also, **Table S2**). The additional contribution of better spin-orbital ordering via SOC is also secondary necessity. However, the

structural changes associated to the JT-distortions in o-LMO, where the Mn-3*d* spin-orbital ordering and local strong electronic-correlations are weakly captured at the standard DFT+*U* methods [152,153]. This is non-trivial to understand at this stage that how these (structure and electronic-correlations) influences the estimated ΔE_{FM} without decoupling it from the reduced structural model of pristine LMOs from the intrinsic JT-distortions. Thus, a comparative analysis of in-plane and out-of-plane ME interactions is quested in the better on-site Hubbard *U* treatment in the pristine and reduced format based on the known exp. limit of reduction in the $LaMnO_{3-x}$ ($0.01< x < 0.04$). This has now become more prominent via broken magnetic symmetries in these LMO crystals by using *point-defects*. The native point-defect is thus, considered with single or double O2/O1-type oxygen vacancies (O_v) in LMOs (see later **Section 4.5** and **4.6**). So, in the next sub-section, we have shown the spin-orbital properties associated to geometries, electronic structures and relative stabilities in these pristine compositions of LMOs within self-consistent on-site U_{self} corrections (with/out SOC and PBE+U_{self}) closely to the existing known exp. spectroscopic data from XPS and XANES [154,155].

4.5 Results from PBE+U_{self}: Self-consistent on-site correlations

4.5.1 Validation of on-site U_{self} Electron-correlations

First of all, we found that the self-consistently (via DFPT) determined on-site U_{self} on Mn(3*d*) sites (say, U_{Mn}) falls in the range 6.15-6.82 eV; and this is in excellent agreement with the earlier investigations using CI cluster model data and exp. data (combined X-ray absorption and photo-emission), proposing U_{Mn} = 6.8 eV in the pristine o-LMO [90,95]. We also see while determining, U_{Mn} jointly with for O-sites (say, U_O), the on-site U_{self} essentially leads to an enhance accuracy of the U_{Mn} [115,116]. Secondly, for r-LMO the predicted U_{Mn} value falls in the range 7.0-7.8 eV for Mn(3*d*), depending upon the choice of U_O correlations. Earlier theory and exp. data had predicted U_{Mn} = 7.5 eV in the FM metallic hole-doped o-LMO [156], thus aligned excellent with the upper bound of the U_{Mn} = 7.8 eV in the current r-LMO.

The observed 3*d*-metal's electronic-correlations in the r-LMO vs. o-LMO phase, is partially stronger U_{Mn} = 7.02 eV vs. 6.15 eV while determined solely at the Mn(3*d*) site. However, the U_{Mn} = 7.83 eV vs. 6.82 eV, while determined jointly with O(2*p*) correlations. Despite having a direct comparison of the previously computed values U_O from other methods, say self-consistent ACBN0 [157,158] or cRPA [159] due to different technical ground of implementations, choice of (pseudo)-potentials and theoretical foundations of *U* corrections within DFT+*U* functionals, the current predicted U_{self} is most affordable determination, and we found U_O ~ 8.4 eV in LMOs. A better description of the Mn-O bond strengths (covalent or mixed valent *etc.*) needs better correlation value not only on the Mn-3*d* but also at the joint determination of U_{self} on the Mn and O-sites via DFPT – a self-consistent first-principles approach. This U_O falls in the upper bound of the predicted range of U_{eff} = 4.8-8.4 eV as known in other 3*d*-metal oxides [44]. Nevertheless, our present first-principles prediction of on-site correlations on the ternary oxide's O(2*p*) is also in line with earlier predictions in some binary oxides electronic and thermal properties [160,161]; and recently validated for the 4*f*-ion doped ZnO [162]. Unfortunately, no such

spectroscopic exp. data is available for the pristine r-LMO as discusses before [12]. Finally, such two competitive electronic-correlations along with/out the JT-distortion in LMOs are taken into account for searching of actual magnetic ground states and could be viable for better understanding of the future high-T_C superconductivity in ternary oxides [153]. Hence, not only correcting the correlation on the Mn(3*d*) orbitals, but also the correct joint correlation treatment of Mn(3*d*)-O(2*p*) orbitals turns out to be very important for a consistent hybridization and better spin-orbital ordering in these LMOs.

We have analysed geometry of LMOs and the stabilization energies from present PBE+U_{self} calculations, and also estimated band gap E_g, and atom site project and total spin-moments, $|M_{Mn}|$, $|M_O|$ and $|M_{tot}|$. In the **Table 3**, we have tabulated these data for both LMOs. The choice of additional on-site U_O on O(2*p*) does not change visibly the lattice parameters, and resulted about +0.5% or less changes in lattice parameters in both LMOs. Besides that, if we see PBE+U_{self} vs. earlier chosen ad-hoc PBE+U_{eff} set-ups, some visible changes (about +1.0-2.0%) on the predicted cell parameters are noted in both LMOs, see also **Table 2** and **Table 3**. More specifically, the currently estimated lattice parameters are respectively, $a = 5.627\text{Å}\ (+1.6\%);\ b = 5.979\text{Å}\ (+0.4\%);\ c = 7.794\text{Å}\ (+1.2\%)$ for the o-LMO, while for the r-LMO bulk phase, $a = b = c = 5.651\text{Å}\ (+1.6\%)$ versus these cell parameters obtained from the previous ad-hoc PBE+U_{eff} set-up [92].

Table 3: Calculated geometry, relative stabilization energies ΔE_{AFM}, and ΔE_{FM} vs. the AFM ground state, spin-magnetic moments Mn^{3+} site ($|M_{Mn}|$), O-site (($|M_O|$)) and total spin-moment, $|M_{tot}|$ and band gap, E_g of the bulk LMOs on the respective AFM and FM ground state of the o-LMO and r-LMO phases with Full-Optm. structure using PBE+U_{self} exchange-correlation functional with Mn-site (U_{Mn}) and or O-sites (U_O).

Parameters	**o-LMO**		**r-LMO**	
	PBE+*U* (U_{Mn} = 6.15 eV)	**PBE+*U* (U_{Mn} = 6.82 eV; U_O = 8.44 eV)**	**PBE+*U* (U_{Mn} = 7.02 eV)**	**PBE+*U* (U_{Mn} = 7.83 eV; U_O = 8.45 eV)**
Lattice Parameters	*a* = 5.605Å; *b* = 5.977Å; *c* = 7.791Å; α=β=γ= 90°	*a* = 5.627Å; *b* = 5.979Å; *c* = 7.794 Å; α=β=γ= 90°	*a* = 5.611Å; *b* = 5.661Å; *c* = 5.661Å; α=β=γ= 61.35°	*a* = 5.651Å; *b* = 5.651Å; *c* = 5.651Å; α=β=γ= 61.17°
Mn-O bond-lengths (Å)	Mn-O1 = 2×2.023; Mn-O2 = 2×1.968; 2×2.272;	Mn-O1 = 2×2.013; Mn-O2 = 2×1.961; 2×2.277;	Mn-O = 6×2.059;	Mn-O = 6×2.067;
Mn-Mn distance (Å)	$(Mn\text{-}Mn)_{\perp}$ = 3.895 Å $(Mn\text{-}Mn)_{\parallel}$ = 4.097 Å	$(Mn\text{-}Mn)_{\perp}$ = 3.897 Å $(Mn\text{-}Mn)_{\parallel}$ = 4.105 Å	$(Mn\text{-}Mn)_{\perp}$ = $(Mn\text{-}Mn)_{\parallel}$ = 4.008 Å	$(Mn\text{-}Mn)_{\perp}$ = $(Mn\text{-}Mn)_{\parallel}$ = 4.032 Å

<Mn-O1-Mn / <Mn-O2-Mn (°)	148.7°/150.0°	150.9°/151.1°	153.5°/153.5°	154.4°/154.4°
ΔE_{AFM} in meV/f.u.	0.00	0.00	0.00	0.00
ΔE_{FM} in meV/f.u.	-30.3	-34.0	-626.0	-714.0
$\|M_{tot}\|$ per cell in μ_B	18.13	18.56	9.74	10.36
$\|M_{Mn}\|$ per Mn^{3+} site ($3d^4$) in μ_B	Mn = 3.60	Mn = 3.66	Mn = 3.85	Mn = 3.95
$\|M_O\|$ per O-site in μ_B	O2 = 0.06	O2 = 0.09	O = 0.13	O = 0.19
Band gap, E_g in eV	0.946 Indirect	1.540 Indirect	Half-metallic	Half-metallic

However, by applying U_{self}, stabilization energies do not show an important change in the sign and order of the ΔE_{FM} = -34 meV vs. -20 meV per f.u. for o-LMO; and ΔE_{FM} = -629 meV vs. -714 meV per f.u. in the r-LMO vs. estimations from ad-hoc PBE+U_{eff}. In fact, this can be primarily explained from geometry point of views (see **Fig. 5**). The enhanced (+0.5%) in-the-plane bond distances $(Mn\text{-}Mn)_{\parallel}$ = 4.105Å (vs. 4.083Å) of the Mn^{3+}—$O2^{2-}$—Mn^{3+} square sub-lattices, resulted flat basal-plane <Mn-O2-Mn angles = 151.1° than the ad-hoc PBE+U_{eff} or even sole U_{self} on the Mn-site set-up estimations as one moves away from the ideal 180° angle for expected AFM ordering [134]. Similarly, in the r-LMO, the estimated $(Mn\text{-}Mn)_{\parallel}$ is resulted about +1.7% elongations with the estimated value 4.032Å (vs. 3.964Å), and also flatter <Mn-O-Mn angles = 154.4°. We also have noted that in Mn-Mn sub-lattices in the out-of-plane side is also expanded by 1.2% [$(Mn\text{-}Mn)_{\perp}$ = 3.897Å vs. 3.851Å] while one uses the PBE+U_{self} exchange-correlation vs. ad-hoc PBE+U_{eff}. This is essentially due to the presence of the JT-distortions in the o-LMO, but absent in the r-LMO which holds identical in-plane and out-of-plane Mn-Mn distances. In the later, both plane's skeleton of Mn^{3+}—O^{2-}—Mn^{3+} contain 6 equal bond lengths, Mn-O = 6×2.059Å and all $(Mn\text{-}Mn)_{\perp/\parallel}$ distances are equal to 4.03Å. Thus, the observed favourable FM type ME interactions could be due to profound manipulation of the geometries and thus, the SE mechanism between half-filled Mn-3*d* ions in the Mn^{3+}—O^{2-}—Mn^{3+} motifs.

Finally, choice of the on-site U_{self} also on O(2*p*) essentially leaves the relative stability to be more profound as FM type ME in r-LMO with the uniform angles < Mn^{3+}—O^{2-}—Mn^{3+}= 154.4°. But due to more buckled angle in o-LMO with <Mn^{3+}—$O2^{2-}$—Mn^{3+}= 150.9° to have JT-distortions, it shows prominent AFM type preference

with ΔE_{FM} ~ -34 meV per f.u. *i.e.*, twice of an order of magnitude less than r-LMO, ΔE_{FM} ~ -714 meV per f.u. (see also **Table 3** and **Fig. 5**). Thus, r-LMO is staying in the FM spin-orbital ordering also in the out-of-plane direction, resulting overall as a robust FM ground state. On other side, the AFM order is favoured in the pristine o-LMO in the similar PBE+U_{self} first-principles calculations set-ups for these La-manganites. It is yet in common line with the failure of band structure theory in the independent particle approximations, even with better on-site Hubbard U_{self} correlations [52].

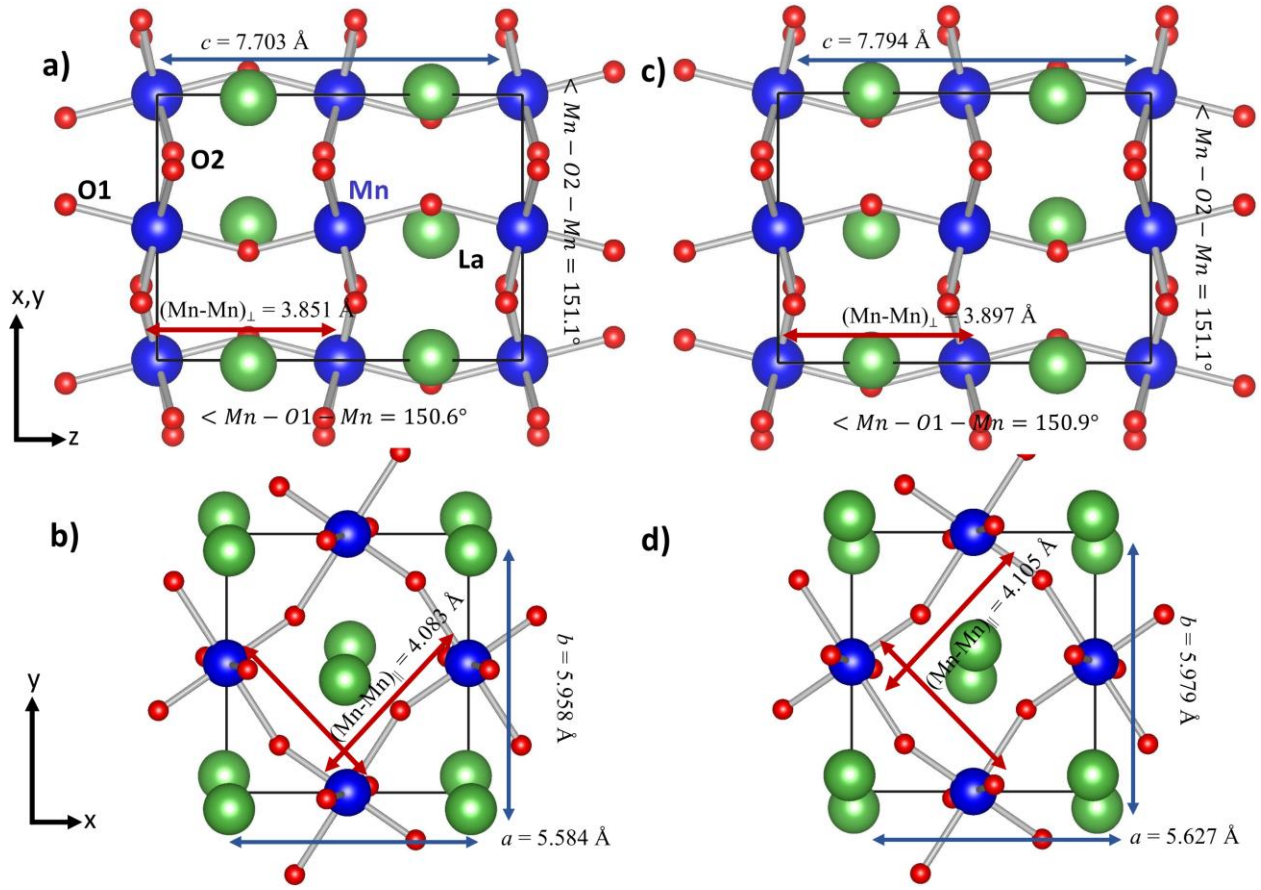

Fig. 5: Unit-cell geometry of the bulk o-LMO after full-relaxation using PBE+U_{self} set-ups with U_{self} = 6.15 eV on Mn(3*d*) panel **a-b)**, and using U_{self} = 6.82 eV for Mn(3*d*) and 8.44 eV for O(2*p*) panel **c-d)** based calculations with side and top views. The marginal changes on the lattice parameters *a*,*b*, and *c* and the Mn-Mn sub-lattices plane distances are marked with fat arrows (blue or red colour), and atoms are labelled with La (green), Mn (blue) and O (red) solids balls in panel **a)**.

Alongside, we have seen application of U_{self} on the both sub-lattices (U_{Mn} and U_O) help to get better high-spin states of the Mn^{3+}($3d^4$) occupancies and much profound E_g of o-LMO phase at the given AFM ordering. While the r-LMO remains in the FM half-metallic type, both the manganites prefer to show the charge-transfer type at the VB and CB edges. Thus, to further understand the role of the on-site U_{self} of U_O along with U_{Mn}, we have plotted the orbital decomposed density of the state of these LMOs with or without U_O, in figures **Fig. 6** and **Fig.**

7, respectively for o-LMO and r-LMO. Primarily, an impact from the U_{eff} = 4.5 & 5.5 eV [92] vs. the U_{Mn} = 6.82 eV & U_O = 8.44 eV within these PBE+*U* set-ups, turn out to be crucial for widening of the same band gap (indirect type), from E_g ~1.2 eV to the ~1.5 eV in the o-LMO phase, and an excellent agreement than the value from known exp. data 1.5-1.7 eV. Secondly, this is even better than the self-consistent Hubbard U_{self} (U_{Mn} = 6.15 eV) while applied only on Mn(3*d*) sites and predicts the same, E_g = 0.946 eV. The current actual band gap, E_g = 1.540 eV is also in reasonable agreement with the previous HSE06 hybrid functional calculations for o-LMO [43,82]. The calculated electronic bands dispersion and electronic transitions from the present set-up of PBE+U_{self} (either with U_{Mn} or both U_{Mn} & U_O set-ups) are also shown with figures **Figure S17** and **Figure S18**, respectively for o-LMO and r-LMO. This is in accordance with the earlier known facts that JT-distortion plays an important role for the transport of o-LMO [163]. This also validates the robustness of the current PBE+U_{self} propositions on the description of the JT-effects in o-LMO with preferred insulating AFM ground state at the modest computational loads.

In case of o-LMO, **Fig. 6.a-b)**, the Mn(3*d*) orbitals are quite strongly localized below 6.0 eV from Fermi level, E_F = 0.0 eV in either choice of the on-site U_{self} for U_{Mn} or both U_{Mn} and U_O set-ups. More specifically, in terms of the 3*d*-2*p* orbitals hybridization the *d*-manifolds in o-LMO *i.e.*, Mn(3*d*:t_{2g}^3) are at lower in energy scale than the Mn(3*d*:e_g^1) orbital. Out of 4 unpaired electrons, 3 parallel electrons (↑↑↑) are located in the Mn-3*d*:t_{2g} manifold (3*d*:t_{2g}^3↑↑↑) and the last one electron (also parallel) at the Mn-3*d*:e_g manifold (3*d*-e_g^1↑) with an empty Mn-3*d*:e_g^0 orbital left in the down spin-channel. Overall, 4 unpaired electrons in o-LMO are distributed into four Mn(3*d*) orbitals and its hybridization with O(2*p*) orbitals, resulting major *p-d* and *p-p* orbital transitions to opening of the indirect E_g in o-LMO, and becomes a charge-transfer insulator consistent with the latest exp. XPS and XAS predictions as mentioned in the previous sub-section [164]. Also, the applied on-site U_{self} on O(2*p*) helps to push up the empty minority (spin-down) levels of Mn(3*d*) into higher energy scale to +7.0 eV and also corroborated with the known exp. data 7.0-7.5 eV [95,141]. As a result, we have seen from **Fig. 6.b)**, an additional Hubbard on-site U_{self} on the O(2*p*) orbitals resulted a knee of O-2*p* pDOS at the valence band top edge below the Fermi level, E_F = 0.0 eV (solid red line plots). As compared to known exp. XPS measurements, the current PBE+U_{self} data also, validates the O-2*p* OO in the o-LMO within the corrected on-site correlations for Mn- and O-sites [154,155]. This was less understood in the earlier discussed ad-hoc PBE+U_{eff} set-ups or even from the current sole U_{Mn} = 6.15 eV set-up. Indeed, the choice of the on-site Hubbard *U* also for the O(2*p*) sites (*i.e.*, U_{Mn} and U_O) is crucial, and that allows us to get the better transport character (*i.e.*, charge-transfer) type of the current o-LMO.

Similar analysis of the orbital decomposed pDOS on the r-LMO phase is also shown in the **Fig. 7.a-b)**, where role of the Hubbard on-site U_{self} also on to the O(2*p*) along with the Mn(3*d*) orbitals is profound. More specifically, the regular environment of the --MnO_6-- motifs with in-the-plane and out-of-plane extension, resulting a quite regular octahedral crystal-field splitting of the Mn(3*d*) orbitals, and thus very distinct and clear 3*d*-orbital occupancies is observed. In spite of the half-metallic nature due to the tail of O(2*p*) is actually passing through the E_F level, but a clear Mn(3d^4) occupancy is observed per Mn-site with spin-moments $|M_{Mn}|$ = 3.95μ_B in r-LMO, which is slightly larger than o-LMO *i.e.*, $|M_{Mn}|$ = 3.66 μ_B for the same reasons discussed before.

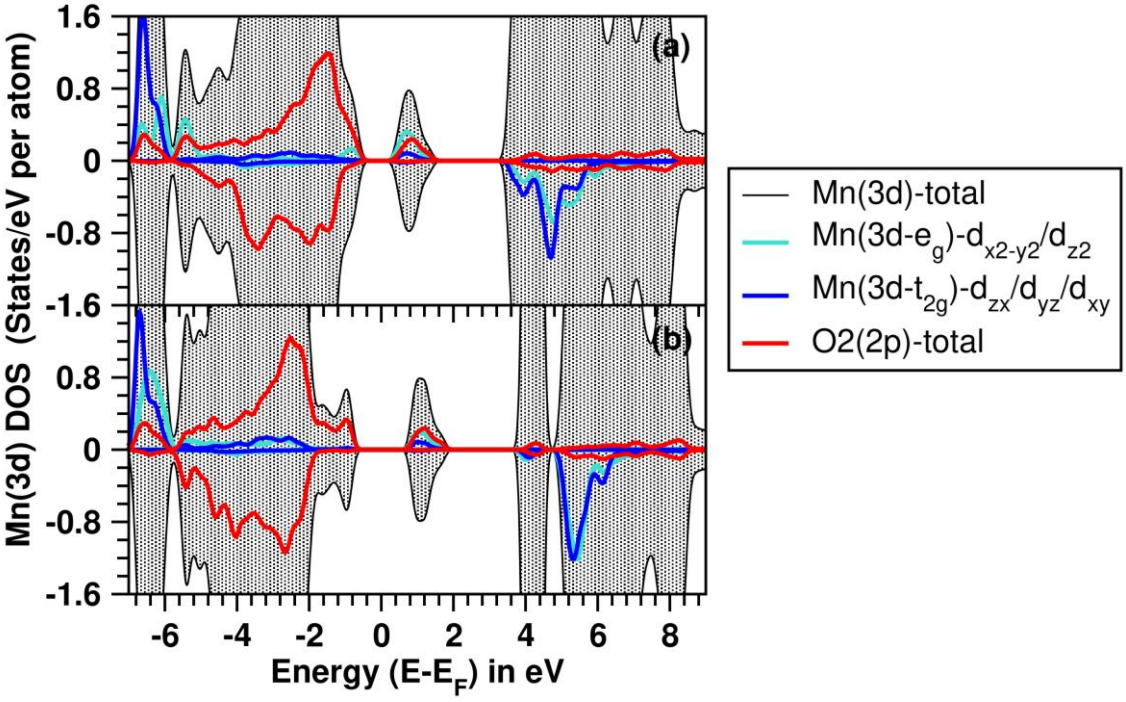

Fig. 6: Calculated Mn(3*d*) orbitals projected density of states per eV per atom of o-LMO bulk crystal using PBE+U_{self} exchange-correlation with U_{self} only on Mn(3*d*) **a)**, or on both sites Mn(3*d*) and O(2*p*) **b)**. In o-LMO applied U_{self} values for Mn(3*d*) = 6.15 eV and set-up with both-site's corrections, Mn(3*d*) = 6.82 eV and O(2*p*) = 8.44 eV, respectively in panel **a)** and **b)** and see also **Table 3**. Different 3*d*-manifolds are plotted with colour solid lines, while the total DOS of the bulk o-LMO is shown with the black shaded area. Fermi level, E_F = 0 eV.

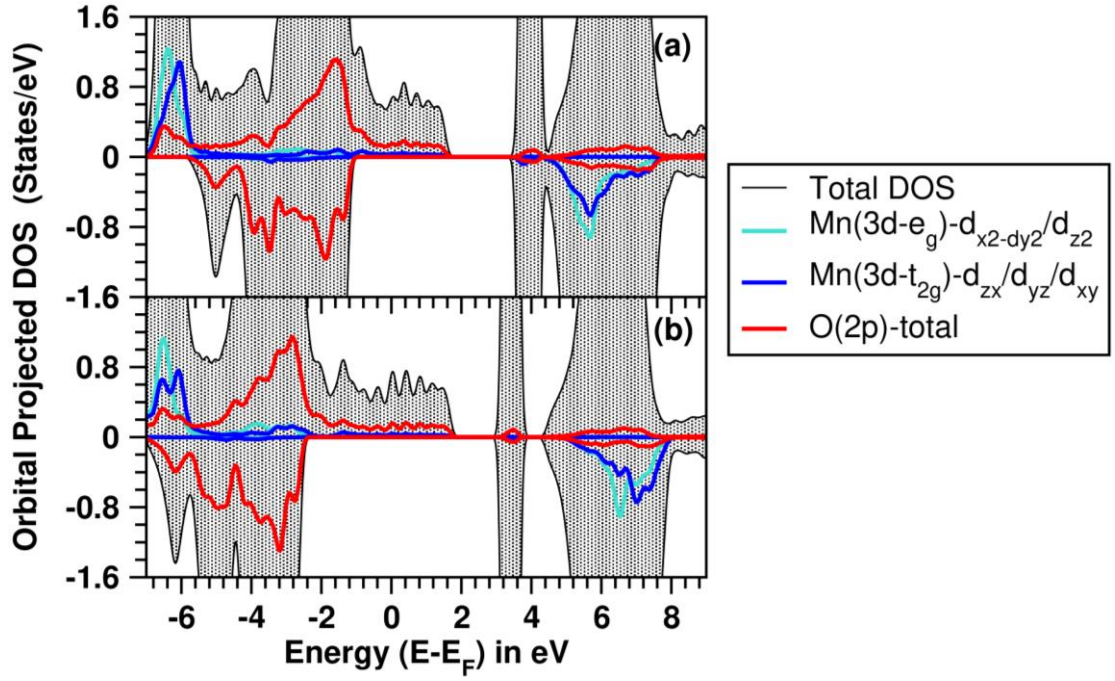

Fig. 7: Calculated Mn(3*d*) orbitals projected density of states per eV per atom (pDOS) of r-LMO bulk crystal using PBE+U_{self} exchange-correlation with U_{self} only on Mn(3*d*) = 7.02 eV **a)**, or both sites Mn(3*d*) = 7.83 eV and O(2*p*) = 8.45 eV in panel **b)**. Fermi level, E_F = 0 eV is set in both panels.

Finally, we seal the choice of the Hubbard U_{eff} vs. U_{self} on both sub-lattices *i.e.*, on Mn(3*d*) & O(2*p*), comes from more preference to the FM ground state relative stability of r-LMO *i.e.*, ΔE_{FM} = -626.0 meV vs. -714.0 meV per f.u. (see **Table 3**), respectively. The same in the o-LMO, ΔE_{FM} = -30.3 meV vs. -34.0 meV per f.u., respectively. In fact, from known XPS spectra on the FM compound obtained with Sr-doped polycrystalline LMO phase shows a supressed electronic density at the sub-states of the Fermi level, E_F = 0 eV, composing the valence band top edge from O-2*p* character [154,155]. This is consistent with present pDOS analysis (solid red line plots) shown in the **Fig. 7.b)**. Electronic transitions among the O(2*p*)-La(4*f*) and O(2*p*)-Mn(3*d*) are quite profound in the down-spin channel (minority spins), and still maintaining the half-metallic nature systematically in the up-spin channel (majority spins) [see also **Figure S18** for the associated band structures]. Thus, the tail of the Mn(3*d*):(t_{2g}+e_g) is less extended across the Femi level, E_F = 0 eV; and this is now pushed down from E_F = 0.0 eV due to the applied U_{self} correction also on the O(2*p*) orbitals in r-LMO. Thus, a stronger non-degeneracy of the O(2*p*) orbitals is resulted at the valence bands in r-LMO with FM ground state, with U_O added. This can be resembled as less covalent character of Mn-O bonds with enhanced net spin-moments from the O(2*p*), $|M_O|$ = 0.2 μ_B per O-sites in r-LMO vs. the $|M_O|$ = 0.1 μ_B in o-LMO.

4.5.2 Role of SOC along with on-site U_{self} correlations

The relative magnetic ground state stability of the host LMO by using PBE+U_{self}+SOC exchange-correlation, is now explored and compared to the known literature data [65,117,165]. Here, by comparing the pDOS data of these LMOs which is obtained from ad-hoc choices of the Hubbard U_{eff} vs. the present U_{self} with SOC – a systematic conclusion can be drawn based on the known reported exp. spectroscopic data combined with XPS, XAS and or XANES on LMOs [95,141,154,155]. First, a distinct nature of the occupied and unoccupied bands is noted from the composing La(4*f*), Mn(3*d*) and O(2*p*) orbitals of LMOs those are shown in **Figure S19.a-b)**. Orbitals with two major m_j quantum numbers, 5/2 and 3/2 for the l = 2 of Mn(3*d*) turns out to be much at lower in energy from Fermi level, E_F = 0.0 eV which indeed results more dominant O(2*p*) character at the top of the valence band, as compared to the ad-hoc PBE+U_{eff} method.

There is a clear shift of the empty La(4*f*) orbitals into the higher energies above E_F = 0.0 eV in o-LMO than the r-LMO. This could be due to more structural distortions imposed by the JT-deformation as compared to the r-LMO phase and hence, more inter-ionic [LaO_{12}]—[MnO_6] interaction is viable in the former case. This essentially fits with the known XPS & XANES data at least for the o-LMO based on the band energy position of *d-f* orbitals [95,155]. Finally, we also noticed that a significant shift of about 1.0 eV to the higher energy of

the La(4*f*) orbitals that compose the bottom of the conduction band in o-LMO than the r-LMO phase. On the other hand, the empty Mn(3*d*) orbitals are also lifted into the higher energies, above the +7.0 eV due to U_{self}, as expected also from these exp. spectroscopic data. Though there is a marginal enhanced splitting of these two majority spins m_j = 5/2, 3/2 of the Mn-3*d* in r-LMO at -7.5 eV, but in either LMOs the present U_{self} parameters are larger than the crystal-fields parameters, *10Dq* and Δ_{JT}, and this is consistent with exp. observation [155] – a necessity beyond the ad-hoc U_{eff} choice.

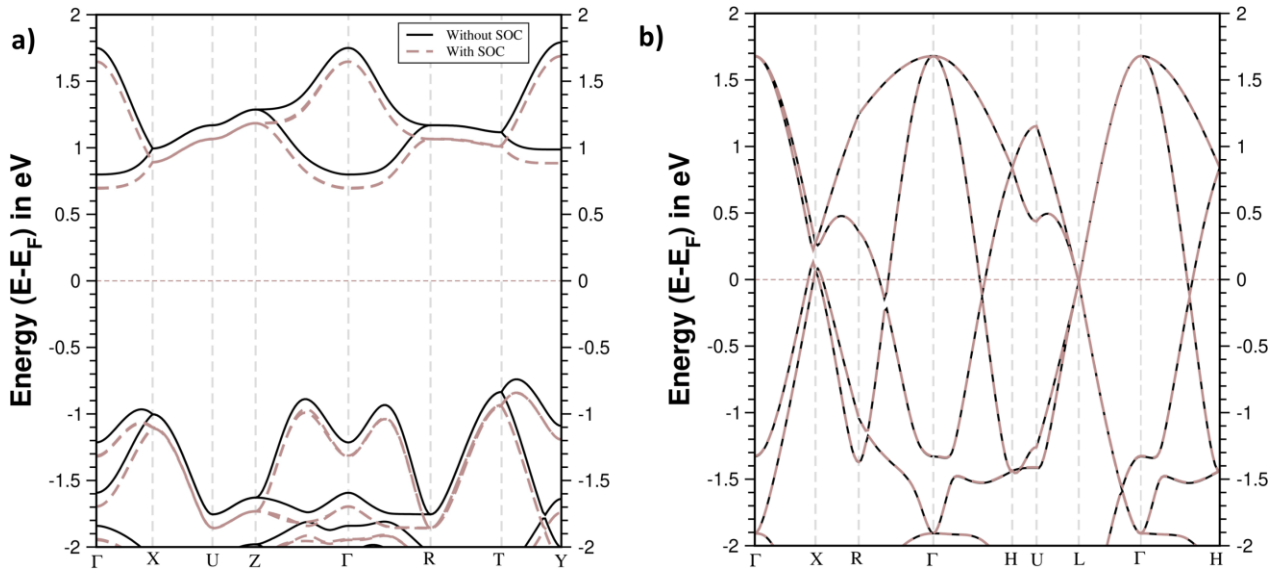

Fig. 8: Calculated total band structures of bulk o-LMO crystal on the full-optimized structure **a)** using PBE+U_{self} +SOC with applied U_{self} for Mn(3*d*) = 6.82 eV and O(2*p*) = 8.44 eV. Panel **b)** shows the same for r-LMO phase with U_{self} on Mn(3*d*) = 7.83 eV and O(2*p*) = 8.45 eV; are plotted in both panels without SOC (black solid energy bands) or with SOC (brown dashed energy bands) corrections. Fermi level, E_F = 0.0 eV is marked with brown thin dotted lines.

The calculated stabilization energies and properties are tabulated in **Table 4**, which clearly shows absence of any visible impacts from SOC (see also **Table 3**). More specifically, with SOC corrections the relative stability is almost unchanged, ΔE_{FM} = -34.0 meV vs. -33.7 meV per f.u. for o-LMO; ΔE_{FM} = -714.0 meV vs. -710.7 meV per f.u. for r-LMO, and also charge-transfer type VB and CB compositions are noted. In the r-LMO phase, the occupied 3*d*-e_g^1 tail is also extended above the Fermi level, E_F = 0 eV, and maintains the half-metallic transport character within the given PBE+U_{self}+SOC set-up (see also, **Figure S19.b**). From this pDOS plots, we see the band-insulator nature of the o-LMO with O(2*p*) character is preserved at the top of VB band-edge compositions. In addition, full structural relaxation with PBE+U_{self} is also to blamed for the invisible relative shift of band-edges in presence of SOC corrections in these 3*d*-metal oxides. Finally, we can also see from bands dispersion plots, **Fig. 8**, a marginal change of the E_g in o-LMO by 10-20 meV at the given PBE+U_{self}+SOC set-up and absent for the r-LMO [166]. In the o-LMO with broken magnetic symmetry (AFM spin-ordering) holds tightly

the JT-distortions on the exp. bulk cell to show SOC splitting (discussed in **Section 4.2**). Possible partial broken JT-distortions (could be $GdFeO_3$-type etc. [140]) during the full structural relaxations with U_{self} set-up resulted VB and CB bands edges shifting in same side of Fermi level, E_F and thus, invisible effects on the estimated band gap, E_g is noted via SOC.

Thus, the necessity of the Hubbard U correlation on O(2p) is quite novel choice in the hierarchy of the JT-distorted host LMOs with Mn^{3+}—O^{2-}—Mn^{3+} octahedral square-cage motifs, and its deformations to maintain the charge-transfer insulating or half-metallic natures [167]. This indeed, indicates different electronic structures, Mn-O hybridizations and hence, its role on the ground stability into two different local minima in the LMOs phases with same stoichiometry *i.e.*, $LaMnO_3$ is crucial to assign the sign and strength of ME terms and this will be discussed next.

Table 4: Calculated relative stabilization energies ΔE_{FM}, and ΔE_{AFM} vs. AFM ground state, as reference, spin-magnetic moments of Mn^{3+}-site ($|M_{Mn}|$), O-site ($|M_O|$) orbital and total moments $|M_{orb}|$ and $|M_{tot}|$, respectively, and electronic band gap, E_g of the bulk LMOs, on the respective AFM and FM ground state of o-LMO and r-LMO using full-optimized structure with PBE+U_{self} set-up and SOC in a single-point calculation. Applied U_{self} values for Mn(3d) = 6.82 (7.83) eV and O(2p) = 8.44 (8.45) eV used for o-LMO (r-LMO). The referential magnetization axis vs. the z-axis and xy-plane was set to the values 0° or 90° and 45° or 30.59° for o-LMO or r-LMO phases, respectively.

Parameters	**o-LMO**			**r-LMO**		
	PBE+U_{self} (Full-Optm.)	**PBE+U_{self} + SOC(1)**	**PBE+U_{self} + SOC(2)**	**PBE+U_{self} (Full-Optm.)**	**PBE+U_{self} + SOC(1)**	**PBE+U_{self} + SOC(2)**
ΔE_{AFM} in meV/f.u.	0.00	0.000	0.000	0.000	0.000	0.000
ΔE_{FM} in meV/f.u.	-34.0	-33.7	-33.7	-714.0	-710.7	-711.0
$\|M_{tot}\|$ per cell in μ_B	18.56	18.55	18.55	10.36	10.36	10.35
$\|M_{Mn}\|$ per Mn^{3+} site ($3d^4$) in μ_B	Mn = 3.66	Mn = 3.66	Mn = 2.59/2.59	Mn = 3.95	Mn = 3.96	Mn = 3.41/2.01
$\|M_{O2}\|$ per O-site in μ_B	O = 0.09	O = 0.09	O = 0.07/0.07	O = 0.19	O = 0.19	O = 0.16/0.09
Band gap, E_g in eV	1.540 Indirect	1.532 Indirect	1.563 Indirect	Half-metallic	Half-metallic	Half-metallic

4.5.3 Estimated magnetic-exchange (ME) terms with on-site U_{self} correlations

Two different exchange-parameters ($J_{\parallel}$ and $J_{\perp}$) in the broken symmetry which were introduced in the last **Section 3** and **Eq. 1-2** for LMOs [81], are now estimated from present first-principles total energy calculations with PBE+U_{self}. As mentioned earlier, the known exp. values of ME are $J_{\parallel}$ = +0.83 meV (in-plane) and $J_{\perp}$ = -0.58 meV (out-of-plane) per Mn-ions in o-LMO [125]. Here, the +Ve and -Ve signs indicate the FM and AFM type ME interactions, respectively. In the limit of Kugel-Khomskii picture with very weaker Hund's exchange *J*, the predicted ME are $J_{\parallel}$ = +0.88 meV and $J_{\perp}$ = -1.15 meV per Mn-ions in the bulk o-LMO phase [152]. In fact, in r-LMO these are actually measured on the hole doped o-LMO with FM ground states and values are in the range of $J_{\perp} \sim J_{\parallel} \sim$ +2.198 to +2.375 meV per Mn-ion, approximately [128,129].

The last reported data by J. Maier and co-authors, 2005 from the first-principles calculations on the o-LMO reported a broad range of the *J*'s value using different exchange-correlations functionals and basis-sets or elemental potentials for o-LMO [127]. The calculated values from their observation of the ME integrals in the classical approach resulted from LAPW calculated data: $J_{\parallel}$ = +2.38 meV and $J_{\perp}$ = -1.75 meV per f.u. [84]; LMTO calculated data: $J_{\parallel}$ = +4.76 meV and $J_{\perp}$ = -1.94 meV per f.u. [39]; LDA+*U* approach with effective *U* only for Mn(3*d*) = 7.3 eV, data: $J_{\parallel}$ = +2.66 meV and $J_{\perp}$ = -1.06 meV per f.u. [153]; and finally with Gaussian LCAO basis-set with GGA exchange-correlation data gives, $J_{\parallel}$ = +3.69 meV and $J_{\perp}$ = -1.47 meV per f.u., and with B3PW values are, $J_{\parallel}$ = +2.50 meV and $J_{\perp}$ = -0.28 meV per f.u. [127]. In comparison to the value from Su *et al.*, 2000 in the Hartree-Fock Approx. (HFA) resulted: $J_{\parallel}$ = +0.88 meV and $J_{\perp}$ = -0.25 meV per f.u. [118], while the DFT values are about one order larger. Nicastro and Patterson, 2002 also same order gives using the HFA: $J_{\parallel}$ = +0.94 meV and $J_{\perp}$ = -0.15 meV per f.u. [64].

We have noticed that most of these values of ME integrals for o-LMO are either overshot or undershot, respectively referential to the values from exp. structure, $J_{\parallel}$ = +1.6 meV and $J_{\perp}$ = -1.2 meV per f.u. [96]. Thus, these earlier first-principles calculations suggest that in-plane Mn^{3+}—$O2^{2-}$—Mn^{3+} motifs have mostly overbound ME integrals with correct sign +Ve (FM-type), while this becomes underbound at the HFA level. Due to use of the exp. crystals, the sign of other out-of-plane ME of the similar Mn^{3+}—$O2^{2-}$—Mn^{3+} motif is resulted with -Ve (*i.e.*, AFM-type) in all these known first-principles theories, that is contrast to the known limitation of the independent-particle bands structure theory for oxides with JT-distortion and limits the predictive power of the first-principles approaches. The obtained range of the ME ratio is $|J_{\perp}/J_{\parallel}|$ = 0.160-0.750; and this is quite broad in range from the known exp. limit 0.699 for o-LMO [96,125].

As discussed before, a spin-polarized SDTF vs. spin-unpolarized CDFT, respectively with on-site Hubbard *U* within first-principles calculations show very interesting comparison of the *spin* exchange-correlation and double-counting errors elimination in the later CDFT+*U* method [52]. However, authors were constrained with only the exp. structure of o-LMO to validate their predictions and interpretations due to the *U* value determined in the cRPA method. The SDFT or CDFT method even with cRPA parameters, essentially fails to disentangle the significant JT-type with/out $GdFeO_3$-type distortions in o-LMO in a fully first-principles calculations. This

is due to the very peculiar *spin-charge-orbital ordering* and *spin-lattice* interactions with multiple (2 in-plane and 3 out-of-plane) Mn-Mn sub-lattices based ME interactions [52]. Authors finally reported, major $J_{||}$ = +1.34 meV (along *x*- or *y*-axis); minor along *xy*-plane, ME term $J_{||}$ = -0.04 meV; and then major along out-of-plane *z*-axis ME term, $J_{\perp}$ = -0.95 meV and minor along the *xz*- or *yz*-plane value, $J_{\perp}$ = -0.27 meV [52]. If we estimate the ratio of these data in the two principal axis values, as $J_{\perp}/J_{||}$ = 0.709 and this is also closer well with known exp. data 0.699.

Our estimation from the present PBE+U_{self} calculations of the in-plane ME integral data are $J_{||}$ = +1.070 meV and +9.807 meV per Mn-ions of o-LMO and r-LMO respectively, and indicating an order stronger FM type ME in the latter non-JT case. Of course, the calculated out-of-plane, ME integral $J_{\perp}$ is positive in either case *i.e.*, +1.051 and +2.713 meV per Mn-ions, respectively in o-LMO and r-LMO phases, which is indicating a favoured (∼thrice) AFM-type ground state stability in o-LMO than the r-LMO – a purely *electronic correlations* mechanism which guided by *orbital* and *charge* ordering as discussed also by Feiner & Oles, 1999 [152]. In spite of the slight differences on the direct distances $(Mn\text{-}Mn)_{\perp}$ = 3.90 Å for o-LMO vs. 4.01 Å for r-LMO (see also **Table 3**), the ME integral value is noticeably larger. Thus, this is indicating a stronger JT-distortions induced *electronic*, *spin*- and *orbital-ordering* in the former to reverse (negative) the sign of ME integral term, $J_{\perp}$. Thus, we have got a reasonable observation from the estimated ME integral value than the known data, with the absolute values ratio of ME terms, $J_{\perp}/J_{||}$ = 0.982 in the present calculations for o-LMO. Thus, we notice more favourable AFM ordering in o-LMO from the current first-principles calculations with PBE+U_{self} and more uniform anisotropy in both directions in a JT-type oxide [152]. But, the asymmetry of ME integrals obtained from the ratio $J_{\perp}/J_{||}$ = 0.277 which indicates a stronger/non-uniform anisotropic energy for the r-LMO and hence more profound difference of ME integrals in two major directions.

Nevertheless, there could be role of anti-site disorder, domain boundaries, and local point-defects, for example oxygen vacancies are predicted with oxygen-deficit magnetic ground states stabilization from a set of PBE+U_{eff} calculations [168,169]. As compared to the other perovskites with alkaline cations *A* = Ca, Sr etc. based manganites, here the size of the *A*-cations, electron doping levels and $[MnO_6]^{3-}$ deformation are crucial consideration for the typical AFM stabilization. Thus, in the next sub-section, we have elaborated these issues with role of the single and double oxygen vacancies (of O1 or O2 type O-atoms) as a case of electron doping. Then, we have taken into account the search of the magnetic ground states of LMOs, and its stabilization and how it is assisted via *magnetic* quasi-particles mediated charge and spin *ordering* around Fermi level and metal site's reductions.

4.6 Reduced $LaMnO_{3-x}$: Results from PBE+U_{self} Calculations

To answer the relative magnetic ground state stability of these LMOs vs. the known exp. data, we have further explored reduced phases with stoichiometric $LaMnO_{3-x}$ $0.00 \leq x \leq 0.04$ *i.e.*, incorporating very small amount of oxygen vacancies (O_v) with concentration 1.0-4.0 at.% (details of VASP calculations in benchmark to the

QE6.8 code data are given in the Method **Section 3** and **Section S1**). The single or double O_v formation energies are also correlated with AFM and FM relative stabilities of these current LMOs. In our current observation from PBE+U_{self} calculations, it shows less than $\pm 0.50\%$ changes for all bulk lattice vectors vs. the highest oxygen deficit o-LMO_{3-x} models in the known exp. structure [165]. To analyse the vacancy formation energies, in the respective single or double vacant O-sites, supercells were relaxed with atomic positions only pertaining to the given cell-volume obtained from full-relaxations of the bulk host lattice in the previous PBE+U_{self} set-up calculations. More technical details of the formation energies calculation can be found elsewhere, which was done on the o-LMO including only on-site Hubbard U for Mn(3d) and the Hund's exchange J [117,169]. Here, the associated electronic structures and magnetic spin-densities are also computed in the given PAW plane-wave calculations [122,123], and plotted in the **Fig. 9** for o-LMO_{3-x}.

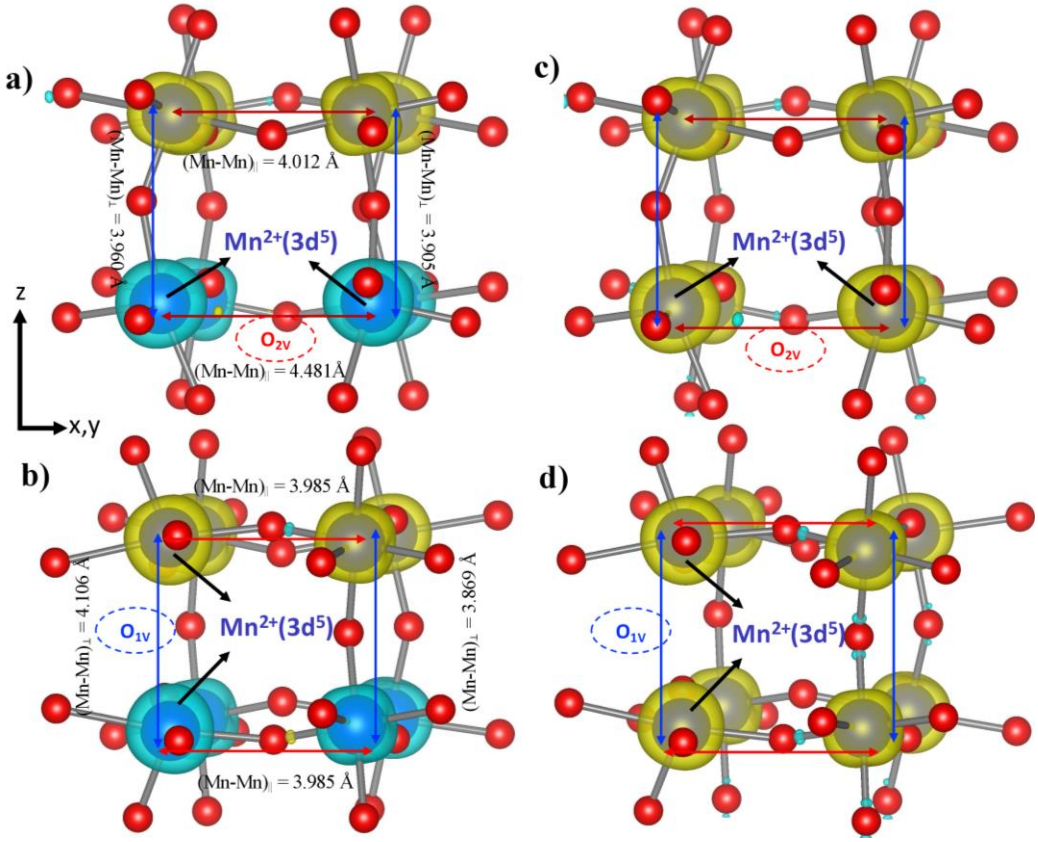

Fig. 9: Calculated spin-densities plots of the reduced o-LMO_{3-x} with $0.00 \leq x \leq 0.04$ from present PBE+U_{self} calculations, for the O2-type in the top two panels **a)-c)** and bottom two panels **b)-d)** for O1-type O_v models. The densities are marked with fine dashed oval shape circles. Reduced $Mn^{2+}(3d^5)$ sites at the 1st NN to the vacancy are marked with a fat black arrow in all panels. Computed majority up and down spin-densities are denoted with yellow and light blue colour electron spin-densities around these Mn-sites (blue solids balls) and plotted with 3D IOS = 0.03 $e^-/Å^3$ using VESTA tool [170].

Spin-densities are calculated from the difference of the up (majority) and down (minority) electronic charge-densities of the given FM or AFM magnetic ground-states of these LMO_{3-x}. This is quite interesting to note that the calculated stabilization energies of the pristine o-LMO, ΔE_{FM} is -11.4 meV and -17.8 meV per f.u. respectively, using on-site U_{self} only on Mn(3*d*) or both sites Mn(3*d*) & O(2*p*) from the current VASP5.4.4 calculations. These are qualitatively and quantitatively excellent than the earlier discussed data using QE6.8 calculations [171]. The both site U_{self}, has not only resulted better E_g values and charge-transfer insulating nature of o-LMO, but also the absolute values of the formation energies are excellent as compared to the earlier reported values 1.0-1.2 eV per O_v sites [168,169]. This makes the PAW and PBE+U_{self} set-up also an equivalent proposition for these La-manganites [169]. Indeed, the estimated formation energies are 1.0-1.4 eV with U_{self} term also on O(2*p*) vs. the 3.1-3.3 eV is obtained from the non-applied U_{self} on the O(2*p*) or say, neglected O(2*p*) correlations. Thus, consideration of local and non-local correlations on the metal and non-metal orbitals, undoubtedly reasonable as soon as one compares such thermochemical properties in the present o-LMO with electron doping.

On the other hand, the O2-sites vacancy needs 1.06-1.08 eV energy per site vs. 1.3-1.4 eV for the O1-site *i.e.*, about 25-30% lower formation energy for the in-plane O_v in the same o-LMO. This could be correlated with JT-distortion induced by shorter and longer bonds, and specifically we noticed that the *shorter* distance 3.85Å of Mn^{3+}—$O1^{2-}$—Mn^{3+} chain in the out-of-plane vs. the *longer* distances 4.10Å of the in-plane Mn^{3+}—$O2^{2-}$—Mn^{3+} chains. Thus, it costs less energy to remove O2-site, see also **Table 3** and **Fig. 5** vs. **Fig. 9**. More specifically, in the **Fig. 9** we show with single O2-site (top panels) or O1-site (bottom panels) O_v pertaining to the AFM and FM ground states, respectively in the left- and right-side panels of this figure. As clearly seen, the majority (yellow colour) and minority (blue colour) spin-densities retain clearly at the AFM, **Fig. 9.a-b**) or the FM, **Fig. 9.c-d**) ground states ordering while stabilizing the single O_v which was created in the host lattice of o-LMO_{3-x}, at the cost of reducing the 1st NN $Mn^{3+}(3d^4)$ ions into a $Mn^{2+}(3d^5)$ ions.

Also, we notice from the **Fig. 9** that, the in-plane bond stiffness *i.e.*, Mn-O2-Mn looks much stronger than the Mn-O1-Mn bonds. Because, the former gets enlarged by 0.47Å (4.01Å vs. 4.48Å) as compared to the later 0.21Å (3.91Å vs. 4.12Å) in the given AFM ground state optimization upon O_v. In the O1-type O_v, we have two mono-polarons (anti-parallel) at the two adjacent out-of-plane Mn^{2+}—• —Mn^{2+} chain, while with O2-type O_v, these are parallel and stay in-the-plane Mn^{2+}—• —Mn^{2+} - are MnO_5-tetrahedral motifs [53]. Thus, the neighbouring Mn-sites are now dressed with excess electrons, the so-called mono *electron* polarons are formed on Mn^{2+} ions, and these aligned AFM type ordering with an extra *electron spin* w.r.t. the 1st NN out-of-plane Mn^{2+} ions. Hence, the O_v planes and polarons formation are strictly following the plane of Mn-O-Mn direction for *charge* and *spin* ordering at the neighbouring Mn(3*d*) empty orbitals in o-LMO – *a prototypical JT-distorted oxide*. In the **Figure S20**, the AFM type spin-densities of the whole supercell are provided with the top and side views, respectively for the single O1 or O2 type O_v in host o-LMO_3.

Corresponding electronic total DOS (black shaded area) and pDOS (red, blue, green, maroon and cyan colours) of the pristine and reduced o-LMO_{3-x} models in the AFM ground state is plotted in the **Fig. 10**. In the AFM type ordering, the O1-site vacancy case is shown in figure **Fig. 10.a-b**), while for the other O2-site vacancy is shown

in the **Fig. 10.c-d**). In these panels, the O1-site and O2-site O_v induced localized doner levels at the adjacent 1st NN Mn-sites is prominent and thus, a sharp pDOS closer to Fermi level, E_F = 0 eV is seen in the panels **b)** and **d)** due to the reduced two $Mn^{2+}(3d^5)$ ions, respectively. As a result, in the lower panels of the **Fig. 10**, we can see majority and or minority spin-density pDOS as a shape peak below Fermi level, E_F = 0.0 eV out of these two Mn^{2+} sites (green solid or brown dashed lines). The extra spin-density also resulted more isotropic spin-densities on the Mn^{2+} sites, as compared to other Mn^{3+} sites, shown in the earlier figure **Fig. 9**. These two Mn^{2+} sites are at the high-spin states in either O_v models out of the O1- or O2-site vacancy which would further manipulate the magnetic AFM or FM exchange integrals in the form of combined direct and or double-exchanges (DE) mechanism with existing super-exchange in o-LMO_{3-x} host.

The next concern is about the relative stability of these LMOs at the reduced limit, and now we discuss the o-LMO_{3-x}. It shows different relative stability trends in the single O1- or O2-type O_v models, say V_{O1} and V_{O2}, respectively. More specifically, in the present case with from V_{O1} model, ΔE_{FM} = -12.7 meV per f.u. and ΔE_{FM} = -19.2 meV per f.u. from the V_{O2} model (see **Table S5**). This indicates that AFM ground state preference comes from the V_{O1} model because of the anti-parallel ME between the two half-filled $Mn(3d^5)$-$Mn(3d^5)$ sites in the $Mn^{2+}(3d^5)$—• —$Mn^{2+}(3d^5)$ skeleton. Thus, the ME is found to relatively negative than the FM type double-exchange (DE) from the kinetic energy gains in the electron doping limits. Then, the U_{self} treatment of correlations in the disrupted Mn(3*d*)-O(2*p*) spin- and charge-ordering is crucial in the chain of Mn-O-Mn skeletons. Thus, for AFM stabilization a better preference is coming from the vacancy at the O1 site (out-of-plane) than the O2 site (in-plane) vacancies. These values and trends are also remaining unchanged even for the twice larger host supercell choice, with 32 f.u. of o-LMO_{3-x} (see also **Table S5.a**).

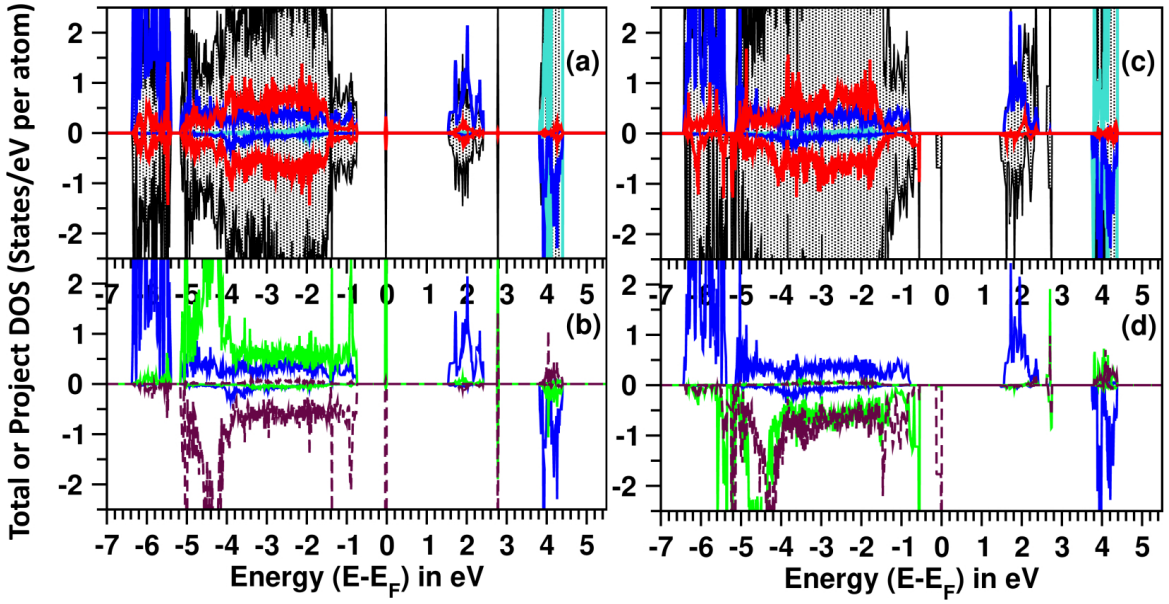

Fig. 10: Calculated Total DOS, and Mn(3*d*) orbitals projected density of states (pDOS) per eV per atom of o-LMO bulk crystal using PBE+U_{self} with U_{self} on the Mn(3*d*) & O(2*p*) in panels **a-b)** with O1-type vacancy or with the O2-type O_v vacancy in panel **c-d)**. In the top panels **a)-c)**, total and pDOS are plotted for the reduced o-LMO_{3-x} model *i.e.*, Total DOS

(black shaded area), other pDOS Mn(3*d*) with blue, O(2*p*) with red, and La(4*f*) with cyan colour solids lines. In the other lower panels, different 3*d*-projected majority (up) and minority (down) spins pDOS are labelled with colour solid or dashed lines for pristine $Mn^{3+}(3d^4)$ [blue solid lines] and its reduced Mn-sites to $Mn^{2+}(3d^5)$ [green solid and maroon dashed lines], respectively in panels **b)-d)**. Fermi level, E_F is set to zero energy scale in all plots.

Thus, to further elaborate these aspects with more electron doping, we also look ground state stability trend as a function of one more O_v sites creation (double vacancy). As a result of the increased vacancies up to double V_{O1} creations, *i.e.*, $x = 0.04$ in o-LMO_{3-x}, we noticed a preference of the AFM ground state is quite enhanced due to the more positive sign of the estimated ΔE_{FM} = -5.42 meV per f.u. However, from the other vacancies with double V_{O2} creations, it remains off or say unaffected with the estimated value of ΔE_{FM} = -19.7 meV per f.u. The associated local spin-densities plots are shown in the **Figure S21**, which also represents a clear favour similarly for the out-of-plane anti-parallel mono-polarons from double O1-vacancies *i.e.*, elevated O_v concentrations. Enhanced AFM type (weak and negative) exchange in the $Mn^{3+}(3d^4)$—O1—$Mn^{2+}(3d^5)$ is much profound in corroboration with possible weaker and negative direct-exchange in the $Mn^{2+}(3d^5)$—• —$Mn^{2+}(3d^5)$ motifs along the out-of-plane [172]. This is schematically depicted in the **Fig. 12.a-b)**.

Possible broken JT-distortions though, is substantial while we removed one of the stiffer basal-plane Mn-O2-Mn bonds, but causes also no significant change in ΔE_{FM} with even with the increased concentration of V_{O2}. So, the V_{O1} introduces a stronger double-exchange type ME in the reduced bulk phase of o-LMO_{3-x} which is relatively negative one as reflected in the calculated ΔE_{FM} = -5.42 meV per f.u., than the pristine FM super-exchange in the only available $Mn^{3+}(3d^4)$—O2—$Mn^{3+}(3d^4)$ motifs in pristine cases. However, the resultant ME remains still with positive sign (FM type) at the current zero temperature and reduced model o-LMO_{3-x} calculations, as interpretated earlier by de Gennes, 1960 [71] and supported by overlapped orbital symmetry rules from Kanamori, 1959 [33]. Hence, the broken JT-distortions of the ideal MnO_6 motifs into MnO_5 polyhedrons in o-LMO through O_v is one of the medium to manipulate its magnetic ground states via different cooperative direct-exchange along with the competition of the native super-exchange and AFM-type DE mechanisms [33,54,165], which is also recently found for other similar non-oxides [173]. Nonetheless, that also validates the current propositions of the applied on-site *U* correlation corrections not only for the metal Mn-site but also for the non-metals O-site in the current o-LMO is profound to stabilize the exp. known charge-transfer insulating AFM ground state – assisted with the magnetic quasi-particles.

In comparison, the r-LMO_{3-x} shows very much distinct electronic structures upon the O-vacancy was seen from calculated vacancy formation energies and relative stabilities (see **Table S5.b**). First of all, as compared to the QE6.8 data, the current VASP5.4.4 data on the relative stability from ΔE_{FM} evaluation in the pristine phase shows similar trend *i.e.*, with an order of enhanced FM stability in the r-LMO vs. o-LMO. The calculated vacancy formation energies at the different O-sites in r-LMO_{3-x} shows very similar thermochemical cost in the range 0.1-0.2 eV per vacancy. This is at least, about an order lower compared to the o-LMO_{3-x} case. This could be associated to the half-metallic nature of the r-LMO_{3-x} with more mobile electrons are available; and resulted

distinct transport of *spins* and *charge* in the reduced format. The net moment out of 2 extra electrons from the single O-vacancy is randomly distributed in the host lattice at four Mn sites (say, Mn7, Mn12, Mn14, Mn21, see **Figure S22**). In this figure we can see ½ of the available electron per Mn-sites, and they partially got reduced to Mn^{2+} ions. Apart from that there are four bridging O-sites, which are now dressed with ½ of an electron with *spins* with opposite sign than neighbouring Mn-site (say, down spin) at dopant (blue colour dumbbells spin-densities). Hence, the so-called Nagaoka-type FM polarons (doublons) are formed [174]. In the **Fig. 11**, we further have plotted the total DOS and pDOS of the La(4*f*), Mn(3*d*) and O(2*p*) of r-LMO_{3-x}, with the atom projection from the Mn8 (pristine) and Mn21 (reduced) Mn-sites at the 1st NN O-vacancy sites. From pDOS plots, it shows clear non-degenerate nature of the O(2*p*) and these $Mn^{2+}(3d^4)$ site's mixed covalent character. This is indeed, manipulating the electronic transitions around the opening of E_g, and is the possibly cause to opening of Mott-type band gap in the reduced r-LMO_{3-x} even at the FM spin-ordering at Mn-sites.

In r-LMO_{3-x}, the calculated spin-moment at the 1st NN Mn-sites *i.e.*, Mn8 and Mn20 of O-vacancy supports as the high-spin centres from $Mn^{2+}(3d^5)$ occupancies with spin-moments, $|M_{Mn}| = 4.6\ \mu_B$ to per site. Subsequently, the bridging O-sites hold dimer like minority spin-densities with calculated spin-moments $|M_O| = 0.6\ \mu_B$ per O-site with dumbbell shape. From these figures, it is clearly visible that in comparison to the other o-LMO_{3-x} models, the current non-JT-distortion induced r-LMO_{3-x} holds also magnetic quasi-particles from spin-densities at the dopant sites – two in-plane and two other dumbbells into the out-of-plane O-sites in the given $Mn^{2+}(3d^5)$—O—$Mn^{4+}(3d^4)$ square-cage skeletons upon the single (or double) O_v models or say, electrons doping (see also **Figure S22)**. Thus, we engender global ferromagnetism in the macroscopic host r-LMO lattice without JT-distortions (say, lattice distortion as compared to the o-LMO) from microscopic induce of the ferromagnetic local magnetic quasi-particles due to electron doping and better on-site added correlations on O-2*p* orbitals.

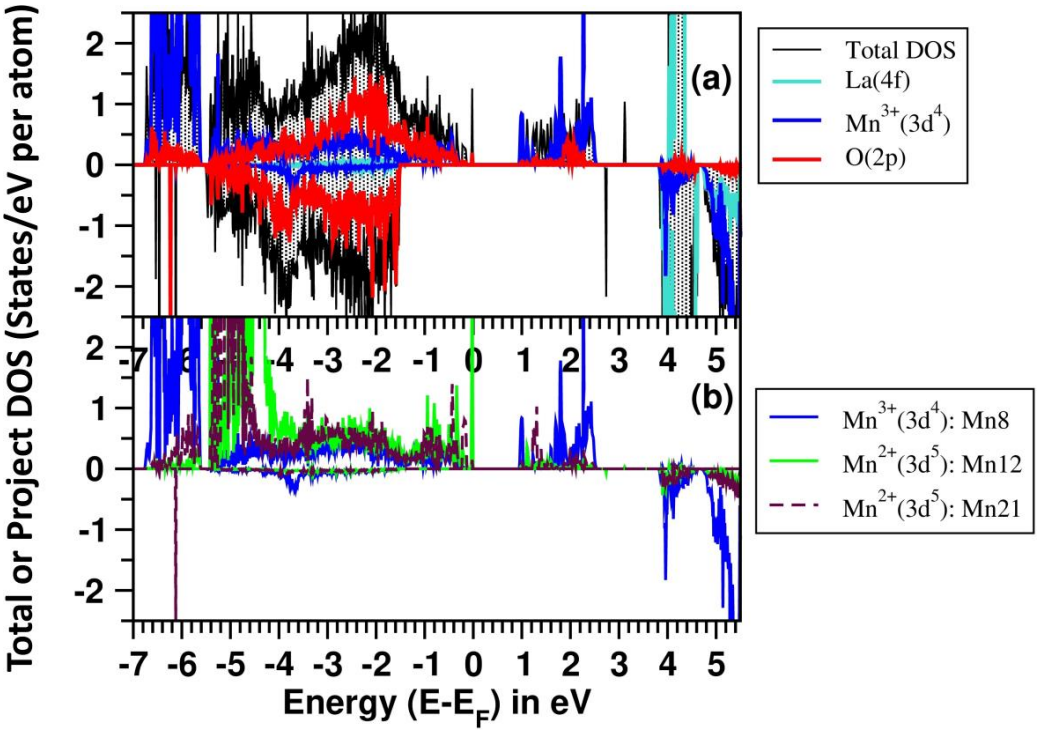

Fig. 11: Calculated Total, Mn(3*d*) orbital projected density of states per eV per atom of r-LMO_{3-x} bulk crystal using PBE+U_{self} set-up with on-site Mn(3*d*) and O(2*p*) and single O-vacancy **a-b)**. In the top panels total and pDOS are plotted for reduced r-LMO_{3-x} model, bottom panel shown only pDOS of Mn(3*d*) in pristine (Mn8) or reduced (Mn12, Mn21). Fermi level, E_F is set to zero energy in all plots.

The so-called *doublons* type magnetic quasi-particles in r-LMO_{3-x}, which results localized FM electron-polarons into these bridging O-sites *i.e.*, spin-polarized electron dressed at the oxygen dopant sites causing an overall FM insulating magnetic ground state. This indeed, separates the spins- and charge-centres away from each other at anion (non-metals) and cation (metals) sites, respectively in the current La-manganite, r-LMO. Thus, the FM spin-ordering remains as the most preferred magnetic ground state even in the r-LMO_{3-x} upon the double or multiple electrons doping in the practical materials, which is an extended 3*d*-metal oxides and consistent with recently proposed bipartite model data on search of Nagaoka FM polarons by Samajdar and Bhatt, 2024 [174]. Indeed, upon extra electrons doping the kinetic energy gain of the 3*d*-itinerant electrons allows to win the FM-type double exchange or direct-exchange in the non-JT model of bulk r-LMO_{3-x} phase over the AFM super-exchange and retained as a FM spin-magnetic ground state – *a signature of the Nagaoka-type FM polaronic magnetic quasi-particles formation in the current manganites* as explored in the ideal theoretical Hubbard model [175,176]. We believe, the itinerant ferromagnetism in this r-LMO phase is a generalization of the FM magnetic ground states in such non-JT oxide r-LMO_{3-x} at larger Hubbard *U* values due to electron doping. This is also consistent with double-exchange mechanism by Zener [70] and de Gennes, 1960 [71] in contrast to the JT-distorted oxide o-LMO_{3-x}.

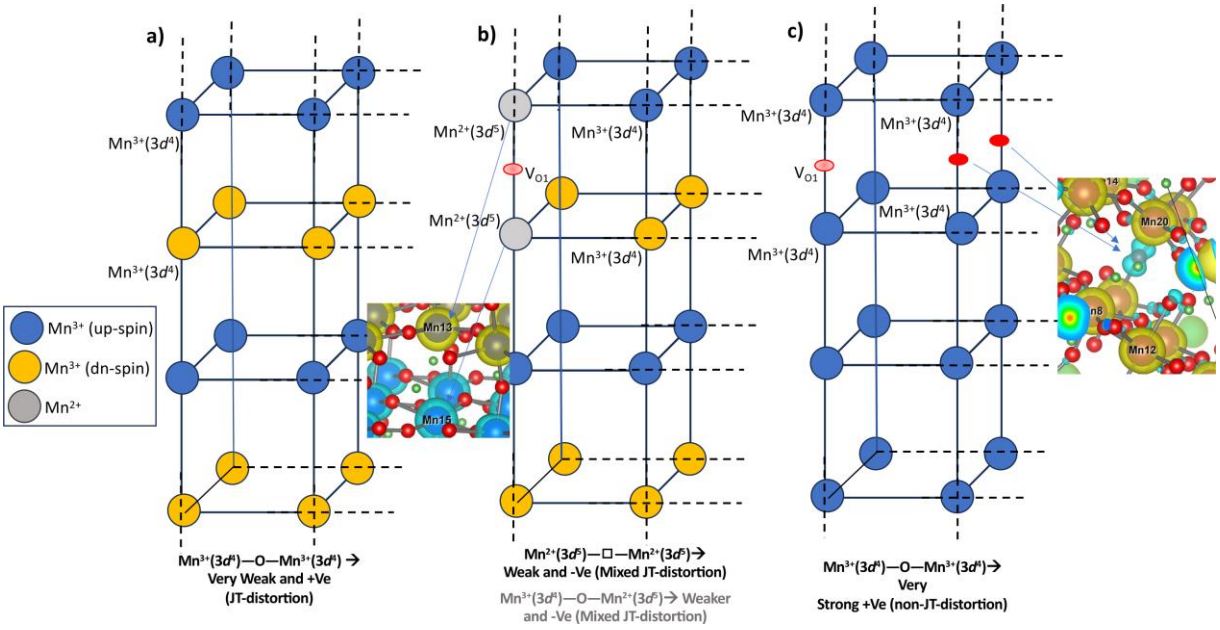

Fig. 12: A schematics of the Mn-Mn sub-lattices ME interactions quantities and signs based on the thermochemical vacancy formations energies, in the pristine model LMO **a)**, and single O_V in the o-LMO **b)** and O_V in r-LMO **c)**. Projected spin-densities of the AFM spin-ordered polarons associated with the reduced Mn^{3+} in o-LMO and FM doublons (*electron-dressed*) at oxygen dopant are marked in panel **b)** and **c)**, respectively with calculated spin-density 3D level of IOS = 0.03 $e^-/Å^3$. Different colour ball (blue or orange) and black/grey sticks are used to draw the Mn-Mn square-skeletons sub-latices (La or O atoms are hidden).

The current observation in r-LMO_{3-x} is also in line with one of our recent observations showing the FM insulating nature and polaronic signature in Sr-doped LMO (say LSMO-0.125) [177]. As similarly to the o-LMO_{3-x}, to summarize the context of the Mn-Mn sub-lattices interactions in LMOs, we have now plotted a schematic of these ME interactions quantities and signs based on the thermochemical stabilization energies and orbital overlap ordering proposed by Kanamori, 1959 [33], and shown in the **Fig. 12.c)** and also see text labelled just below of these panels.

5. Future Implications

Defect induced magnetism in the oxides are fertile ground of research to future advancing materials design, novel experimental techniques to stabilise these defects, and thus, quested more advanced theoretical models and methods to interpret their physical properties [1,2]. Thus, manipulation of point-defects (vacancy, anti-sites, or interstitials etc.), line-defects (dislocations in 1D-imperfections) or planar-defects (2D- or interface-imperfections etc.) are known to vital to manipulate the ferrro- and or anti-ferro-magnetic ground state of oxides. We hope, the current study will find a valuable place in the broader community working in the physics, chemistry of the ternary oxides, especially oxide perovskite thin-films and its peculiar polaronic nature to the transport and magnetic properties due to intrinsic O-vacancy formations (electron doping) or additional *A*-cation doping (say, hole-doping) for better spintronics, orbitronics and room temperature superconductivities to catalysis applications via local or non-local spin-ordering from defects.

For instance, the first example of the anion intercalation in the pseudocapacitor applications due to mobile oxygen ions and vacancies are crucial fact in bulk or nano-crystalline LMOs for energy storage applications via solid fuel-cells or Li-ion Air battery [178,179]. The current observation would impact on many existing observations in the use of the ABO_3 type perovskites for efficient catalytic and solar energy storages device including the recent observation by Z. Weng et al., 2023 [180] and efficient LMO pseudocapacitor by Lin et al. 2023 [181], where mobile electronic charge in the LMOs is viable to reconsider. This possibly caused due to the quasi-particle formations as a function of the native point-defects (electron doping) and modulations via JT-distortions. The role of the corrected on-site Mn-3*d* and O-2*p* correlations and better transport character of LMOs was better justified. Thus, we realized that the cooperative control of the BO_6-octahedral tilting via Y^{3+}

doping may result very exciting control of host $LaMnO_3$ for next generation ABO_3-oxide based clean energy device making [180].

Lin et al., 2023 also have reported the sub-surface H-intercalation and profound pseudocapacitive application of the LMO [181], Nonetheless, our current study may also sheds light on domain of the high-T_c superconductivity research using oxides from the earth abundant manganites, r-LMO [153,160]. In particular, the non-local and local spins of the Mn-3*d* electrons are crucial for such materials, where one can have orbital selective properties of electrons in solids for example, in ABO_3 type oxide perovskites.

In the future work, the current theoretical propositions are aimed to be applied for the Supercapacitors, LIBs and post-LIB applications [182]. Also, other applications not only limited to the such catalysis, but also in spintronics, orbitronics or CMR via multi-orbital model oxides and spin-valve applications using such earth abundant 3*d*-metal perovskites, as competitive to the earlier known 4*d*-oxides or rare-earth metal oxides with proper estimation of the *d*- and *p*-orbital's electronic-correlation [167]. While going from the bulk to the thin-film geometry by switching FM to AFM ground states as a function of oxygen pressure or point-defects, and structural modulation through JT-distortions of these pseudo-cubic to orthorhombic and rhombohedral symmetries, actually opens up new technological applications of LMOs and broader interests in the communities of materials physics and engineering, solid-state chemistry and materials sciences [183,184].

6. Summary and Conclusions

We have revisited the pristine La-manganite perovskites (LMOs) and investigated its reduced stoichiometric say, LMO_{3-x} ($LaMnO_{3-x}$, $0 \leq x \leq 0.04$) by using comparative first-principles calculations and benchmarked to the known experimental evidences from spectroscopic, magnetic and transport measurements. Though the Hubbard on-site U_{eff} electronic correlations correction in the Mn(3*d*) & O(2*p*) of binary oxides are known to be a prominent approach merging the computational cost and accuracies [160,161], however, such studies were lacking in the current ternary ABO_3 perovskite models, where we determined *U* from the choice-free theoretical approach *i.e.*, self-consistent on-site Hubbard *U* calculations via DFPT (density functional perturbation theory). The LMOs models are associated to the presence and absence of the Jahn-Teller distortions in the main metal-non-metal skeletons. Thus, in this scope, we have calculated a transferable and efficient choice of *U* in the DFPT and PBE+U_{eff} formulations at modest computational loads in these two proto-type bulk manganite phases with/out JT-distortions in orthorhombic and rhombohedral. The DFPT method results self-consistent on-site Hubbard *U* (U_{self}) for metals and got excellent accuracy while determined jointly with non-metals and it is excellent corroboration with the known spectroscopic XAS and XPS data at least for Mn-3*d* correlations.

More specifically, out of known three different range of the ad-hoc U_{eff} values (smaller, medium and larger), in the PBE+U_{eff} approach in first-principles calculations, the geometry of the o-LMO was better described with medium U_{eff}, while applied on the Mn(3*d*) only or on both sites, U_{Mn} = 4.5 eV on Mn(3*d*) and U_{O} = 5.5 eV on

O(2*p*) orbitals, respectively. But the electronic band gap, E_g is likely to be a Mott-insulator type with calculated E_g = 1.2 eV vs. known charge-transfer type in the exp. data E_g ~1.5-1.7 eV in any of these U_{eff} set-ups.

The reason was due to lower value of the *U* correlation, U_{eff} = 4.5 eV on Mn(3*d*) in o-LMO vs. known exp. observation U_{eff} = 7.5-7.8 eV. These data were elaborated with the calculated structural and magnetic properties (**Table 1**) at the three different on-site ad-hoc *U* correlations in the **Sections 4.1-4.3**. In the **Fig. 1** and **Fig. 2**, we have shown the full optimized crystal structure and associated density of states (DOS) with orbital projections (pDOS) in the orthorhombic or rhombohedral symmetry of these two LMOs. The DOS and pDOS are shown, respectively in left and right-side panels of **Fig. 2**. Though, the exp. crystal structures of LMOs are retained to the exp. known ground states respectively, AFM and FM for the o-LMO and r-LMO phases at the smaller U_{eff} on the Mn(3*d*), but it is broken with the medium or larger PBE+U_{eff} set-ups. Calculated one order higher FM ordering stability (ΔE_{FM}) in the r-LMO vs. the o-LMO was also explained from the observed in-plane and out-of-plane JT-distortions of Mn-O-Mn angles, and discussed in the **Section 4.2** from the dynamical vs. localized electronic-correlations treatment of Mn-3d orbitals in La-manganites. In fact, in this section we also have rechecked the ΔE_{FM} as a function of different exchange-correlation using PBE and PBEsol with on-site Hubbard *U* with applied Hund's exchange, *J* and non-sphericity term, *B*. The structure, electronic and magnetic properties were also listed in the **Table 2** after full relaxation of crystal structure within ad-hoc PBE+U_{eff} set-up at the medium U_{eff} value. An underestimation of the band gaps by 50-70% from any of ad-hoc PBE+U_{eff} set-ups were noted which limits further the choice for predictive study of physical properties of bulk and finite size LMOs.

Though the band gap of o-LMO was better in the medium U_{eff} set-up, Mott-type insulating nature resulted from the computed atom and/or orbital projected DOS plots which were shown in the **Fig. 3** and shown in the **Section 4.3**. Not only, the orbital ordering was wrongly described in the energy scale, but also width of the Mn(3*d*) bands and La(4*f*) orbitals were less accurate at this ad-hoc set-up of PBE+U_{eff}, than the known exp. XPS and XAS *etc.* spectroscopic data. In the end of this same **Section 4.3**, we also have shaded light on the estimated Mn(3*d*) orbital occupancies in the o-LMO and r-LMO, and geometry and electronic structures were listed in the **Table 2** from the fully first-principles volumes. From a set of systematic PBE+U_{eff} and the SOC (non-collinear spin-polarized) calculations, we noticed that it enlarged band gap, E_g = 1.46 eV as soon as the SOC is included even in the PBE+U_{eff}+SOC approach (*i.e.*, E_g = 1.2 eV without SOC), and shown in the **Fig. 4** and discussed in the **Section 4.4**. The estimated relative stability, ΔE_{FM} was improved also with this ad-hoc PBE+U_{eff}+SOC calculations, but the orbital ordering was not accurate enough for these LMOs. The spin-orbital anisotropy in orthorhombic symmetry to the rhombohedral (hexagonal) one was explored from the presence of centre of inversions in these manganites.

Thus, the necessity of the self-consistent on-site Hubbard *U* is proposed due to the difficulty to explain the consistent magnetic, spin- and orbital ordering in the current LMOs with/out JT-distortions, and shown in **Section 4.5**. Avoiding the large range of choices of these on-site *U* correlations and unavoidable errors from human choices in the calculation strategies available in the literature, our study systematically scrutinised study

of these limitations and we propose a rational PBE+U_{self} set-up with/out electron doping, and discussed in these **Sections 4.5-4.6**.

In the **Section 4.5**, we have first validated on-site Hubbard U_{self} solely on the Mn(3*d*) vs. the U_{self} applied on the both sites, U_{Mn} & U_O very systematically. The origin of the larger U_{Mn} = 7.0-7.8 eV in the r-LMO vs. the 6.2-6.8 eV in o-LMO is explained from the structures, JT-distortions and electronic structures. The on-site U_O = 8.4-8.5 eV, *i.e.*, correlations also on the O(2*p*) orbital occupancies are shown herein **Sub-section 4.5.1** and present theoretical data are compared to the other known theory from cRPA or ACBN0; and few exp. spectroscopic observations at least on the o-LMO. In both LMOs, in-plane and out-of-plane and internal coordinates were relaxed in PBE+U_{self} and very much distinctly evolved during the full optimizations of crystal structures of LMOs. In the orthorhombic crystal symmetry of o-LMO, the JT-distortions were preserved, while the other one r-LMO with rhombohedral symmetry was also maintaining the non-JT-distortions at any set-up first-principles calculations. Here, the calculated pDOS from the two set-ups of U_{self} on Mn(3*d*) only or applied on both sites Mn(3*d*) & O(2*p*) are shown in the **Figs. 6-7**, and structure, and physical properties were tabulated in the **Table 3**. In fact, from the PBE+U_{self} calculations, change on the orbital-ordering at the extrema of the band edges was remarkable, specially resulted LMOs as a charge-transfer like insulator due to dominant O(2*p*) & Mn(3*d*) orbital ordering at the valence band top and conduction band bottom, respectively. No changes on the calculated E_g = 1.53-1.54 eV from PBE+U_{self} approach vs. exp. known 1.5-1.7 eV is found with applied SOC, in the current PBE+U_{self}+SOC functional set-up due to constrains from the centre-of-inversion. More specifically, orthorhombic symmetry in the o-LMO crystal constraints in the self-consistent full optimization of LMOs crystals, was affected and converted into the $GdFeO_3$-type distortions [139]. However, the r-LMO remains insensitive to any U_{self} (or U_{eff}), due to its hexagonal symmetry and complete lacks of JT-distortions before or after full first-principles volume determinations. Besides, an accuracy limit of the estimated E_g in o-LMO (less than 5.0% vs. exp. data) was good enough as like the range-separated hybrid functional based calculation results and known for other similar binary metal oxides [78].

Finally, with/out SOC though the current PBE+U_{self} se-up even was unable to predict the ideal AFM ground state of the pristine o-LMO, but it is still resulted relatively more AFM type magnetic exchange (at least twice of an order of magnitude of relative stability energy ΔE_{FM}) than the FM ordering of r-LMO (see **Tables 3-4**). It does matter whether U_{self} was applied only on the Mn(3*d*) or on the both Mn(3*d*) & O(2*p*) orbitals, because of the better VB and CB compositions of LMOs; discussed and shown in **Fig. 6** and **Fig. 7** in **Section 4.5.1-4.5.2**. Thus, we shed light on the actual electronic correlations treatment of Mn and O sites in LMOs, and spin-orbital effects in such 3*d*-metal oxides to get better description of the Mn-O bond strengths – across the covalent and mixed covalent regime. The limitations of the first-principles electronic structure theory on the accurate reproduction of the AFM ground state were known earlier, and now we extended our discussion into the electron doping models of LMOs. At the end of the **Section 4.5.3**, different magnetic integrals ME term, were calculated and compared to exp. and other known theoretical values.

We realized that by applying PBE+U_{self} on the reduced geometry of o-LMO_{3-x} ($LaMnO_{3-x}$, $0 \leq x \leq 0.04$) with as low as possible concentrations of oxygen vacancy, O_v up to 1.0-4.0 at.% per f.u. of LMOs, it shows the

possible resultant AFM spin-ordered ground state stabilization in o-LMO_{3-x}, while the r-LMO_{3-x} retains as in the FM ordered in r-LMO_{3-x}. We thus, finally was able to show that the cost of two broken O1-sites, substantially drops the relative stabilization energy, ΔE_{FM} down to -5.42 meV from about -34.0 meV per f.u. in o-LMO_{3-x} with self-consistent Hubbard U_{self} and electron doping, while it remains insensitive of two such O2-site vacancies in the r-LMO_{3-x}. This is in excellent corroboration to the known data from experimental studies with the increase of O-deficit or electron doping, and thus profound AFM ground state as discussed in the **Section 4.6**. The electronic spin-densities from the single O1- (out-of-plane) and O2-type (in-plane) oxygen vacancies in LMOs are shown in the **Fig. 9** and associated orbital decomposed pDOS plots are shown in the **Fig. 10** for the o-LMO_{3-x}. The origin of the FM and AFM ordered electron polarons (electron and phonon coupling and magnetic quasi-particles formations) are observed in the o-LMO_{3-x} models, while doublons magnetic quasi-particles are viable in the r-LMO phase due to absence of the JT-distortions (see **Fig. 11**). In the later phase, the FM insulating state is also noted in such minimal electron doping limits in r-LMO_{3-x} models. Compared to the known two major ME values are $J_{\parallel}$ = +0.83 meV (in-plane) and $J_{\perp}$ = -0.58 meV (out-of-plane) per Mn-ions in o-LMO, the estimated ratio of these two ME integrals is 0.982 and 0.277 for current o-LMO and r-LMO, respectively – defining their anisotropic natures. A summary of such ME interpretations is shown in the **Fig. 12**, and labelled with the possible sign and strength from the current investigation.

More specifically, as a function of the O-vacancy concentration in the format, $LaMnO_{3-x}(0.0 \leq x \leq 0.04)$, our findings are also in line with the earlier Zener's DE mechanism where the spin-orbital ground state stability of o-LMO is derived from the electron-hopping along the in-plane direction vs. the lower preference of hoping into the out-of-plane direction, which is anti-ferromagnetic ME. Thus, it provides an AFM-type resultant magnetic ground state in the o-LMO_{3-x} upon the electron doping [185,186]. This is also found to be guided by JT-distortions, and quasi-particles formation and its interaction with host lattices for manipulating the metal into insulator transition in non-JT type oxide r-LMO_{3-x} [17]. The local and non-local electronic correlations limit of the Mn-3*d* and O-2*p* orbitals with orbital selective nature of spins and charge kinetics are expected to be viable for the specific spintronic and orbitronics applications of these LMOs [17,174]. To further validate our findings, with necessary future experimental measurements on these LMOs samples pertaining to the low and high oxygen vacancies are undertaken [53,187].

Thus, the use of such computationally affordable PBE+U_{self} opens an important scope of future implications to use for applications which are discussed in the **Section 5**. The aim of the current work is thus, to overcome difficulties to designing novel earth abundant metal oxides related devices modelling from the affordable first-principles calculations – *a way to enhance the predictive power of the band structure theory in a strong-correlation metal perovskites with JT-distortions*. The desired transport, magnetic and optical properties for possible novel spintronics, orbitronics, and optoelectronic applications are crucial to better understand at the finite sizes, which need also affordable computational loads. These have now been expected to come out by using this computationally cheaper exchange-correlation set-up adapted in current state-of-art DFT+U_{self} first-principles calculations for 3*d*-metal oxides – in particular for earth abundant *manganites*.

Acknowledgements

T.D. acknowledge and thanks to the research grant for Ramanujan Fellow provided by **Anusandhan National Research Foundation (ANRF)** and Science and Engineering Research Board (SERB), Govt. of India, File No. RJF/2021/000120. T.D. also glad to acknowledge National Supercomputing Mission (NSM) for providing computing resources of "PARAM Shakti" at IIT Kharagpur, which is implemented by C-DAC and sup- ported by the Ministry of Electronics and Information Technology (MeitY) and Department of Science and Technology (DST), Government of India. We thank Dr. I. Timrov for fruitful discussions. T.D. also acknowledge useful discussion with Prof. A. Roy, Dept. of Physics, IIT Kharagpur, WB, India and also thanks to Prof. Xavier Rocquefelte, Univ. of Rennes 1, France for insightful suggestions. We also thankful to Prof. Sujit Das, Materials Research Centre, IISc Bangalore, India for a fruitful discussions and help us conducting the initial experimental measurements on these LMO samples (On-going).

CONFLICT OF INTEREST

Authors declare they have no competing potential financial or non-financial conflicts or interests.

DATA AVAILABILITY

All data generated or analysed during this study are included in this published article and its Supplementary Information files.

AUTHOR'S CONTRIBUTION

P.S.P. and T.D. have performed all the calculations, analysed data and drafted the scientific reports. S.T., G.P.D. and T.D. have supervised overall works, contributed to the discussions and preparation of the first draft of the manuscript. T.D. have supervised final overall activities, contributed to the discussions and wrote the final version of the manuscript.

References

[1] P. Esquinazi, W. Hergert, D. Spemann, A. Setzer, and A. Ernst, IEEE Trans. Magn. 49 (2013) 4668–4674.
[2] E. Brand et al., Appl. Phys. Rev. 12 (2025) 011327.
[3] K. Hirose, R. Sinmyo, and J. Hernlund, Science 358 (2017) 734.
[4] D. Maiti et al., Energy Environ. Sci. 11 (2018) 648-659.
[5] J. Park et al., Chem. Mater. 34 (2022) 6108-6115.
[6] S. Moharana, T. Badapanda, S. K. Satpathy, R. N. Mahaling, R. Kumar, Perovskite Metal Oxides, Synthesis, Properties, and Applications, 1st Edition - May 30, 2023, ISBN: 9780323995290
[7] T. Saha-Dasgupta, Mater. Res. Express 7 (2020) 014003.
[8] T. H. Jin et al., Science 264 (1994) 413.
[9] A. Fujimori and Y. Toruka, Proceedings of the 17th Taniguchi Symposium Kashikojima, Japan, Springer Series in Solid State Sciences 119 (1994) 95.
[10] E. O. Wollan and W. C. Koehler, Phys. Rev. 100 (1955) 545; W. C. Koehler and E. O. Wollan, J. Phys. Chem. Solids 2 (1957) 100.

[11] X. Li and J. Yang, Natl. Sci. Rev. 3 (2016) 365.
[12] F. Ma et al., ACS Appl. Mater. Inter. 10 (2018) 36088.
[13] W. E. Pickett and D. J. Singh, Phys. Rev. B 53 (1996) 1146.
[14] I. Solovyev, N. Hamada, adìnd K. Terakura, Phys. Rev. Lett. 76 (1996) 4825.
[15] R. von Helmolt et al., Phys. Rev. Lett. 71 (1993) 2331.
[16] Casey Israel, María José Calderón, and Neil D. Mathur, Materialstoday 10, (2007) 24.
[17] Evgeny A. Stepanov, and Silke Biermann, Phys. Rev. Lett., 132 (2024) 226501.
[18] D. Jo, D. Go, and G-.M. Choi, and H.-W. Lee, npj Spintronics, 2 (2024) 19.
[19] P. Hohenberg and W. Kohn, Phys. Rev. 136 (1964) B864.
[20] W. Kohn and L. Sham, Phys. Rev. 140 (1965) A1133.
[21] R. Qiu, J. Chem. Theory Comput. 21 (2025) 1360-1368.
[22] M. Uhrin et al. npj Comput. Mater. 11 (2025) 19.
[23] O. K. Andersen, Phys. Rev. B 12 (1975) 3060.
[24] O. Gunnarsson, O. Jepsen, and O. K. Andersen, Phys. Rev. B 27 (1983) 7144.
[25] V. Anisimov, J. Zaanen, and O.K. Andersen, Phys. Rev. B 44 (1991) 943.
[26] I. Solovyev, N. Hamada, and K. Terakura, Phys. Rev. Lett. 76 (1996) 4825.
[27] S. Pathak, P. Das, T. Das, G. Mandal, B. Joseph, M. Sahu, SD Kaushik, V. Siruguri, Acta Crystal. C: Structural Chemistry 76 (2020) 1034.
[28] S. Homkar, B. Chand, S. Singh Rajput, S. Gorantla, T. Das, R. Babar, S. Patil, R. Klingeler, S. Nair, M. Kabir, A. Bajpai, ACS Appl. Nano Mater. 4 (2021) 9313.
[29] L. A Cipriano, G. Di Liberto, S. Tosoni, G. Pacchioni, J. Chem. Theory Comput. 16 (2020) 3786.
[30] J. Perdew and A. Zunger, Phys. Rev. B 23 (1981) 5048.
[31] P. Mori-Sánchez, A. Cohen, and W. Yang, J. Chem. Phys. 125 (2006) 201102.
[32] Chen Zhou et al., Chem. Sci. 13 (2022) 7685-7706.
[33] J. Kanamori, J. Phys. Chem. Sol. 10 (1959) 87-98.
[34] J. -H. Park et al., Phys. Rev. Lett. 76 (1996) 4215.
[35] H. Sawada, Y. Morikawa, K. Terakura, and N. Hamada, Phys. Rev. B 56 (1997) 12154.
[36] H. Sawada, Y. Morikawa, N. Hamada, and K. Terakura, J. Magn. Magn. Mater. 177-181 (1998) 879.
[37] H. Sawada and K. Terakura, Phys. Rev. B 58 (1998) 6831.
[38] E. A. Kotomin, R. A. Evarestov, Y. A. Mastrikov, and J. Maier, Phys. Chem. Chem. Phys. 7 (2005) 2346.
[39] R. Lorenz, R. Hafner, D. Spišák, and J. Hafner, J. Magn. Magn. Mater. 226-230 (2001) 889-891.
[40] J. P. Perdew, J. A. Chevary, S. H. Vosko, K. A. Jackson, M. R. Pederson, D. J. Singh, and C. Fiolhais, Phys. Rev. B 46 (1992) 6671.
[41] M. Nicastro and C. H. Patterson, Phys. Rev. B 65 (2002) 205111.
[42] J. H. Lee et al, Phys. Rev. B 88 (2013) 174426.
[43] H. Banerjee et al., Phys. Rev. B 115 (2019) 115143.
[44] K. J. May and A. M. Kolpak, Phys. Rev. B 101 (2020) 165117.
[45] G. Sai Gautam and E. A Carter, Phys. Rev. Mater. 2 (2018) 095401.
[46] Julien Varignon, M. Bibes and A. Zunger, Nat. Commun., 10 (2019) 1658.
[47] T. Ogawa et al., J. Mag. Mag. Mater. 290-291 (2004) 933-936.
[48] T. A. Sidorov, Russ. J. Ing. Chem., 58 (2013) 706-710.
[49] Nadgorny et al., Phys. Rev. B 63 (2001) 184433.
[50] Dowben and Skomski, J. Appl. Phys. 95 (2004) 7453-7458.
[51] B Nadgorny, J. Phys.: Condens. Matter 19 (2007) 315209.
[52] S. W. Jang, S. Ryee, H. Yoon, and M. Joon Han, Phys. Rev. B 98 (2018) 125126.
[53] R. Cortés-Gil et al., J. Phys. Chem. Solids 67 (2006), 579-682.
[54] G. H. Jonker, Physica XXII (1956) 707-722.
[55] S. L. Dudarev, G. A. Botton, S. Y. Savrasov, C. J. Humphreys, and A. P. Sutton, Phys. Rev. B 57 (1998) 1505.
[56] G. Trimarchi, N. Binggeli, Phys. Rev. B 71 (2005) 035101.
[57] T. Das, S. Tosoni, and G. Pacchioni, Comput. Mater. Sci. 191 (2021) 110324.
[58] R. Mahajan, I. Timrov, N. Marzari, and A. Kashyap, Phys. Rev. Mater. 5 (2021) 104402.
[59] E Finazzi, C Di Valentin, G Pacchioni, A Selloni, J. Chem. Phys. 129 (2008) 154113.

[60] E Finazzi, C Di Valentin, G Pacchioni, J. Phys. Chem. C, 113 (2009) 3382.
[61] A. Revcolevschi, A.H. Moudden, Phys. Rev B 57 (1998) R3189-R3192.
[62] J.A. Alonso, M.J. Martınez-Lope, M.T. Casais, and M.T. Fernandez-Dıaz, Inorg. Chem. 39 (2000) 917.
[63] A. Urushibara, Y. Moritomo, T. Arima, A. Asamitsu, G. Kido, and Y. Tokura, Phys. Rev. B 51 (1995) 14103.
[64] M. Nicastro and C. H. Patterson, Phys. Rev. B 65 (2002) 205111.
[65] T. Hashimoto, S. Ishibashi, and K. Terakura, Phys. Rev. B 82 (2010) 045124.
[66] Thomas A. Mellan et al., Phys. Rev B 92 (2015) 085151.
[67] P. Dai et al., Phys. Rev. B 54 (1996) R3694(R).
[68] P. Dai et al., Phys. Rev. B 61 (2000) 9553.
[69] Q. Qian, T. A. Tyson, C.-C. Kao, M. Croft, and A. Yu. Ignatov, Appl. Phys. Lett. 80 (2002) 3141-3143.
[70] C. Zener, Phys. Rev. 81 (1951) 440; 82 (1951) 403; J. Phys. Chem. Solids 8 (1959) 26.
[71] P. G. de Gennes, Phys. Rev. 118 (1960) 141.
[72] J. Muscat, A. Wander, N. M. Harrison, Chem. Phys. Lett. 342 (2001) 397-401.
[73]M. Marsman, J. Paier, A. Stroppa, G. Kresse, J. Phys.: Condens. Matter 20 (2008) 064201.
[74] C. Adamo, V. Barone, J. Phys. Chem. 110 (1999) 6158.
[75] M. Gerosa, C.E. Bottani, C. Di Valentin, G. Onida, G. Pacchioni, J. Phys.: Condens. Matter 30 (2017) 044003.
[76] J. He, C. Franchini, J. Phys.: Condens. Matter 29 (2017) 454004.
[77] F. Tran, P. Blaha, K. Schwarz, P. Novák, Phys. Rev. B 74 (2006) 155108.
[78] T. Das, G. Di Liberto, S. Tosoni and G. Pacchioni, J. Chem. Theory Comput. 15 (2019) 6294-312.
[79] T. Das, G. Di Liberto and G. Pacchioni, J. Phys. Chem. C 126 (2022) 2184.
[80] T. Das and S. Tosoni, Sol. State Ions. 392 (2023) 116165.
[81] D. Munoz, N. M. Harrison, and F. Illas, Phys. Rev. B 69 (2004) 085115.
[82] P. Rivero, V. Meunier, and W. Shelton, Phys. Rev B 93 (2016) 024111.
[83] J. Rodrıguez-Carvajal, M. Hennion, F. Moussa, A.H. Moudden, L. Pinsard, and A. Revcolevschi, Phys. Rev. B 57 (1998) 3189.
[84] N. Hamada, H. Sawada, I. Solovyev, and K. Terakura, Physica B, 237-238 (1997) 11.
[85] P. Ravindran, A. Kjekshus, H. Fjellvåg, A. Delin, and O. Eriksson, Phys. Rev. B 65 (2002) 064445.
[86] P. Norby, I. G. K. Andersen, E. K. Andersen, N. H. Andersen, J. Solid State Chem. 119 (1995) 191-196.
[87] V. Sedykh, Physica C 433 (2006) 189-194.
[88] L.C. Moreno et al., J. Mag. Mag. Mater. 320 (2008) e19–e21.
[89] S. Satpathy, Zoran S. Popovic and Filip R. Vukajlovic, Phys. Rev. Lett. 76 (1996) 960.
[90] A. E. Bocquet, T. Mizokawa, T. Saitoh, H. Namatame, and A. Fujimori, Phys. Rev. B 46 (1992) 3771.
[91] I. Solovyev, J. Phys. Soc. Jpn. 78 (2009) 054710.
[92] Ailbhe L. Gavin, Graeme W. Watson, Sol. State Ion. 299 (2017) 13-17.
[93] J.H. Jung, K.H. Kim, D.J. Eom, et al., Phys. Rev. B 55 (1997) 15489.
[94] T. Arima, Y. Tokura, and J. B. Torrance, Phys. Rev. B 48 (1993) 17006.
[95] T. Saitoh, A.E. Bocquet, T. Mizokawa, H. Namatame, A. Fujimori, M. Abbate, Y. Takeda, M. Takano, Phys. Rev. B 51 (1995) 13942.
[96] N. N. Kovaleva et al., Phys. Rev. Lett. 93 (2004) 147204.
[97] S. Yamaguchi, Y. Okimoto, K. Ishibashi, Y. Tokura, Phys. Rev. B 58 (1998) 6862-6870.
[98] A. E. Nikiforov and S. E. Popov, Adv. Quntum. Chem. (Book Series) 44 (2003) 587.
[99] P. Giannozzi et al., J. Phys.: Condens. Matter 21 (2009) 395502.
[100] P. Giannozzi et al., J. Phys.: Condens. Matter 29 (2017) 465901.
[101] P. Giannozzi et al., J. Chem. Phys. 152 (2020) 154105.
[102] H. J. Monkhorst and J. D. Pack, Phys. Rev. B 13 (1976) 5188.
[103] F. P. Lindner et al. 2022, Comput. Mater. Sci., 237 (2024) 112890.
[104] J. P. Perdew, K. Burke and M. Ernzerhof, Phys. Rev. Lett. 77 (1996) 3865.
[105] M. Cococcioni and S. de Gironcoli, Phys. Rev. B 71 (2005) 035105.
[106] A. I. Liechtenstein, V. Anisimov, and J. Zaanen, Phys. Rev. B 52 (1995) R5467.
[107] V. I. Anisimov, F. Aryasetiawan, A. I. Liechtenstein, J. Phys.: Condens. Matter 9 (1997) 767.
[108] I. Timrov, F. Aquilante, L. Binci, M. Cococcioni, and N. Marzari, Phys. Rev. B 102 (2020) 235159.
[109] W. E. Pickett, S. C. Erwin, and E. C. Ethridge, Phys. Reb. B 58 (1998)1202.

[110] V. L. Campo Jr and M. Cococcioni, J. Phys.: Condens. Matter 22 (2010) 055602.
[111] I. Timrov, N. Marzari, and M. Cococcioni, Phys. Rev. B, 98 (2018) 085127.
[112] I. Timrov, N. Marzari, and M. Cococcioni, Phys. Rev. B, 103 (2021) 045141.
[113] R. Fletcher, Practical Methods of Optimization, 2nd ed. (Wiley, Chichester, 1987).
[114] N. Marzari, D. Vanderbilt, A. De Vita, and M. C. Payne, Phys. Rev. Lett. 82 (1999) 3296.
[115] Iurii Timrov, Nicola Marzari, and Matteo Cococcioni, Comput. Phys. Commun. 279 (2022) 108455.
[116] M. Cococcioni and N. Marzari, Phys. Rev. Mater. 3, 033801 (2019).
[117] Ricca, Chiara, I. Timrov, M. Cococcioni, N. Marzari, and U. Aschauer, Phys. Rev. B 99 (2019) 094102.
[118] Y.-S. Su, T. A. Kaplan, S. D. Mahanti, and J. F. Harrison, Phys. Rev. B 61 (2000) 1324.
[119] P. Reinhardt et al., Chem. Phys. Lett. 319 (2000) 625-630.
[120] Iberio de P. R. Moreira and Francesc Illas, Phys. Rev. B 55 (1997) 4129.
[121] Coen de Graaf and Francesc Illas, Phys. Rev. B 63 (2000) 014404.
[122] G. Kresse and J. Hafner, Phys. Rev. B 47 (1993), 558; G. Kresse and J. Furthmüller, Comput. Mater Sci. 6 (1996) 15; Phys. Rev. B 54 (1996) 11169.
[123] G. Kresse and D. Joubert, Phys. Rev. B 59 (1999) 1758.
[124] Y. Nohara, and A. Yamasaki, S. Kobayashi, T. Fujiwara, Phys. Rev. B 74(6) (2006) 064417.
[125] F. Moussa, M. Hennion, J. Rodriguez-Carvajal, H. Moudden, L. Pinsard, and A. Revcolevschi, Phys. Rev. B 54 (1996) 15149.
[126] Kazuma Hirota, Nobuhisa Kaneko, Akinori Nishizawa, and Yasuo Endoh, J. Phys. Soc. Jpn. 65 (1996) 3736-3739.
[127] R. A. Evarestov, E. A. Kotomin, Y. A. Mastrikov, D. Gryaznov, E. Heifets, and J. Maier, Phys. Rev. B 72 (2005) 214411.
[128] T. G. Perring et al., Phys. Rev. Lett. 77 (1996) 711.
[129] J. W. Lynn et al., Phys. Rev. Lett. 76 (1996) 4046.
[130] R. Laskowski, N. E. Christensen, P. Blaha, B. Palanivel , Phys. Rev. B 79 (2009) 165209.
[131] L. Lajaunie, F. Boucher, R. Dessapt, P. Moreau, Phys. Rev. B 88 (2013) 115141.
[132] T. Das, X. Rocquefelte, R. Laskowski, L. Lajaunie, S. Jobic, P. Blaha, K. Schwarz, Chem. Mater., 29 (2017) 3380-3386.
[133] J. B. A. A. Elemans, B. van Laar, K. R. van der Veen and B. O. Loopstra, J. Solid State Chem. 3 (1971) 238.
[134] J. B. Goodenough, Phys. Rev. 100 (1951) 564.
[135] For example, changing the basis-set from ultrasoft to the PAW (projector augmented wave) type to pseudopotentials (USPP), it does not change the trend with the calculated value i.e., ΔE_{FM} = +8.0 meV (or -325.0 meV) per f.u. for o-LMO (for r-LMO) vs. AFM ground state. This is as good as like +4.0 meV/f.u. (or -349.0 meV/f.u.), derived from the USPP choices. Varying the energy cut-offs 25-30% and convergence criteria down to 2-3 order lower are also not showing any visible changes on these calculated relative stabilities, not even by 1.0 meV per f.u. in either case. Thus, the choice of DFT convergence and parameters are quite robustly chosen and shown the main text methodology Section 3.
[136] C. Franchini et al., Phys. Rev. B 75 (2007) 195128.
[137] Finally, we rechecked the relative stability at the given I. Solovyev, 2009 proposition along within PBEsol exchange-correlation and as before these results are visibly remaining intact with calculated values, ΔE_{FM} = +2.0 meV (or -343.0 meV) per f.u. for o-LMO (or r-LMO) vs. the AFM ground state, respectively. Thus, we conclude that the current calculations and hence interpretations, are free from any technical and/or human choices even on such a fine and smaller (few meV order energy per f.u.) energy differences in the current first-principles calculations in LMOs. This independence is also maintained regardless of the level of pseudopotential as long as the exp. geometry remain fixed for such Jahn-Teller (JT) type distorted oxides. In fact, we noted that the choice of the PBEsol and PBE versions of the GGA functional on binary oxide like MnO_2 and also for the current $LaMnO_3$, the changes in the cell volume relaxation are less than 1.1-2.2%.
[138] Earlier noted that the computed ΔE_{FM} trend is maintained and also remain true for the r-LMO phase, where the FM ground state is preserved irrespective to the choice of PBE+U_{eff} set-ups with the different effective Hubbard on-site U_1 and U_2 with Hund's J and B terms. The calculated spin-magnetic moment on the Mn sites and the unit-cell average absolute values in the present test case retain the same trend while compared to the previous data without Hund's J and non-sphericity B term.
[139] J. Rodriguez-Carvajal, M. Hennion, F. Moussa, A. H. Moudden, L. Pinsard, A. Revcolevschi, Phys. Rev. B 57(6) (1998) R3189.

[140] Pavarini, Eva and Koch, Erik, Phys. Rev. Lett. 104 (2010) 086402.
[141] J. Garcia, G. Subıas, M. C. Sanchez and J. Blasco, Physica Scripta. T115 (2005) 594-596.
[142] Yoshiro Nohara, Susumu Yamamoto, and Takeo Fujiwara, Phys. Rev. B 79 (2009) 195110.
[143] M. M. Schmitt, Y. Zhang, A. Mercy, P. Ghosez, Phys. Rev. B 101 (2020) 214304.
[144] Priya Mahadevan, N. Shanthi, and D. D. Sarma, Phys. Rev. B 54 (1996) 11199.
[145] F. Rortais, S. Lee, R. Ohshima, S. Dushenko, Y. Ando, and M. Shiraishi, Appl. Phys. Lett. 113 (2018) 122408.
[146] R. F. Pierret, Advanced Semiconductor Fundamentals (Addison-Wesley Publishing Co, Reading, Massachusetts, 1987), p. xii.
[147] H. Xu, R. Chen, Q. Sun, W. Lai, Q. Su, W. Huang, and X. Liu, Chem. Soc. Rev. 43 (2014) 3259.
[148] P. R. Anandan et al., Appl. Phys. Rev. 10 (2023) 041312.
[149] S. Ishihara et al., Phys. Rev. B 55 (1997) 8280.
[150] E. Saitoh et al., Nature 410 (2001) 180.
[151] T. Das, S. Tosoni, G. Pacchioni, Comput. Mater. Sci. 163 (2019) 230-240.
[152] Louis Felix Feiner and Andrzej M. Oles, Phys. Rev. B 59 (1999) 3295.
[153] W. Y. Hu et al., Phys. Rev. B 61 (2000) 1223.
[154] S Lafuerza et al., J. Phys.: Condens. Matter 23 (2011) 325601.
[155] J. L. Ortiz-Quiñonez, L. García-González, F. Enrique C. Gordillo, U. Pal, Mater. Chem. Phys. 246 (2020) 122834.
[156] J. Inoue and S. Maekawa, Phys. Rev. Lett. 74 (1995) 3407.
[157] N. J. Mosey and E. A. Carter, Phys. Rev. B 76 (2007) 155123.
[158] N. J. Mosey, P. Liao, and E. A. Carter, J. Chem. Phys. 129 (2008) 014103.
[159] T. Miyake, F. Aryasetiawan, and M. Imada, Phys. Rev. B 80 (2009) 155134.
[160] A. Consiglio, Z. Tian, Sci Rep 6 (2016) 36875.
[161] K. Harun, Nor A. Salleh, B. Deghfel, M. K. Yaakob, A. A. Mohamad, Res. Phys. 16 (2020) 102829.
[162] L. He, Junling Meng, J. Feng, Fen Yao, L. Zhang, Z. Zhang, X. Liu, and H. Zhang, ChemPhysChem 21 (2019) 51-58.
[163] A. J. Millis et al., Phys. Rev. B 54 (1996) 5389; 54 (1996) 5405.
[164] G Zampieri, M Abbate, F Prado, A Caneiro, E Morikawa, Physica B: Condensed Matter, 320 (2002) 51-55.
[165] Ole H. Hansteen, Yohann Bréard, Helmer Fjellvåg, Bjørn C. Hauback, Sol. State Sci. 6 (2004) 279.
[166] Flaviano Jose dos Santos, and N. Marzari, Phys. Rev. B 107 (2023) 95122.
[167] C. M. Varma, Phys. Rev. B 54 (1996) 7328.
[168] U. Aschauer, R. Pfenninger, and S. M. Selbach, T. Grande, and N. A. Spaldin, Phys. Rev. B 88 (2013) 054111.
[169] C. Ricca, Nicolas Niederhauser and Aschauer Ulrich, Phys. Rev. Res. 2 (2020) 042040.
[170] K. Momma, and F. Izumi, J. Appl. Cryst. 44 (2011) 1272–1276.
[171] But absolute values are almost halved compared to the estimation from QE6.8 data, See **Table 3**. We can take into account the difference arises from the USPP and PAW pseudopotentials for supercell calculations with defects (oxygen vacancies).
[172] A. J. Freeman and R. E. Watson, Phys. Rev. 124 (1961) 1439.
[173] Meng-Chien Wang and Ching-Ray Chang, J. Electrochem. Soc. 169 (2022) 053507.
[174] R. Samajdar, and R. N. Bhatt, Phys. Rev. B 109 (2024) 235128.
[175] Y. Nagaoka, Phys. Rev. 147 (1966) 392.
[176] Y. Li, K. Liu, and G. W. Bryant, Phys. Rev. B 110 (2024) 245141.
[177] S. Mekap, J, Tiwari, A. Baro, T. Das, S. Ghosh, and A. Roy, Phys. Rev. B 109 (2024) 241411.
[178] J. Mefford, W. Hardin, S. Dai et al. Nature Mater. 13 (2014) 726-732.
[179] V. Sankar Devi, M. Athika, Perumal Elumalai, ChemistrySelect 7 (2022) e202202554.
[180] Z. Weng et al. 2023, Adv. Mater., DOI: 10.1002/adma.202311102
[181] M.-H. Lin, M.-Y. Lu, H.-L. Chou, G. Wan, and C.-C. Chen, Chem. Mater. 35 (2023) 10487-10494.
[182] C. Li et al., J. Phys. Chem. Solid. 113 (2018) 151–156.
[183] N. Driza et al., Nat. Mater. 11 (2012) 675-681.
[184] Xu Wen Zhao et al., Appl. Phys. Lett. 121 (2022) 162406.
[185] G. Martínez and P. Horsch, Phys. Rev. B 44 (1991) 317.
[186] K. Bieniasz, Mona Berciu, and Andrzej M. Oleś, Phys. Rev. B 95 (2017) 235153.
[187] Collaboration: Prof. Sujit Das, Materials Research Centre, IISc Bangalore, India (on-going work, 2025)